Title	Enhancement of Access Network through Utilization of Optical Resources
Author(s)	椎名, 亮太
Citation	大阪大学, 2022, 博士論文
Version Type	VoR
URL	https://doi.org/10.18910/88146
rights	© 2022 The Institute of Electronics, Information and Communication Engineers.
Note	

Enhancement of Access Network
through Utilization of Optical Resources

Submitted to
Graduate School of Information Science and Technology
Osaka University

January 2022

Ryota SHIINA

List of Publications by the Author

I. Journals

[1] **Ryota Shiina**, Toshihito Fujiwara, Tomoki Sugawa, Tomohiro Taniguchi, "Novel Digital Transmission System for Multi-Channel Radio-Frequency Broadcasting Video Signals Using Digitized-Radio-over-Fiber," *IEICE Trans. Commun.*, vol.J100-B, no. 11, pp.901-911, July 2017.

[2] **Ryota Shiina**, Toshihito Fujiwara, Tomohiro Taniguchi, and Satoshi Ikeda, "DRoF-based Optical Video Re-transmission of Commercial RF Broadcast Signals," *IEEE/OSA Journal of Optical Communications and Networking*, vol. 11, no. 11, pp.559–567, Sept. 2019.

[3] **Ryota Shiina**, Shinya Tamaki, Kazutaka Hara, Tomohiro Taniguchi, Shunsuke Saruwatari and Takashi Watanabe, "Implementation and Evaluation of Novel Architecture using Optical Wireless for WLAN Control Plane," *IEEE Access*, vol.9, pp.133611-133624, Sept. 2021.

II. International Conferences

[1] **Ryota Shiina**, Toshihito Fujiwara, Tomoki Sugawa, "Optical Video Transmission System of Terrestrial Broadcasting by Digitized-RoF Technology with Rate Reduction Method," *Proc. European Conference on Optical Communication (ECOC)*, M.1.B.5, Sept. 2017.

[2] **Ryota Shiina**, Toshihito Fujiwara, Satoshi Ikeda, "3-Bit Digitized-RoF Retransmission of 12ch 16APSK Broadcast Signals with Improved Nonlinear Compression," *Proc. European Conference on Optical Communication (ECOC)*, Th2.64, Sept. 2018.

[3] **Ryota Shiina**, Kazutaka Hara, Tomohiro Taniguchi, Toshiro Nakahira, Tomoki Murakami, Satoshi Ikeda, "VLC/RF Channel Switching Process Adapting to User Mobility in Coexistence Architecture," *Proc. 24th Optoelectronics and Communications Conference/Photonics in Switching and Computing (OECC/PSC)*, WA3-3, July 2019.

III. Domestic Conferences

[1] **Ryota Shiina**, Toshihito Fujiwara, Naotaka Shibata, Tomohiro Taniguchi, Tomoki Sugawa, "Clipping Effects of Multi-Channel Digital Terrestrial Television Broadcasting Signals for DRoF Transmission," *IEICE General Conference*, B-8-6, Sept. 2015. (in

Japanese)

[2] **Ryota Shiina**, Toshihito Fujiwara, Tomohiro Taniguchi, Tomoki Sugawa, "Quantized Bit Reduction by Clipping of Multi-Channel OFDM Signal for DRoF Transmission," *IEICE General Conference*, B-8-23, Mar. 2016. (in Japanese)

[3] **Ryota Shiina**, Toshihito Fujiwara, Tomoki Sugawa, "Quantized Bit Reduction by Nonlinear quantization of Multi-Channel DTT Signals for DRoF Transmission," *IEICE General Conference*, B-8-36, Sept. 2016. (in Japanese)

[4] Toshihito Fujiwara, **Ryota Shiina**, Hisao Yoshinaga, Tomoki Sugawa, "A Study on DRoF Transmission of Broadcasting Satellite Signals," *IEICE General Conference*, B-8-25, Mar. 2017. (in Japanese)

[5] **Ryota Shiina**, Toshihito Fujiwara, Tomoki Sugawa, Satoshi Ikeda, "A Study on Required Quantization Bit for Optical Video Distribution System Using Digitized-Radio-over-Fiber Transmission," *IEICE General Conference*, B-8-21, Sept. 2017. (in Japanese)

[6] **Ryota Shiina**, Kazutaka Hara and Satoshi Ikeda, " Optical / RF Hybrid Wireless Systems for Realizing Stabilized Wireless Environment," *IEICE General Conference*, B-8-2, Sept. 2018. (in Japanese)

[7] **Ryota Shiina**, Kazutaka Hara, Tomohiro Taniguchi and Satoshi Ikeda, "The Study on Switching Method for Optical / RF Hybrid Wireless Systems," *IEICE General Conference*, B-8-32, Mar. 2019. (in Japanese)

[8] **Ryota Shiina**, Shinya Tamaki, Kazutaka Hara, Tomohiro Taniguchi, Toshiro Nakahira, Tomoki Murakami and Satoshi Ikeda, "A study on application of optical wireless to control plane in optical / RF hybrid wireless system," *IEICE General Conference*, B-8-19, Sept. 2019. (in Japanese)

[9] **Ryota Shiina**, Shinya Tamaki, Kazutaka Hara, Tomohiro Taniguchi, Toshiro Nakahira, Tomoki Murakami and Satoshi Ikeda, "A study on optical transmission method for the application of optical wireless to RF control plane," *IEICE General Conference*, B-8-15, Mar. 2020. (in Japanese)

[10] **Ryota Shiina**, Toshihito Fujiwara, Tomohiro Taniguchi and Tomoki Sugawa, "Proposal of The Optical Video Distribution System Using Digitized-Radio-over-Fiber Transmission," *IEICE Tech. Rep.*, vol. 116, no. 346, CS2016-52, pp.39-43, Dec. 2016. (in Japanese)

[11] **Ryota Shiina**, Toshihito Fujiwara, Tomoki Sugawa and Satoshi Ikeda, " [Invited] A Study on Bit Reduction for Optical Video Distribution System Using Digitized-RoF Transmission," *IEICE Tech. Rep.*, vol. 117, no. 156, CS2017-26, pp.65-70, July. 2017. (in Japanese)

[12] Tomohiro Taniguchi, **Ryota Shiina**, Kazutaka Hara and Satoshi Ikeda, "A study on

applicable use cases of optical-wireless communication systems cooperating with Wi-Fi," *IEICE Tech. Rep.*, vol. 119, no. 6, CS2019-6, pp.31-36, April 2019. (in Japanese)

[13] Kazutaka Hara, **Ryota Shiina**, Shinya Tamaki, Tomohiro Taniguchi, Toshiro Nakahira, Tomoki Murakami, Yasuhiro Suzuki, Satoshi Ikeda, "Data Transmission and Radio Resource Control by applying Optical/RF Hybrid Coordinated Systems," *IEICE Tech. Rep.*, vol. 119, no. 183, CQ2019-80, pp.119-124, Aug. 2019. (in Japanese)

IV. Patents

[1] JP6534915B, THE METHOD OF SIGNAL CONVERSION, A SIGNAL CONVERSION APPARATUS AND SIGNAL CONVERSION PROGRAM

[2] JP6527492B, COMMUNICATIONS SYSTEM

[3] JP6912701B, TRANSMISSION SYSTEM, TRANSMISSION METHOD, AND COMPRESSION PROCESSING

[4] JP2020-017855A, OPTICAL/RF WIRELESS HYBRID COMMUNICATION SYSTEM AND CONTROL METHOD

[5] JP2020-043446A, OPTICAL/RF WIRELESS HYBRID COMMUNICATION SYSTEM AND CONTROL METHOD

[6] PCT/JP2019/026359, COMMUNICATION SYSTEM, BASE STATION, AND COMMUNICATION METHOD

[7] PCT/JP2019/024584, WIRELESS COMMUNICATION SYSTEM, WIRELESS COMMUNICATION METHOD, AND TERMINAL DEVICE

[8] PCT/JP2019/031260, WIRELESS COMMUNICATION SYSTEM, WIRELESS TERMINAL DEVICE, WIRELESS BASE STATION DEVICE, AND WIRELESS COMMUNICATION METHOD

[9] PCT/JP2019/049198, TERMINAL DEVICE, COMMUNICATION METHOD, AND COMMUNICATION SYSTEM

[10] PCT/JP2019/049199, TERMINAL DEVICE, COMMUNICATION METHOD, AND COMMUNICATION SYSTEM

[11] PCT/JP2020/002409, TERMINAL DEVICE, COMMUNICATION METHOD, AND COMMUNICATION SYSTEM

[12] PCT/JP2020/015148, RADIO COMMUNICATION SYSTEM, RADIO COMMUNICATION METHOD, BASE STATION CONTROL DEVICE, AND BASE STATION CONTROL PROGRAM

[13] PCT/JP2020/035424

[14] PCT/JP2021/000022

V. Awards

[1] Encouraging Award of Technical Committee on Communication Systems, "Proposal of The Optical Video Distribution System Using Digitized-Radio-over-Fiber Transmission," The Institute of Electronics, Information and Communication Engineers, Technical Committee on Communication Systems, July 2017.

[2] Young Researcher's Award, "Optical/RF Hybrid Wireless Systems for Realizing Stabilized Wireless Environment," The Institute of Electronics, Information and Communication Engineers, Mar. 2019.

Abstract

This paper is a summary of the research results on "Enhancement of Access Network through Utilization of Optical Resources". This research was conducted during the author's affiliation with the Department of Information Networking, Graduate School of Information Science Technology, Osaka University and NTT Access Network Service System Laboratories. This paper is composed of chapters 1 to 5.

Chapter 1 is an introduction and explains the current state of access networks and changes in research areas for the future as the background of this research. Furthermore, the optical video re-transmission service and wireless local area network (LAN) service are outlined. Then, the purpose of this research is described.

Chapter 2 describes the optical re-transmission service of broadcast signals as one of the various services to be accommodated in the access network. Conventional systems used for optical re-transmission are equipped with coaxial network interfaces that are widely used at both ends of the network, but there are some problems caused by analog transmission. In analog transmission, it is necessary to deploy a large number of re-transmission facilities near the user facilities due to the transmission distance limitation. Therefore, we propose an optical re-transmission system based on digitized radio-over-fiber (DRoF) technology. In the proposed system, optical re-transmission is possible through a shared communication digital network with coaxial interfaces at both ends of the network. Since the transmission rate of the proposed system is increased by digitizing the radio frequency (RF) signal compared to the transport stream (TS) signal, we also propose a static and simple method to reduce the transmission rate. We evaluate the effect of transmission rate reduction through re-transmission experiments using 9ch of

commercial digital terrestrial broadcasting signals.

Chapter 3 describes the transmission rate reduction scheme focusing on satellite broadcasting among the broadcasting signals targeted by the optical re-transmission service. In satellite broadcasting, signals are received at re-transmission antennas via RF band channels in the 11 GHz to 12 GHz. Compared to digital terrestrial broadcasting, satellite broadcasting is more susceptible to rainfall attenuation due to its high frequency band. Therefore, the carrier-to-noise ratio (CNR) of the input signal to the re-transmission facility fluctuates. In the conventional system, it is necessary to set the compression parameters assuming the lowest CNR for the CNR fluctuation, which reduces the transmission rate reduction efficiency and spectrum utilization efficiency. Therefore, we propose a DRoF-based optical re-transmission system using adaptive combinatorial compression for broadcasting signals. In the proposed system, the optical re-transmission rate of broadcasting satellite (BS) / communication satellite (CS) signals is reduced as much as possible while accommodating the variation of input CNR. This ensures the transmission rate of communication signals in time division multiplexing (TDM) transmission and realizes network sharing of communication signals and broadcast signals through passive optical network (PON). Experimental evaluation based on the prediction model of ITU-R P.618-13 is used to evaluate the effect of quantization bit number reduction (transmission rate reduction) on service time.

Chapter 4 describes a wireless LAN system using optical wireless to solve the problems in hotspot services, such as the difficulty of providing location-based services and the fluctuation of network quality due to the variation of user equipment (UE) distribution. In order to realize location-based network provision and control, we propose a location aware wireless system architecture that divides the wireless service area into smaller

optical cells and centrally controls the user equipment (UE) connections under each optical cell. Our system transmits an optical identifier (ID) specifying connection information to the UE. The received optical ID indicates the optimum connection destination. To realize simple and low-cost transmission and reception of optical ID, we propose an optical ID transmission / reception method using Internet of Things (IoT) lighting and illuminance sensors. The proposed method reduces the transmission/reception error rate while reducing the matching cycle of the optical ID. The reduction rate of the matching cycle and the transmission/reception error rate are evaluated by experiments. In addition, an optical cell control algorithm is also proposed in order to suppress deterioration of network quality due to fluctuations in UE distribution. We propose two types: ScanLine-based, which controls the optical cell in a scanning line, and MinDist-based, which considers the positional relationship between the optical cell and the access point (AP). The simulation evaluates the 1user average capacity difference between APs and the perspective of total capacity.

Finally, in Chapter 5, we summarize the results obtained through the above research and conclude this paper.

Acknowledgments

First at all, I would like to express my deep and sincere gratitude to my advisor, Professor Takashi Watanabe of the Department of Information Networking in Graduate School of Information Science and Technology, Osaka University, for all his valuable advice and comments on my research. He graciously accepted me as a working doctoral student and guided my research in a better direction.

A special gratitude I give to Associate Professor Shunsuke Saruwatari of Information Networking in Graduate School of Information Science and Technology, Osaka University, for his constructive suggestions and guidance.

I would like to express my deep gratitude to Professor Masayuki Murata, Professor Toru Hasegawa, Professor Hirozumi Yamaguchi and Professor Morito Matsuoka of the Department of Information Networking in Graduate School of Information Science and Technology, Osaka University for serving as members on my dissertation committee.

I owe a deep debt of gratitude to Assistant Professor Takuya Fujihashi of the Graduate School of Information Science and Technology, Osaka University, for his continuous support.

I would like to express my appreciation to Satoshi Ikeda Project Manager (currently Director of NTT West R&D Center), Koji Tsuji Project Manager (currently NTT Advanced Technology Corp.), Tomoki Sugawa Project Manager (currently NTT Advanced Technology Corp.), Yuuichi Kido Research Director and Junichi Kawataka Project Manager of NTT Access Network Service Systems Laboratories, for giving us the opportunity to carry out these studies at NTT Access Network Service Systems

Laboratories.

I am particularly grateful to Tomohiro Taniguchi Group Leader, Toshihito Fujiwara Senior Researcher, Shinya Tamaki Senior Researcher, Tatsuya Fukui Senior Researcher, Yuki Sakaue Research Engineer, Hiroya Ono Researcher, Ryohei Tsugami Researcher of NTT Access Network Service Systems Laboratories for giving great deal of cooperation in advancing the research.

Finally, I would like to thank my irreplaceable family for supporting me at all times.

Contents

List of Figures

List of Tables

Chapter 1

Introduction

1.1   Background

The demand for network traffic is increasing every year. With the start of the fiber-to-the home (FTTH) service in the early 2000s, the spread of broadband has accelerated, and networks have achieved remarkable development [1]. In recent years, with the change in lifestyle due to the epidemic of covid-19, remote work has been actively promoted, and broadband has become more widespread [2]. Fig. 1.1 shows FTTH subscribers in fixed broadband in Japan. As can be seen from Fig. 1.1, the number of FTTH subscribers is
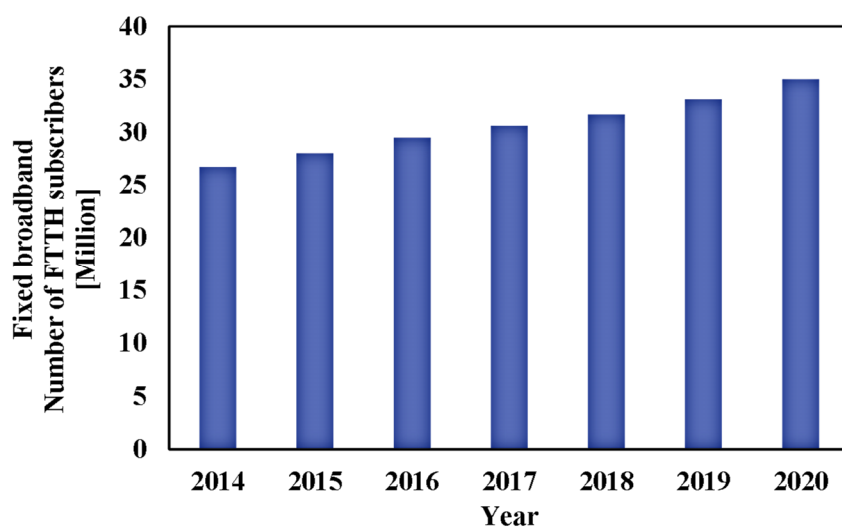
Fig. 1.1: Number of fixed broadband FTTH subscribers in Japan [2].
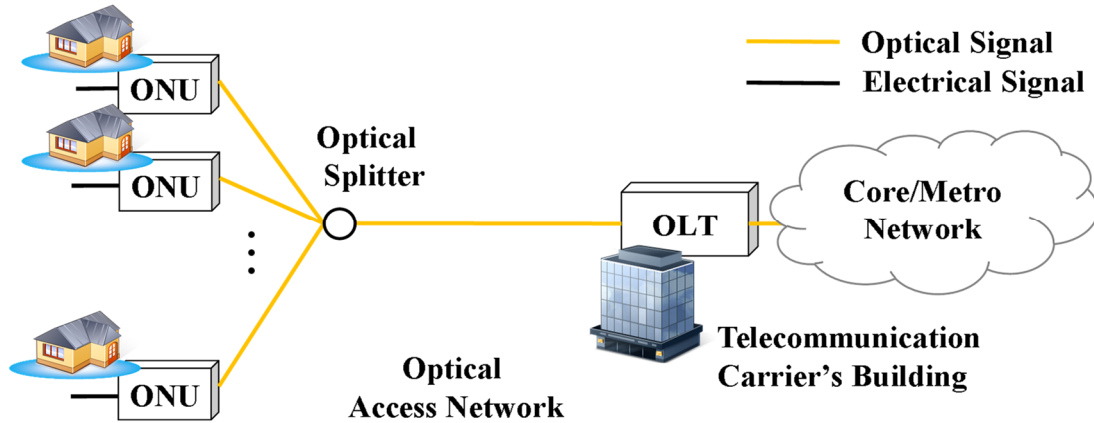
Fig. 1.2: Access network configuration using passive optical network.

increasing year by year. Among the broadband services, FTTH service is widely provided in Japan. In this FTTH service, passive optical networks (PON) are widely used in the access network [3].

Figure 1.2 shows the configuration of the access network using PON. A PON-based optical access network consists of an optical line terminal (OLT), an optical splitter, and an optical network unit (ONU). The OLT sends and receives optical signals as a terminal device installed in a telecommunications carrier's building. An optical splitter is a device for branching an optical signal. An ONU is a subscriber-side termination device that converts between optical and electrical signals. The signal transmitted from the OLT is branched by the optical splitter and received by the ONU. The received optical signal is converted into an electrical signal.

There are various signal multiplexing methods in PON. For example, widely used commercial system such as GE-PON use time division multiplexing (TDM) -based PON system [97]. In TDM-based PON system, downlink signals are multiplexed by time division multiplexing (TDM). Each ONU uses the assigned time slot to communicate
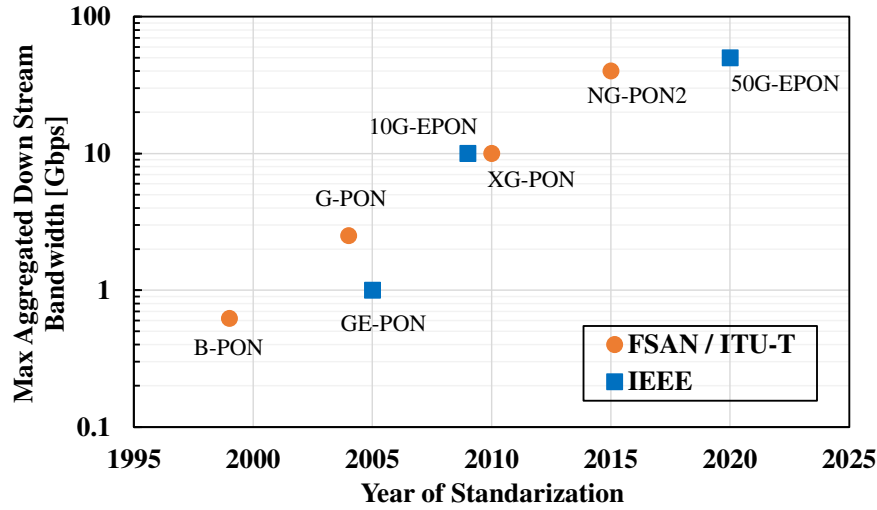
Fig. 1.3: Standardization trends in passive optical network [5].

with the OLT. On the other hand, the uplink signal is multiplexed using time division multiple access (TDMA). In TDMA, the connection with OLT is established so that the collision of the uplink signal from each ONU does not occur. In the current commercial system, different wavelengths are used for the uplink and downlink signals, and strictly speaking, a combination of TDM and wavelength division multiplexing (WDM) is used. On the other hand, there is WDM-based PON in which each ONU is assigned a specific wavelength to communicate with the OLT [98]. Since an ONU can exclusively use one wavelength, high-speed communication can be achieved without being affected by the communication status of other users in the PON segment.

Figure 1.3 shows the standardization trends of PON systems. The standardization of PON systems has been promoted by two organizations, Institute of Electrical and Electronics Engineering (IEEE) and International Telecommunication Union-Telecommunication Standardization Sector (ITU-T) / Full Service Access Network (FSAN). In the current PON system, 1 Gbps class and 10 Gbps class systems have been
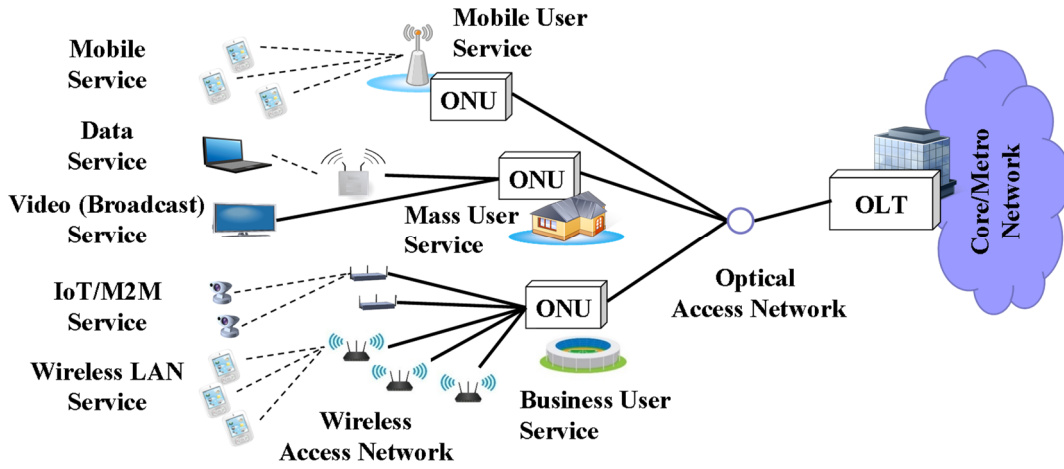
Fig. 1.4: Accommodating various services using passive optical network.

used commercially. On the other hand, as shown in Figure 1.3, the standardization of high-speed PON systems exceeding 10 Gbps has been progressing in recent years [99, 4, 5]. For example, in 2015, ITU-T standardized a 40 Gbps class system called Next-Generation Passive Optical Network Stage 2 (NG-PON2). NG-PON2 realizes high-speed communication of 40 Gbps by TWDM-based PON, which is an approach that combines TDM / TDMA and WDM [100]. In addition, 50G-EPON has been standardized as a new standard that realizes 50 Gbps. A 50G-EPON is also realized by TWDM-based PON system utilizing two wavelengths [101, 102].

Since the establishment of the PON system, the mainstream of research has been the realization of ultra-high-speed communication. There has also been active research on low power consumption related to ONU and OLT [6, 7, 8]. On the other hand, in recent years, with the advent of standardized high-speed system standards exceeding 10 Gbps, new research directions are being found. Assuming a high-speed system standard, technologies related to flexibly accommodating various services, improving economic efficiency, and reducing maintenance operations are being actively proposed. For

example, efforts are being made to virtualize, softwareize, and componentize the functions of communication equipment such as OLT for telecommunications carriers [16, 17, 18]. As a basic idea, the functions for realizing various services are concentrated in the upper level, and the other devices use simple general-purpose devices. This makes it easy to add or remove functions. In addition, by adopting a highly common device configuration, maintenance parts can be minimized and operation procedures can be simplified.

Also, as shown in Figure 1.4, research to accommodate a variety of services in PON-based access networks is being conducted for each service. For example, data communication services, video distribution services, Internet of Things (IoT) / Machine to Machine (M2M) services, wireless local area network (LAN) services, and mobile services will be accommodated. In order to realize various service accommodations, it is considered that the flexibility and economic efficiency of the system are strongly required. For example, in mobile services, research for using PON as the backbone network of mobile networks is being discussed [9, 10, 11, 12]. Furthermore, for IoT / M2M services as well, architectures using PON have been proposed and are considered as one of the leading services [13, 14, 15]. In addition to system flexibility and economics, future access networks will also be required to ensure and improve the quality of accommodated services from the service perspective. Therefore, research has been conducted to improve quality for various services such as mobile communication, video or audio, and wireless LAN systems. [19, 20, 21].

As mentioned above, in future access networks, it will be required to flexibly provide various services while maintaining high quality based on the high-speed standard PON system. For these future access networks, this paper focuses on two research topics:

optical video distribution services and wireless LAN services.

1.2　Optical Video Distribution Service

One of the research scopes is the optical re-transmission service for broadcasting, which is an important source of income for telecommunications carriers as one of various services. There are two types of video distribution service provided in FTTH: video on demand (VOD) and broadcast [22]. The latter is further classified into Internet Protocol (IP) schemes and radio frequency (RF) schemes [23, 24]. The IP scheme sends video signals in the form of IP packets. In the RF scheme, multiple signals that are carrier modulated in the RF band are frequency multiplexed and then transmitted. Especially, in Japan, the RF scheme is widely used for optical re-transmission of broadcast signals by pass-through [15]. In the RF scheme, the same RF signal as the antenna reception is output from the subscriber's equipment. Therefore, the existing coaxial wiring in the premises or the home environment can be used. In addition, the RF scheme does not require a dedicated receiver such as a set top box (STB), and the television can be used directly as a receiver. Traditional optical re-transmission systems that use RF schemes are based on analog transmission of frequency division multiplexing (FDM) signals. Therefore, there are problems due to analog transmission. For example, in the most popular systems using subcarrier multiplexing (SCM), it is difficult to increase the transmission distance from the viewpoint of signal quality because the broadcast signal is transmitted by optical intensity modulation [26, 27]. Therefore, in order to accommodate a large number of subscribers, it is necessary to deploy a large number of re-transmission facilities near the user receiver.

There is also frequency modulation (FM) conversion scheme standardized by ITU-T J.185 [25, 28]. In the FM conversion scheme, the input FDM signal is directly converted

into a wideband FM signal. The high immunity to noise and distortion that are characteristic of FM signals allows for long-distance transmission in FM conversion scheme. However, the FM conversion scheme cannot be shared with digital communication network because it is difficult to electrically multiplex with other analog and digital signals. Therefore, communication carriers need to provide network equipment for video distribution in addition to network equipment for communication, which increases capital expenditure (CAPEX) and operating expense (OPEX).

For existing systems, we consider approaches to digitize signal and utilize shared communication network while preserving the coaxial interfaces at both ends of the network. Especially in a shared network, it is assumed that communication signals and broadcast signals are multiplexed in the time domain. Our approach utilizes a transmission technology called digitized radio-over-fiber (DRoF) [29, 30, 31]. DRoF is a technology that directly digitizes RF signals and transmits them via optical fiber. However, since the waveform information of the RF signal is digitized, the amount of data increases dramatically with respect to the original data. Therefore, the rate for optical transmission increases. To deal with such technical problems, the DRoF-based optical re-transmission system for digital transmission of broadcast signals and the signal compression method for efficient network sharing will be discussed in the following chapter.

1.3 Wireless LAN Service

There is a wireless LAN hotspot service as one of the commercial services via fixed optical broadband. Wireless LAN uses an unlicensed band and is one of the wireless standards that makes it easy to develop services [32, 33]. Therefore, the wireless LAN hotspot service is considered as one of the promising services. In recent years, various business providers including telecommunications carriers have provided services in

public facilities and commercial facilities.

Previously, wireless LAN services were mainly used for mobile offload, but they are changing to services that provide new added value [34]. In particular, commercial facilities such as cafes and malls tend to utilize wireless LAN services as an added value for commercial services. If there is a problem with the quality of the communication environment provided, customer satisfaction with the entire commercial service will be reduced [35, 36, 37].

With the current wireless LAN service, there are problems that it is difficult to provide services according to the location and control the network. For example, with existing systems, it is difficult to provide network connection to just the user equipment (UE) in a specific region within the wireless access area. In other words, it is difficult to limit the usage area based on location [38]. This means that there is a lack of flexibility in the provision of hotspot services. Network access restriction is generally achieved by distributing different passwords to the UEs to differentiate the target areas, but there is a concern that this will reduce usability [39].

Furthermore, in a high-density wireless LAN system that accommodates many UEs, deterioration of communication quality according to the distribution of UEs becomes a technical problem. In a situation where the user position distribution fluctuates with time, the communication quality also fluctuates. Therefore, various approaches have been proposed for such deterioration of communication quality. One approach is for each UE to make its own access point (AP) selection decisions depending on their state. Each UE calculates the optimal AP by itself and connects to the destination under its own initiative [40, 41]. The second approach is to collect network information from a central AP or controller and then determine the connection destination for each UE based on that

information. In this approach, network parameters including received signal strength indicator (RSSI) between UE and AP are used to determine the connection destination [42, 43]. However, in an environment where a large number of UEs and an extremely concentrated user distribution occur, it is difficult to perform fine-grained connection control, so an approach that considers the absolute UE position is also being considered. In order to improve the accuracy of UE position determination, one approach utilizes not only the radio waves themselves but also other media [44, 45]. By utilizing such position determination, it is possible to calculate the optimum connection destination. Unfortunately, this approach makes it necessary to modify UE hardware and software to add the functions needed.

Therefore, we focus on an approach that uses light waves as another medium. Light waves are defined as frequency resources above 3 THz and have abundant frequency resources [46]. Optical frequency resources are also known to be license-free. Due to its frequency characteristics, light is less diffracted than RF and has a strong straightness. In addition, visibility is one of the features in the wavelength range of visible light [46]. We consider an approach to apply this optical resource as a control plane for wireless LAN system. The wireless LAN service provision area is divided by small cells created by light, and the connection management and load balancing of UEs existing in the small cells are centrally controlled in small cell units. With such an approach, for example, it is possible to realize connection restrictions according to the area, and to improve quality deterioration due to fluctuations in the distribution of users by area-based connection control. In order to realize centralized control in small cell units, it is necessary to transmit connection information to the UE via the optical cell. In addition, to reduce the cost that is a barrier to introduction, a mechanism that realizes the transmission of connection

information is required without using dedicated transmission / reception hardware such as Light-Fidelity (Li-Fi) [47].

Therefore, in the following chapters, schemes for transmitting and receiving control information using smart lighting and the illuminance sensor provided in smartphones is discussed without relying on dedicated hardware. In addition, assuming a case where connection control is performed for each optical cell, an optical cell control scheme aimed at suppressing deterioration of communication quality due to fluctuations in the distribution of users is also discussed.

Chapter 2

Optical Video Re-Transmission of RF Broadcast Signals by Using Digitized Radio-over-Fiber

2.1 Introduction

As an optical re-transmission system for broadcast signals, a system using ITU-T J.186 is widely used [26]. This system is based on SCM. SCM is an optical transmission method in which carrier-modulated signals in the RF band are frequency-multiplexed and then transmitted to the subscriber side by optical intensity modulation.

Figure 2.1 shows the architecture for overlaying and providing optical re-transmission services in areas where PON-based communication services are widespread [26, 48, 49]. The communication network consists of an access network close to the subscriber side and a core/metro network, which is a long-distance relay network. On the other hand, the broadcast signal is received as a radio wave by the head-end antenna. The received signal is frequency-multiplexed in the head-end and then output. The output FDM signal is electrically input to the transmitter (Tx) of the re-transmission facility. In Tx, the FDM signal is light intensity modulated and output as an optical signal. The output optical signal is wavelength division multiplexed with the communication signal and then
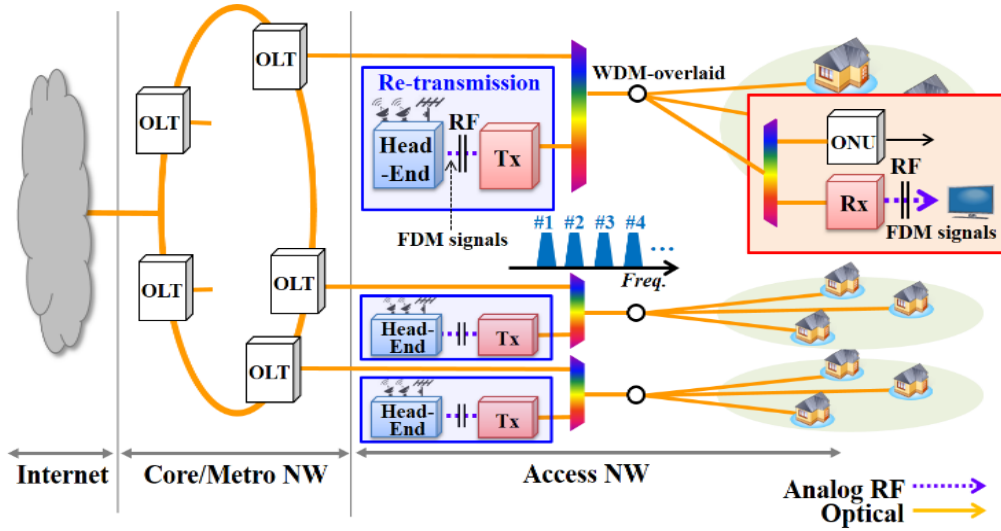
Fig. 2.1: Conventional optical re-transmission system using SCM scheme.

transmitted to the subscriber side. On the subscriber side, the wavelength division multiplexing (WDM) signal is separated into a communication signal and a broadcast signal via a WDM device. The communication signal is terminated by the ONU. On the other hand, the broadcast signal is received by the dedicated receiver (Rx) and converted from the optical signal to the same electrical signal as the radio signal received at the head-end. Finally, the signal is input to the television and viewed via demodulation processing.

A feature of such an SCM-based system is that it has coaxial interfaces at both ends of the optical re-transmission network. The electrical coaxial interface is an interface that is highly compatible with the hybrid fiber-coaxial (HFC) network of community antenna television (CATV) service operators [50]. Also, on the subscriber side, it is recognized as a fairly popular interface. There is an advantage that such an interface can be used.

However, the conventional system has a problem in terms of accommodating economical and efficient broadcasting services. As described above, in the SCM-based

system, analog transmission by optical intensity modulation is performed in the optical network. Therefore, the transmission distance in optical transmission is limited. Due to this transmission distance limitation, the retransmission facility must be deployed near the subscriber equipment. This means that if the system accommodates a large number of subscribers, a large number of re-transmission equipment must be deployed in the access network. This significantly increase CAPEX and OPEX in telecommunications carriers. Furthermore, in the SCM-based system, the communication signal and the broadcast signal are wavelength-multiplexed and transmitted in the access network. Since WDM equipment is generally expensive, this also leads to an increase in CAPEX and OPEX. In addition, it is necessary to deploy WDM equipment on the subscriber side as well, which leads to higher cost of service provision.

In this chapter, as opposed to conventional systems, we propose an optical re-transmission system that applies DRoF technology for shared networks. The proposed system is equipped with the same coaxial interfaces as the conventional system at both ends of the optical re-transmission network, and realizes the transmission of broadcast signals by the shared communication network. Section 2.2 describes the details of the proposed system and the signal processing configuration of the system. Next, we discuss the number of quantization bits in the transmitter to satisfy the quality of the required signal in the receiver through signal-to-noise ratio (SNR) analysis of the system. Section 2.3 discusses the technical challenges of DRoF-based systems, increasing transmission rates. In addition, a transmission rate reduction method for solving these problems will be described. Section 2.4 describes the results of implementing the transmission rate reduction method proposed for the DRoF-based system and evaluating the system by
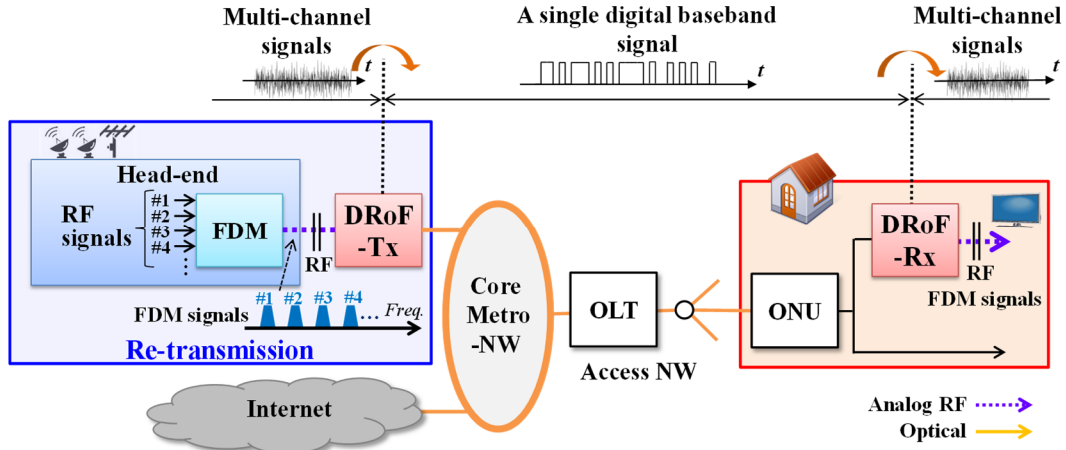
Fig. 2.2: Proposed DRoF-based optical video re-transmission system.

optical re-transmission experiments. Section 4 describes the results of system evaluation by optical re-transmission experiments. In the experiment, a commercial digital terrestrial broadcasting (DTT) signal of 9ch was used. The effect of the transmission rate reduction method is shown quantitatively.

2.2 Proposed Optical Re-Transmission System

2.2.1 DRoF-based Optical Re-Transmission System

For overcoming the problems of existing system, we propose a novel optical video re-transmission system based on DRoF technology [29, 30, 31]. Fig. 2.2 shows the proposed system and network architecture. In the head-end, the RF signals are received and frequency division multiplexed. Then, the multi-channel FDM signals are converted into a single digital baseband signal and optically transmitted via the core / metro network and access network by sharing the transmission capacity with regular communication signals. That is, the broadcast RF signal is time-division multiplexed with the communication signals. The customer premises DRoF-Rx re-converts the digital baseband signal into the

multi-channel RF signals, and outputs them via a coaxial cable.

By applying DRoF technology, RF signals are digitally transmitted across the core / metro network and access network while maintaining the conventional analog coaxial interfaces at both ends of the network.

This approach brings major advantages. By digitizing the signal transferred, Re-amplification, Re-timing and Re-shaping (3R) regenerators can be applied at each node [51]. 3R regeneration ensures the predetermined quality at both ends of the network. Therefore, CAPEX and OPEX can be drastically reduced since telecommunication carriers only need to arrange one re-transmission facility (i.e. head-end and DRoF-Tx) at the higher-layer node. The benefit of being aggregated on higher-layer node is that the number of expensive optical re-transmission facility including large-scale antennas, receiving equipment, and optical converters can be reduced. In a conventional system, it is necessary to deploy an optical re-transmission facility in an area close to the user side, which means that a large number of optical re-transmission facilities need to be deployed. Furthermore, since these optical re-transmission facilities require a large amount of costs for maintenance and operation including inspections, it is required to provide services with a small number of optical re-transmission facilities. On the other hand, in the core metro network, the optical re-transmission traffic flows by using the proposed system, so that the traffic increases. However, since the characteristic of the target signal is broadcast and most of it is common content, it is considered that the optical re-transmission credit traffic can be regarded as a relatively small scale traffic in the core metro network.

Having standard coaxial interfaces at both ends of the network allows CATV service operators to re-transmit video signals without reconstruction of network interfaces. Therefore, CATV service operators will be able to provide optical re-transmission
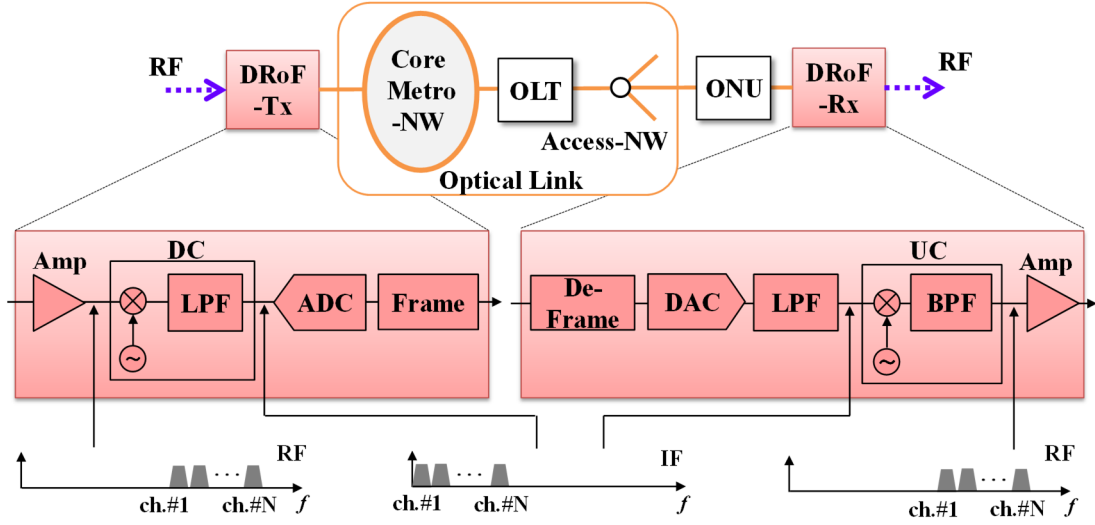
Fig. 2.3: Block diagram of signal processing for proposed system.

services for broadcast signals using optical networks (i.g. FTTH, Fiber-to-the Curve (FTTC), and Fiber-to-the Building (FTTB)) owned by telecommunications carriers.

2.2.2 Signal Processing of the Proposed System

Figure 2.3 shows signal processing configurations in DRoF-Tx and DRoF-Rx. RF signals are input to DRoF-Tx and amplified. To reduce the sampling frequency of the analog-to-digital (A/D) conversion, the amplified multi-channel FDM signals are collectively down-converted from RF to intermediate frequency (IF) with a mixer and a low-pass filter (LPF). In the analog-to-digital converter (ADC), the signals are A/D converted, and transmitted through an optical core/metro network and access network (i.e. Optical-Link) after framing processing (i.e. Frame) such as Ethernet.

The signal input to the DRoF-Rx is an electrical signal yielded by optical signal conversion at the ONU. The electrical signal is de-framed, and digital-to-analog (D/A) converted by the digital-to-analog converter (DAC). After D/A conversion, the signals are filtered by the LPF to cut the high-order harmonics generated by DAC sampling. The

multi-channel signal output from the LPF is up-converted from IF to RF using a mixer

and band-pass filter (BPF). The up-converted signal is amplified and finally output from

DRoF-Rx.

Table 2.1: SNR of system components.

System Component	SNR	SNR Equation		Abbreviation	
Amplifier	SNR_{Amp_Tx} [52]	SNR_{Amp_Tx} [dB] $= S_{Power\_Tx} - NF_{Tx} - 10\log_{10}(k_B BT)$	(2.1)	S_{Power_Tx}: S_{Power_Rx}: NF_{Tx}: NF_{Rx}: k_B: T: B:	Input Signal Power to Tx Amp [dBm] Input Signal Power to Rx Amp [dBm] Noise Figure of Tx Amp [dB] Noise Figure of Rx Amp [dB] Boltzmann Constant [JK^{-1}] Temperature [K] Total Bandwidth [Hz]
	SNR_{Amp_Rx} [52]	SNR_{Amp_Rx} [dB] $= S_{Power\_Rx} - NF_{Rx} - 10\log_{10}(k_B BT)$	(2.2)		
Down -Converter	SNR_{DC} [53]	SNR_{DC} [dB] $= -20\log_{10}(2\pi\sigma_{DC}f_{LO})$	(2.3)	σ_{DC_LO}: σ_{UC_LO}: f_{LO}:	Jitter of DC LO [sec] Jitter of UC LO [sec] Frequency of LO [Hz]
Up -Converter	SNR_{UC} [53]	SNR_{UC} [dB] $= -20\log_{10}(2\pi\sigma_{UC}f_{LO})$	(2.4)		
Quantization	$SNR_{Quantization}$ [54,55]	$SNR_{Quantization}$ [dB] $= 6.02n + 10\log_{10}3 - PAR$	(2.5)	n: PAR:	Quantization Bit Peak-to-Average Power Ratio [dB]
ADC	SNR_{ADC_Jitter} [56]	SNR_{ADC_jitter} [dB] $= -20\log_{10}(2\pi\sigma_{ADC}f_c)$	(2.6)	σ_{ADC}: σ_{DAC}: f_c:	Jitter of ADC [sec] Jitter of ADC [sec] Carrier Frequency [Hz]
DAC	SNR_{DAC_Jitter} [56]	SNR_{DAC_jitter} [dB] $= -20\log_{10}(2\pi\sigma_{DAC}f_c)$	(2.7)		
Optical-Link	$SNR_{Optical\_Link}$ [57]	$Signal\ Power = \dfrac{V_{max}^2\left[(2^n)^2 - 1\right]}{3\cdot(2^n)^2}$	(2.8)	$P_{Optical\_Link}$: V_{max}:	Bit Error Rate of Optical Link Maximum Voltage of the Sampled Signal [V]
		$Noise\ Power_{Optical\_Link} = \dfrac{4\cdot V_{max}^2\left[(2^n)^2 - 1\right]}{3\cdot(2^n)^2}P_{Optical\_Link}$	(2.9)		
		$SNR_{Optical\_Link} = \dfrac{Signal\ Power}{Noise\ Power_{Optical\_Link}}$	(2.10)		

Table 2.2: SNR Calculation Parameters.

Symbol	Quantity	Value
S_{Power_Tx} [dBm]	Input Signal Power to Tx Amp	-18.9
S_{Power_Rx} [dBm]	Input Signal Power to Rx Amp	-17.3
NF_{Tx} [dB]	Noise Figure of Tx Amp	6
NF_{Rx} [dB]	Noise Figure of Rx Amp	6
k_B [JK^{-1}]	Boltzmann Constant	1.38×10^{-23}
T [K]	Temperature	300
B [MHz]	Total Bandwidth	54
σ_{DC_LO} [ps]	Jitter of DC LO	0.2
σ_{UC_LO} [ps]	Jitter of UC LO	0.2
f_{LO} [MHz]	Frequency of LO	500
f_c [MHz]	Carrier Frequency	125
n	Quantization bit	3-18
PAR [dB]	Peak-to-Average Power Ratio	14.33
σ_{ADC} [ps]	Jitter of ADC	0.2
σ_{DAC} [ps]	Jitter of DAC	0.2
$P_{Optical\_Link}$	Bit Error Rate of Optical Link	1.0×10^{-10}

2.2.3 SNR analysis for proposed system

The signal quality is degraded by signal processing in DRoF-Tx and DRoF-Rx, and the

magnitude of the degradation depends on the DRoF-Tx and DRoF-Rx components. The

degradation can be theoretically analyzed.

Table 2.1 shows the SNR calculation formulas for DRoF-Tx and DRoF-Rx signal

processing operations; the optical-link amplifier generates amplifier noise due to noise

figure (NF) and thermal noise [52]. In down-conversion (DC) and up-conversion (UC),

the signal's SNR is degraded by jitter noise caused by the frequency fluctuation of the

local oscillator [53]. In the ADC, the SNR is degraded by quantization noise (dependent

on the quantization bit number (n)) and jitter noise caused by the frequency fluctuation
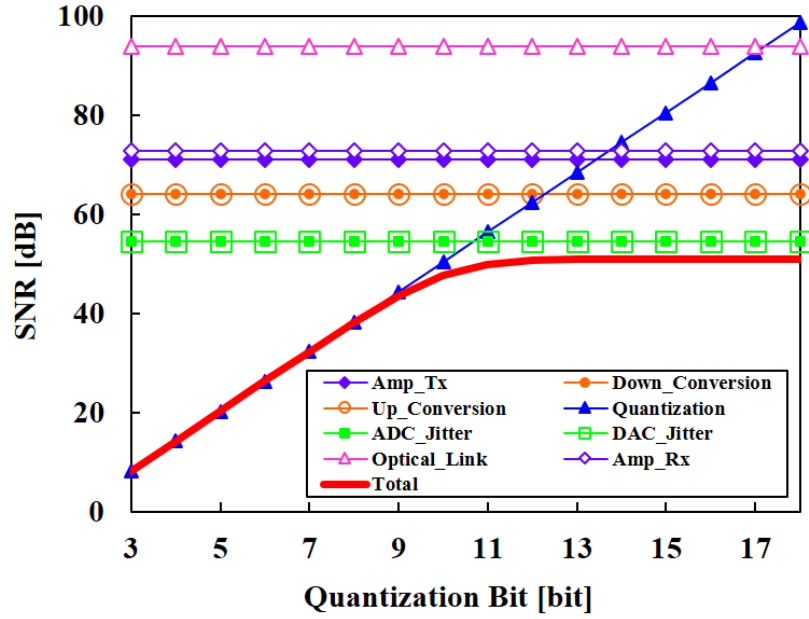
Fig. 2.4: Quantization bit dependency of the SNR.

of the sampling clock [54, 55, 56]. As in the ADC, the jitter noise caused by frequency fluctuation of the sampling clock of the DAC is a factor degrading the SNR [56]. In the Optical-Link, the SNR is degraded according to the bit error of the signal. Assuming Ethernet as the Optical-Link, the bit-error-ratio (BER) must be conformed to the standard. For example, in case of a gigabit ethernet-passive optical network (GE-PON) system, the BER requirement is 1.0×10^{-10} [58]. This value is defined in consideration of deterioration factors in the optical subsystem (e.g. driver and modulator nonlinearity, fiber dispersion and the square-law detection at the photo detector).

Using equations (2.1) to (2.10) in Table 2.1, the total SNR of the entire system (SNR_{Total}) is expressed by the following equation (2.11):

$$
\begin{aligned}
SNR_{Total}^{-1} = & \ SNR_{Amp\_Tx}^{-1} + SNR_{DC}^{-1} + SNR_{Quantization}^{-1} \\
& + SNR_{ADC\_Jitter}^{-1} + SNR_{Optical\_Link}^{-1} \\
& + SNR_{DAC\_Jitter}^{-1} + SNR_{UC}^{-1} + SNR_{Amp\_Rx}^{-1}.
\end{aligned}
\tag{2.11}
$$

19

Fig. 2.4 shows the SNR plots for the system components considering each degradation factor as determined by equations (2.1) to (2.10); the parameters used in the calculations are shown in Table 2.2. These parameters conform to generally accepted specifications. For S_{Power_Tx} and S_{Power_Rx}, values within the range of input and output powers defined by the regulations for broadcasting were used [59]. Some of the parameters represent the specifications of the equipment used in the experiments described later. The total channel number is set to nine, which is the maximum channel number of Japanese DTT signal. Fig. 2.4 plots the SNR_{Total} considering each degradation factor. From Fig. 2.4, when the quantization bit number is under 8, it is understood that the contribution of jitter noise in ADC/DAC and amplifier noise to the SNR_{Total} is negligible, and signal degradation due to ADC quantization is the dominant factor.

On a different note, when the input signal quality to DRoF-Tx (CNR_{Tx_Input}) and the output signal quality from DRoF-Rx (CNR_{Rx_Output}) are given, the required carrier-to-noise ratio (CNR) of the entire system including the Optical-Link ($CNR_{Required}$) is determined. Here, the relationship among $CNR_{Required}$, CNR_{Tx_Input} and CNR_{Rx_Output} is represented by equation (2.12):

$$CNR_{Required}^{-1} = CNR_{Rx\_Output}^{-1} - CNR_{Tx\_Input}^{-1}. \tag{2.12}$$

$CNR_{Required}$ can be easily converted into $SNR_{Required}$ by considering the channel interval and occupied bandwidth of the target signal. For example, in the case of the DTT signal, since the channel interval and occupied bandwidth are 6 MHz and 5.6 MHz, respectively, the conversion is written as equation (2.13):

$$SNR_{Required}\,[\text{dB}] = CNR_{Required}\,[\text{dB}] + 10\,log_{10}\,(5.6/6). \tag{2.13}$$

20
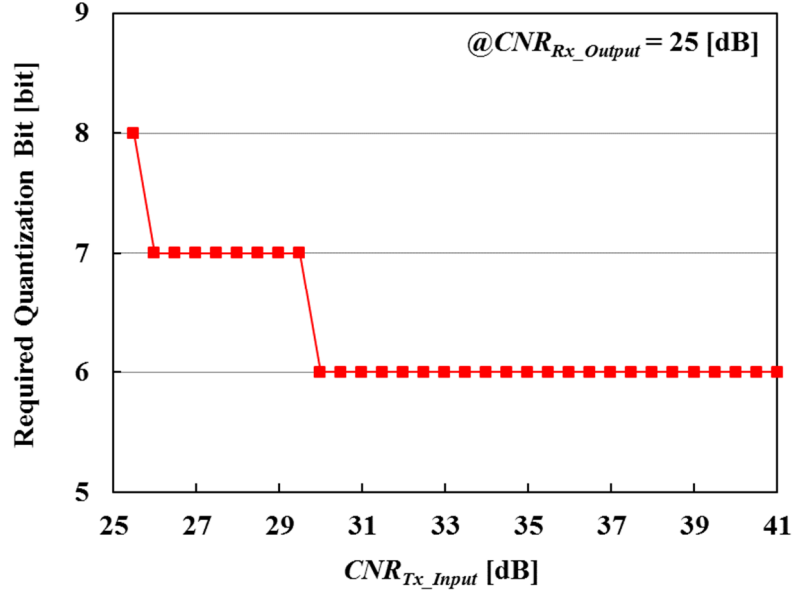
Fig. 2.5: CNR_{Tx_Input} dependency of required quantization bit analytically obtained. CNR_{Rx_Output} is set as the worst case of 25 dB which is defined by the broadcasting law.

By using the $SNR_{Required}$ expressed by equation (2.13) and SNR_{Total}, the required quantization bit for re-transmission at the ADC in DRoF-Tx is calculated as the minimum quantization bit number satisfying equation (2.14):

$$SNR_{Total}\ [\text{dB}] \geq SNR_{Required}\ [\text{dB}]. \tag{2.14}$$

Fig. 2.5 plots the relationship between CNR_{Tx_Input} and the required quantization bit number. Here, CNR_{Rx_Output} is set as the worst case of 25 dB as specified by broadcasting regulations [59]. As can be seen from Fig. 2.5, increasing CNR_{Tx_Input} mitigates $SNR_{Required}$ and thus the required quantization bit number. For example, at the worst input condition specified by broadcasting regulations, in which is CNR_{Tx_Input} = 27dB, the required quantization bit number is 7-bit from Fig. 2.5. In this way, the minimum quantization bit number at the DRoF-Tx ADC can be obtained analytically when using the proposed

21

system to re-transmit DTT signals. Fixing the quantization bit number determines the transmission rate in the optical network. Therefore, understanding the quantization bit number is critical for designing of optical networks.

While this paper uses a DTT signal in explaining the proposal, this system can be generically applied to other broadcast signals such as digital video broadcasting-terrestrial / terrestrial 2 (DVB-T / T2) and advanced television systems committee 2.0 / 3.0 (ATSC 2.0 / 3.0) [60, 61, 62]. For these signals as well, the quantization bit number (i.e. signal transmission rate) is analytically calculated by determining the signal quality of the input signal to DRoF-Tx and the output signal quality from DRoF-Rx.

2.3 Optical Transmission Rate Reduction

2.3.1 Optical Transmission Rate for DRoF-based System

The optical transmission rate of the proposed DRoF-based system is generally determined by the quantization bit number and the sampling frequency of the DRoF-Tx ADC. Quantization with high bit numbers and high sampling frequencies is preferred to maximize the SNR of the signal, but in an actual network, both parameters should suit the available network capacity. In particular, in the proposed system, since the signal is transmitted by TDM together with regular communication signals, the transmission rate of the rebroadcast RF signal needs to be as low as possible. When referring to the minimum quantization bit number (7-bit) calculated under the worst case scenario, CNR_{Tx_Input} is 27 dB, the transmission rate is calculated to be 0.875 Gbps by using the sampling frequency of 125 MHz. This sampling frequency is the value of the ADC used in the experimental study. This was decided as a value larger than the Nyquist frequency of the 9ch multiplexed DTT signals which have 54 MHz bandwidth. For example, when

realizing re-transmission by a GE-PON in the access network, by using the proposed

system, the rebroadcast RF signals occupy most of the network capacity [63]. That is, the

communication signals have scant resources. Therefore, it is necessary to further reduce

the transmission rate. On the other hand, in future PON systems, high-speed systems that

combine WDM and TDM have been standardized based on the improved transmission

rate per wavelength. In order to accommodate the optical re-transmission service of

broadcast signals while maintaining high bandwidth utilization efficiency in such future

PON systems, it is required to reduce the transmission rate of broadcast signals as much

as possible. In addition, as one of the purposes of this research, by verifying how much

the transmission rate can be reduced in an actual system, it will be possible to obtain the

prospect of bandwidth design required in the system in the future.

2.3.2 Optical Transmission Rate Reduction Technique

Transmission rate reduction is generally realized by reducing the quantization bit number

during A/D conversion. Fig. 2.6 describes the Block diagram of bit reduction processing

after 16-bit ADC. In Fig. 6 (a), bit reduction is realized by simply re-quantizing with a

quantization bit smaller than 16 bits. Fig. 2.6 (b) and (c) show a mu-law based

quantization process and a proposed improved nonlinear quantization (INL) process,

respectively. For example, in mobile common public radio interface (CPRI), Mu-law is

already being used for compression in the network between the base band unit (BBU) and

remote radio head (RRH) [64]. Implementation of the Mu-law method is, as shown in Fig.

2.6(b), realized by combining nonlinear transformation and linear quantization. As shown

in Fig. 2.6(b), an A/D converted signal with a sufficiently large quantization number such

as 16-bit is nonlinearly converted. Here, the 16-bit ADC in Fig. 2.6 represents the ADC

used in the experiment described later. The function used for nonlinear transformation is

(a) w/o

16-bit ADC

Bit Reduction Processing (Compressor)

n-bit Re-Quantizer

(b) w/ mu-law

16-bit ADC

Nonlinear Transformer

n-bit Re-Quantizer

(c) w/ INL

16-bit ADC

Clipper

Nonlinear Transformer
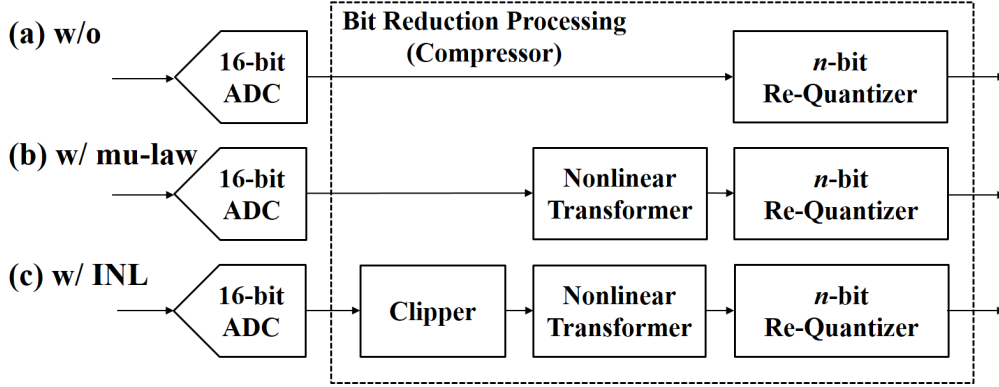
n-bit Re-Quantizer

Fig. 2.6: Block diagram of bit reduction processing. Only the basic re-quantization process is performed by (a). (b) and (C) represent the processing in the case of using Mu-law and INL, respectively.

written as:

$$u = A_{max} sgn(s) \log\left(1 + \beta|s|/A_{max}\right)/\log(1 + \beta),$$

$$(2.15)$$

$$\left[-A_{max} \leq s \leq A_{max}\right]$$

where β and s are the nonlinear parameters determining the nonlinearity of the function and the input signal, respectively. A_{max} is the maximum peak amplitude of s. After nonlinear transformation, the signal is re-quantized with n-bit quantization in which $n <$ 16. This nonlinear transformation allows the quantization interval to be controlled according to the probability distribution of the instantaneous voltage of the signal. For example, when the probability distribution of the instantaneous voltage of the signal is a Gaussian distribution, the amplitude center is quantized densely and the region away from the center is quantized sparsely. This improves *SNR* compared with uniform quantization shown in Fig. 2.6(a); as a result, quantization bit number can be reduced. By using this Mu-law, quantization error in the region where the probability distribution of the

instantaneous voltage is large can be reduced. However, to further reduce the quantization

error, quantization bits must be allocated to regions where the probability distribution of

the instantaneous voltage is extremely small.

In order to obtain stronger compression than the Mu-law method, we propose the INL

method; it performs nonlinear quantization after clipping the amplitudes of regions that

small probability distribution of instantaneous voltage. Fig. 2.6(c) shows the signal

processing proposed.

The 16-bit A/D converted signal is clipped to reduce the peak-to-average power ratio

(PAPR) of the signal. The clipping depth, expressed as clipping ratio, R_{clip}, is given by the

following equation:

$$R_{clip}\,[\mathrm{dB}] = 20\log_{10}\left(A_{clip}\,/\,\sigma_{RMS}\right),\tag{2.16}$$

where A_{clip} and σ_{RMS} are the clipped amplitude and the root mean square of the signal

amplitude, respectively. Representing the input/output signal to/from the clipping

processing block by $s(t)$ and $s_{clip}(t)$ yields equation (2.17):

$$S_{clip}\,(t) = \begin{cases} s(t) & \text{for } s(t) \le A_{clip} \\ A_{clip} & \text{for } s(t) > A_{clip}\,. \end{cases}\tag{2.17}$$

Nonlinearly transformed signal u' after clipping is given by equation (2.18):

$$u' = \sigma_{RMS}\cdot 10^{\,R_{clip}\,/20}\cdot sgn\left(s_{clip}\right)$$
$$\cdot\log\left\{1+\beta\left|s_{clip}\right|\Big/\left(\sigma_{RMS}\cdot 10^{\,R_{clip}\,/20}\right)\right\}\Big/\log\left(1+\beta\right).\tag{2.18}$$

$$\left[-\sigma_{RMS}\cdot 10^{\,R_{clip}\,/20} \le s_{clip} \le \sigma_{RMS}\cdot 10^{\,R_{clip}\,/20}\right]$$

The transformed signal is re-quantized with quantization interval Δq given by Equation

(2.19):
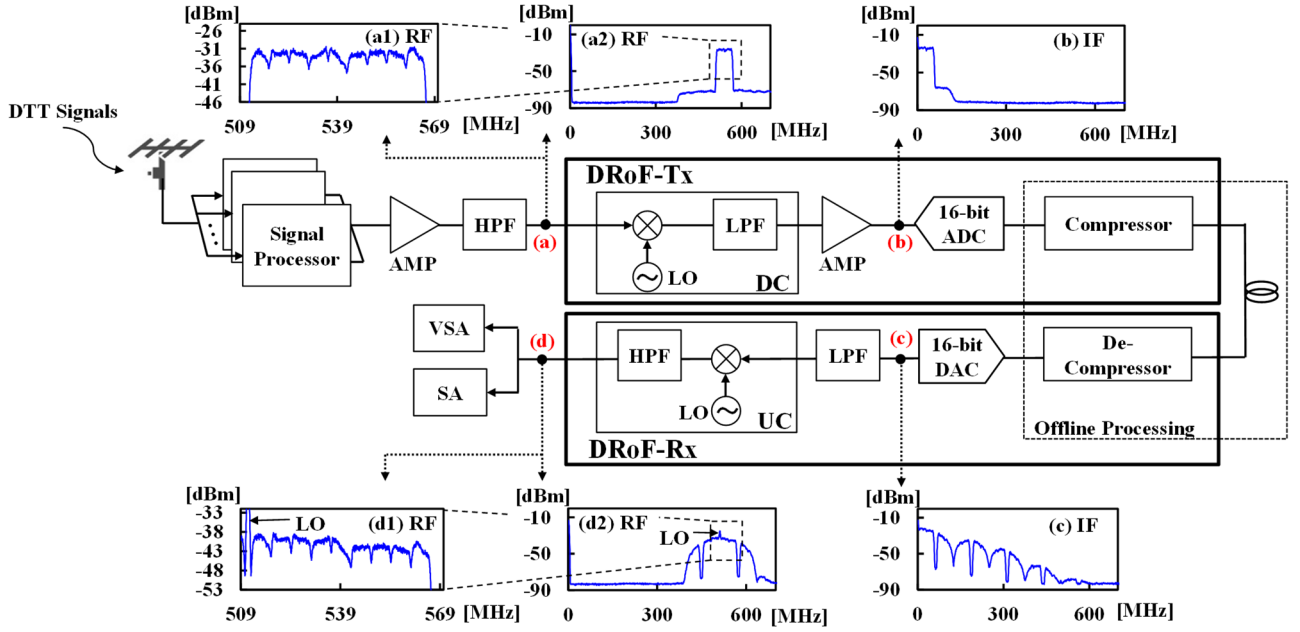
Fig. 2.7: Experimental setup for re-transmission of actual broadcasting signals. Insets show the spectrum of the 9 ch multiplexed DTT signals which are proved at the point of (a), (b), (c) and (d). At the compressor, the bit reduction processing expressed in Fig. 2.6 are performed.

$$\Delta q = \left(2\sigma_{RMS} \cdot 10^{R_{clip}/20}\right)\Big/\left(2^n - 1\right) , \qquad (2.19)$$

where *n* is the re-quantization bit number in each bit reduction part.

2.4   Evaluation

2.4.1 Experimental Setup

Figure 2.7 show that the experimental setup used to confirm the performance of the proposed system. Actual 9 ch DTT signals were received by an antenna, and the level of the signals were adjusted by individual signal processors. The controlled signals were amplified and filtered by a high pass filter (HPF) to eliminate the amplifier's out-of-band noise. The RF spectra of the signals at point (a) shown in Fig. 2.7(a1) and (a2), have some undulations. The DTT signals comply with integrated services digital broadcasting-

terrestrial (ISDB-T) mode 3, and so use orthogonal frequency division multiplexing (OFDM) with 5617 subcarriers having 64-quadrature amplitude modulation (QAM) using 5.6 MHz [65]. Here, convolutional coding (3/4) and reed-solomon coding (204,188) are used for inner and outer coding, respectively. The center frequencies of the 9 channels were allocated from 512.142 to 566.142 MHz at 6 MHz intervals. The input DTT signals were down-converted to IF ranging from 1 to 55 MHz with a local oscillator and filtered to eliminate the image components. The converted DTT signals were amplified, and passed through the ADC with 16-bit resolution yielding the spectrum shown in Fig. 2.7(b). ADC sampling frequency was 125 MHz. The digitized ADC output was off-line processed for Mu-law and INL with the compressor shown in Fig. 2.6 to reduce the transmission rate. After n-bit quantization at the re-quantizer, the signals were output by DRoF-Tx. The input signals to the de-compressor in DRoF-Rx were off-line processed for nonlinear inverse transformation. De-compressor output was input to a DAC, having sampling rate of 125 MHz and 16-bit resolution. The spectra of the DAC output signals, shown in Fig. 2.7(c), display both zero-order hold and image components caused by 125 MHz sampling. After LPF processing to eliminate the image components, the DTT signals were up-converted from IF to RF at up-convertor (UC) composed of LO and HPF, and finally output. Fig. 2.7(d1) and (d2) show spectra of the DRoF-Rx output signals, these signals were reallocated from 512.142 to 566.142 MHz.

The constellation diagrams were measured by a vector signal analyzer (VSA). The carrier-to-noise ratio (CNR) of the output signals was also measured by an ISDB-T video signal analyzer (SA).

2.4.2 Parameter Determination

In our INL transmission rate reduction method, there are two key parameters: R_{clip} and β.
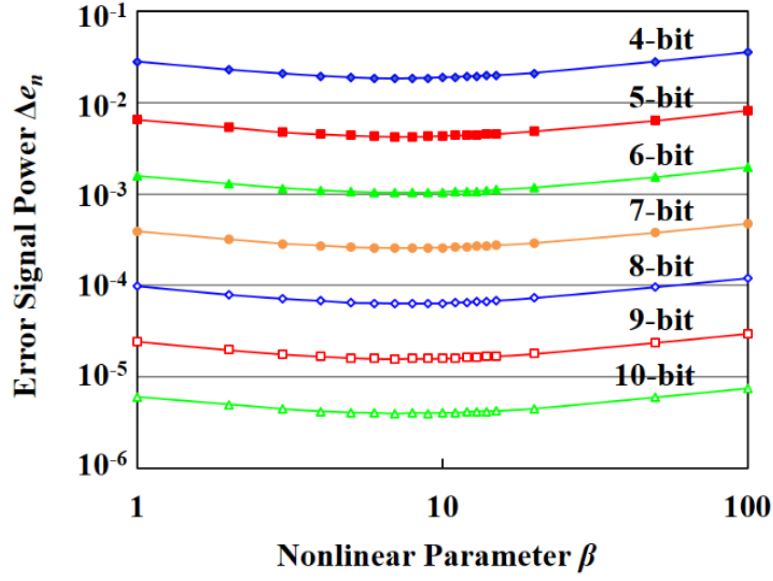
Fig. 2.8: The parameter optimization results for Mu-law. Nonlinear Parameter β dependency of Error signal power Δe_n . The 9ch DTT signal was re-quantized with $n = 4$ to 10 bit.

Since the probability distribution of the instantaneous voltage of the signal varies with R_{clip}, the optimal β also changes. The optimum parameters for Mu-law could not be used with INL, so different β and R_{clip} values were required.   In the optimization process, input signal to compressor, $s(t)$, and output signal from de-compressor, $s_n'(t, R_{clip}, \beta)$, are compared, and difference signal, Δs_n, was evaluated. By using Δs_n, the error signal power, Δe_n, defined by equation (2.20) can be evaluated.

$$\Delta e_n \left(R_{clip} , \beta \right) = \sum_{k=0}^{k=N} \Delta s_n^{\,2} \Big/ N \,, \tag{2.20}$$

where N is the total sampling number. The optimal parameters that minimize Δe_n can be evaluated by using equation (2.21):

$$^{\forall}\beta > 0, \; ^{\forall}R_{clip} > 0, \; minimize \; \left\{ \Delta e_n \left(R_{clip} , \beta \right) \right\}. \tag{2.21}$$
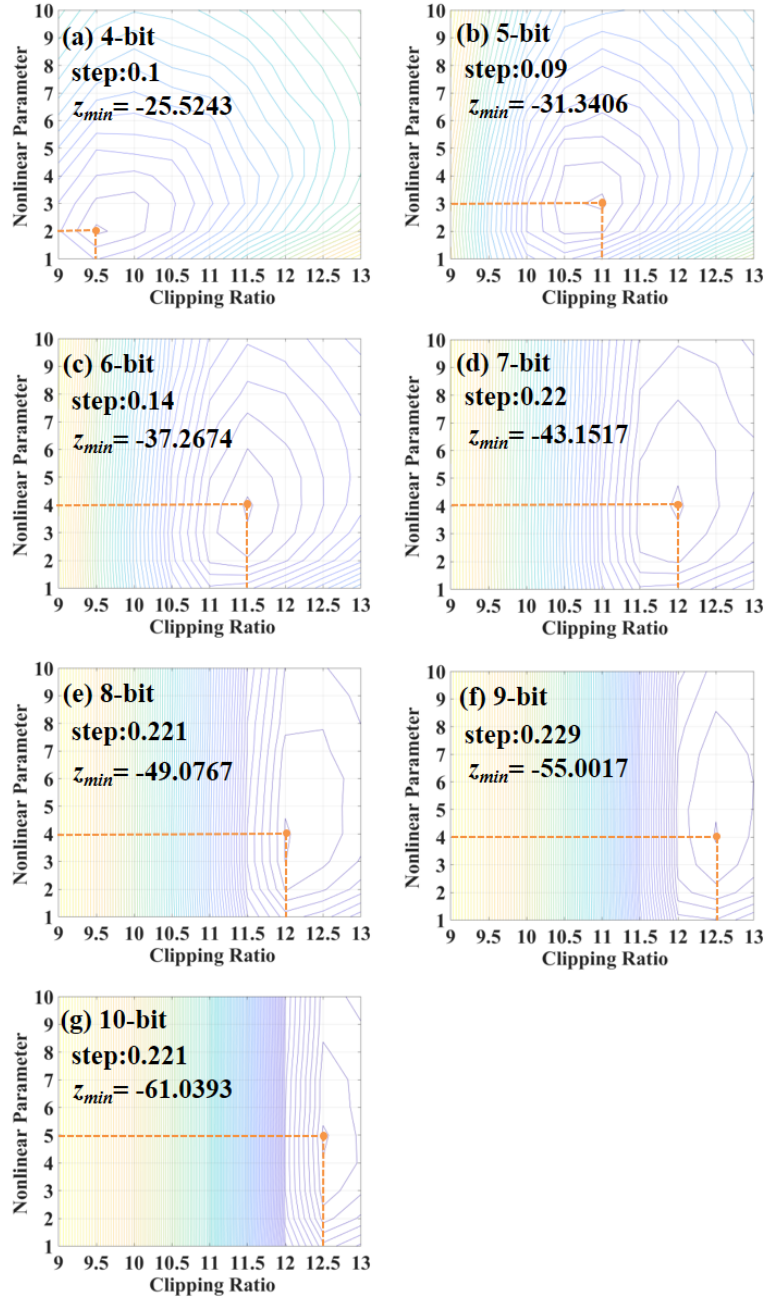
Fig. 2.9: The optimization results for INL. A plot of contours to optimize nonlinear parameter and clipping ratio. The z values in the combination of the parameters of nonlinear parameter and clipping ratio are plotted. The step indicates the interval between contour lines. z_{min} represents the minimum value of z.

Here, R_{clip} and β are optimized for each n. Fig. 8 shows the parameter optimization results for Mu-law by plotting the error signal power dependence on β for $n = 4$ to 10. As can

be seen from Fig. 2.8, for Mu-law, the optimum value was obtained at just $\beta = 7$ for n

values of 4, 5, 6, 7, 8, 9, 10. On the other hand, the optimization results for INL are shown

in Fig. 2.9. Fig. 2.9 shows the contour lines that plot the z value defined as,

$$z = 10 \log \left\{ \Delta e_n \left(R_{clip}, \beta \right) \right\}. \tag{2.22}$$

R_{clip} is shown on the horizontal axis and β is shown on the vertical axis. From these figures,

the combination of R_{clip} and β that minimizes Δe_n can be extracted. As a result, Δe_n was

minimized under the condition at (R_{clip}, β) = (9.5, 2), (11, 3), (11.5, 4), (12, 4), (12, 4),

(12.5, 4), (12.5, 5) for n = 4, 5, 6, 7, 8, 9, 10, respectively.

2.4.3 Results of Re-Transmission Experiment of Actual DTT Signals

The first re-transmission experiment examined the required quantization bit when neither

Mu-law nor proposed INL was applied. That is, the compressor of Fig. 2.7 implemented

only the n-bit re-quantizer shown in Fig. 2.6(a). In order to determine the minimum

quantization bit satisfying the requirement, the output signal from DRoF-Rx was captured

and its CNR was evaluated. Fig. 2.10 shows the channel #N dependency of the output

CNR from DRoF-Rx. Here, the dashed line shows the required CNR value which defined

by regulations for broadcasting [59]. Tx-Input indicates the input CNR to DRoF-Tx, that

is, CNR_{Tx_Input}. Each channel had a different CNR_{Tx_Input}. This is due to deterioration in the

radio wave section. CNR deteriorates as the quantization bit decreases. From Fig. 2.10,

since the CNR_{Tx_Input} of all channels other than ch. #9 exceeded 30 dB, the CNR

requirement is satisfied with 6-bit quantization. To fully satisfy the requirement, 7-bit

quantization is required. These results are consistent with the theoretical results shown in

Fig. 2.5. Therefore, it can be seen that the required quantization bit number for all
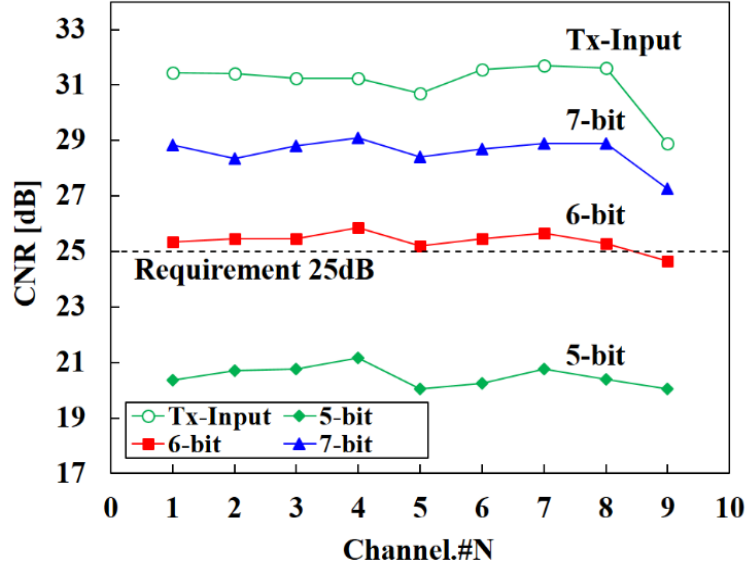
Fig. 2.10: The channel #N dependency of output CNR from DRoF-Rx. The legend indicates the case of re-quantization with 5-bit, 6-bit and 7-bit at the *n*-bit re-quantizer. The Input indicates the CNR of the input signal to DRoF-Tx. The dashed line shows 25 dB which is the required condition of CNR.

channels is 7-bit.

Fig. 2.11 plots DRoF-Rx output CNR versus quantization bit (*n*) at the re-quantizer. Channel #9, which demonstrated the worst performance in Fig. 2.8, was measured. The dashed line shows the required CNR [59]. By applying Mu-law, CNR is improved, which reduces the required minimum quantization bit number. As can be seen from Fig. 2.11, transmission with 6-bit is possible with Mu-law. On the other hand, INL, our proposed method, improves CNR significantly. The improvement in CNR at 5-bit is 6.2 dB.

Fig. 2.12 shows the constellation diagrams for 5-bit quantization in channel #9. It can be understood that the signal quality is clearly improved by the proposed INL. Overall, these results indicate that our INL proposal offers a 2-bit reduction in quantization bit number compared with the case of using just the re-quantizer.
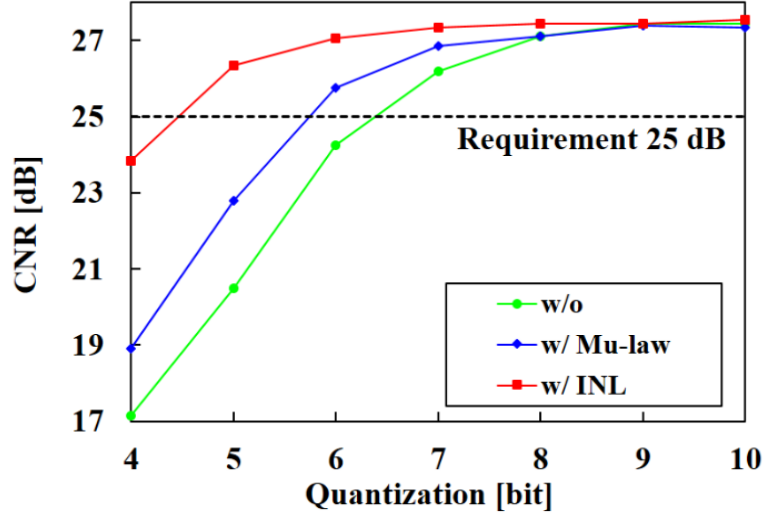
Fig. 2.11: Quantization bit dependency of CNR with Mu-law and INL method. The dashed line indicates CNR requirement. Channel #9 is measured.

(a) w/o   (b) w/ Mu-law   (c) w/ INL
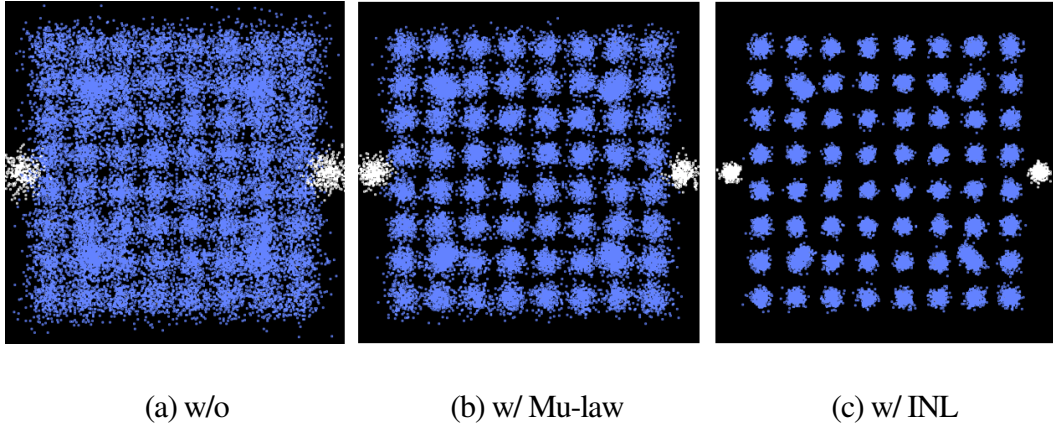
Fig. 2.12. The constellation diagram of the signal. Channel #9 is measured. (a) shows the case of w/o bit reduction method and 5-bit quantization, (b) shows the case of Mu-law and 5-bit quantization, and (c) shows the case of INL and 5-bit quantization.

2.4.4 Transmission Rate Reduction Effect

Furthermore, the measured transmission rate reductions achieved by the three methods is shown in Fig. 2.13. Without using the bit reduction method, the minimum quantization number capable of transmitting a 9-channel multiplexed DTT signal was 7-bit, and its
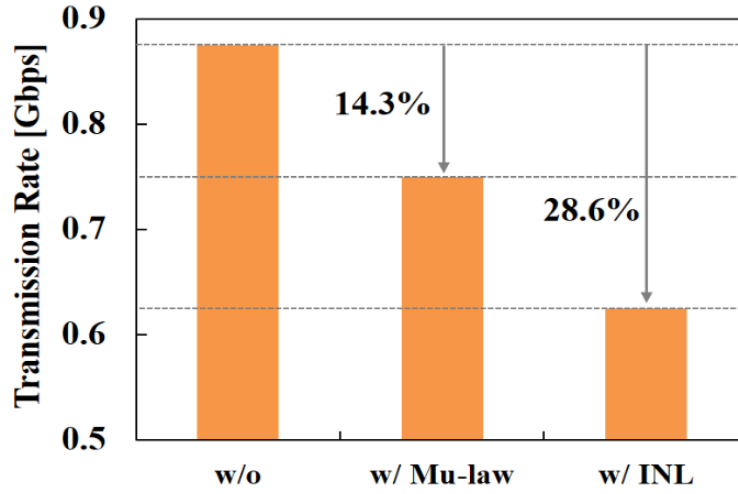
Fig. 2.13: Transmission rate reduction effect with bit reduction. The w/o indicates the case of 7-bit quantization without bit reduction method. w/ Mu-law and w/ INL is the case of 6-bit and 5-bit, respectively.

transmission rate was 0.875 Gbps. By using Mu-law, 1-bit quantization bit reduction was obtained. This represents a transmission rate reduction of 14.3 %.

On the other hand, by using INL, we achieved further reduction of 2-bit from the minimum quantization number 7-bit. This means that we achieved a reduction of 28.6% which is larger than using existing mu-law. As a result, by using the INL, it is possible to transmit a 9-channel multiplexed DTT signal at a transmission rate of 0.625 Gbps.

For example, assuming a GE-PON used in an existing access network, when the quantization bit reduction method is not applied, most of the transmission rate occupied by the broadcast signal. However, our results mean that the transmission rate of the communication signal is secured according to the 28.6% transmission rate elimination effect obtained by the reduction of the quantization bits.

These results confirm that the proposals will yield practical RF broadcasting video re-transmission systems.

2.5   Summary

In this chapter, we have proposed DRoF-based optical video re-transmission system that realizes digital transmission via the regular optical network while maintaining the existing RF interface at the both ends of the network.   Experiments demonstrated optical re-transmission of actual 9 ch multiplexed commercial DTT signals. Both theoretical and experimental results clarified that optical re-transmission can be realized with 7-bit quantization while satisfying the technical requirements. To improve the practicality of the proposed system, we also proposed an enhanced INL method to reduce the quantization bit number needed for ADC and showed that a 2-bit reduction was possible (7-bit to 5-bit). By reducing the minimum quantization bit of the proposed scheme, the transmission rate was reduced by 28.6%. This means that a 9 ch multiplexed DTT signal can be re-transmitted at 0.625 Gbps. These results show that re-transmission of DTT signals is practical in the current PON system.

Chapter 3

Optical Video Re-Transmission System for Rain Attenuated Satellite Broadcast Signals

3.1 Introduction

Broadcasting services in Japan include broadcasting satellite (BS) / communication satellite (CS) in the super-high frequency (SHF) band in addition to DTT in the ultra-high frequency (UHF) band. The BS / CS service realizes 2K / 4K broadcasting by using right/left-hand circularly polarized waves [66]. In particular, in Japan, 4K/8K ultra-high definition (UHD) BS/CS broadcasting services has been underway since 2018 and is currently in the process of spreading [67]. These BS/CS signals are received via satellite channels at RF band from 11 GHz to 12 GHz band as shown in Fig.3.1 [67, 68]. For
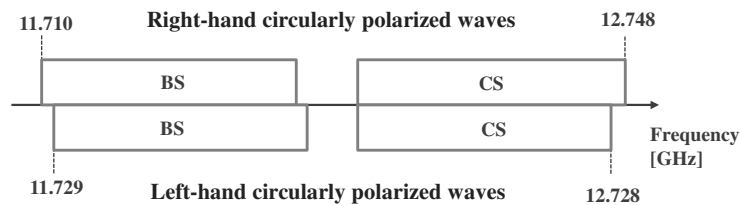
Fig. 3.1: Details of RF band in satellite broadcasting service.

Fig. 3.2: Details of IF band in satellite broadcasting service

example, in the satellite broadcasting service, instead of inputting this RF signal to the TV receiver, the signal down-converted from 1GHz to the 3 GHz band (i.e. IF band) as shown in Fig. 3.2 is input to the TV receiver [68]. Similarly, in the optical re-transmission of BS/CS signals, the down-converted signal to the intermediate frequency band is optically distributed to the subscriber side. Therefore, a higher frequency band is used in the wireless section compared with DTT.

In general, the attenuation in the wireless section due to weather conditions can be significant depending on the frequency band [69]. UHD BS/CS using the 12 GHz band has a larger attenuation than DTT. Therefore, CNR, which is an important quality index of the signal received at the head-end, fluctuates depending on the weather conditions. When the CNR of received signal changes, the acceptable CNR margin in the network section also changes. Since there is a trade-off between the signal compression ratio and the signal quality at the network, it is necessary to relax the compression ratio by assuming the worst case of the received signal at the head-end in order to satisfy the required CNR at the receiver. Our previous system simply assumed the fixed case of the received signal CNR at the head-end and assigned a fixed compression parameter at the DRoF-Tx.

The proposed system described in Chapter 2 is highly effective when the fluctuation of

the antenna reception CNR is relatively small, such as DTT. Therefore, assuming a fixed case of the received signal CNR at the head-end, we assigned the fixed compression parameter with DRoF-Tx. In this chapter, we discuss the system configuration for more efficiently and economically accommodating the optical video re-transmission service assuming BS / CS broadcast signals. To reduce the transmission rate of optical re-transmission of BS / CS broadcast signals as much as possible in the face of fluctuations in CNR due to rain attenuation, we propose a DRoF-based adaptive optical re-transmission system based on combination compression. The proposed system reduces the transmission rate for more broadcast signals by dynamically assigning compression parameters that take into account actual fluctuations in the input CNR to the DRoF-Tx due to rainfall attenuation. As a result, PON sharing in the time domain by the communication signal and the broadcast signal is realized.

Section 3.2 describes the detailed configuration of the proposed system and adaptive transmission rate reduction method. Section 3.3 describes modeling the antenna received signal at the head-end for detailed level design in the proposed system. Section 3.4 describes the experimental system evaluation results. The DRoF-Tx input CNR is calculated from the head-end input CNR modeled in Section 3.3. Experiments evaluate the proposed adaptive rate reduction effect for the input CNR to the DRoF-Tx. Finally, by using the prediction model of ITU-R P.618-13, the adaptive rate reduction effect on the service operating time is evaluated [70].
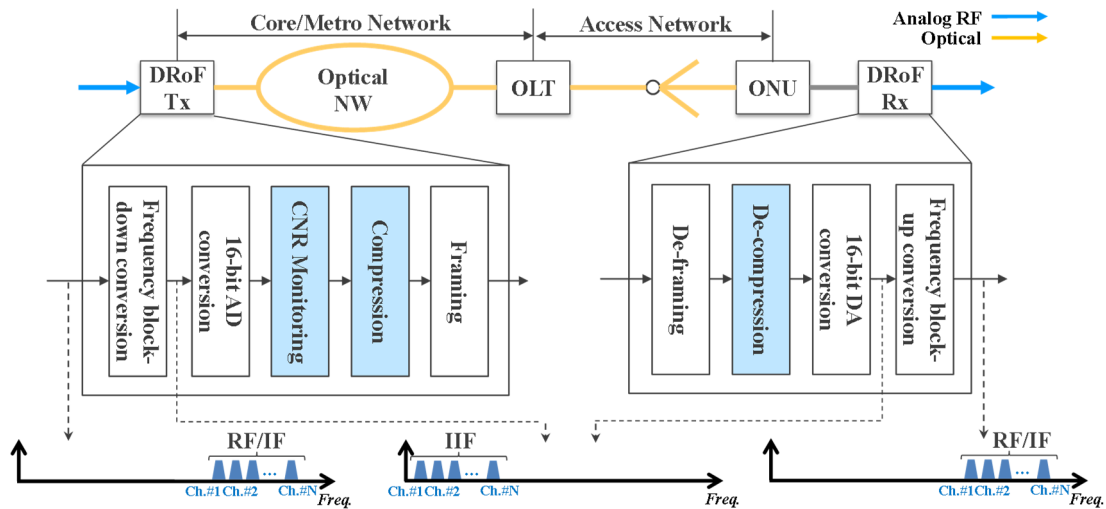
Fig. 3.3: Processing scheme in the proposed DRoF-based adaptive optical video re-transmission system.

3.2 Proposed Adaptive Optical Video Re-Transmission System

3.2.1 DRoF-based Adaptive Optical Video Re-Transmission System

Our adaptive optical video re-transmission system offers coexistence with communication systems. Our proposal changes the compression rate applied in RF/IF signal processing to suit the input CNR in order to minimize, as much as possible, the transmission rate decreases of the communication system. Figure 3.3 shows the processing flow of the proposed system. The proposed system deploys DRoF-Tx and DRoF-Rx at both ends of the network. Frequency multiplexed multi-channel RF / IF broadcast signals are input to DRoF-Tx. The RF / IF signal is block down-converted to the internal intermediate frequency (IIF). The frequency-converted signal is input to a 16-bit ADC, and is quantized for processing in the digital domain. After A/D conversion, the
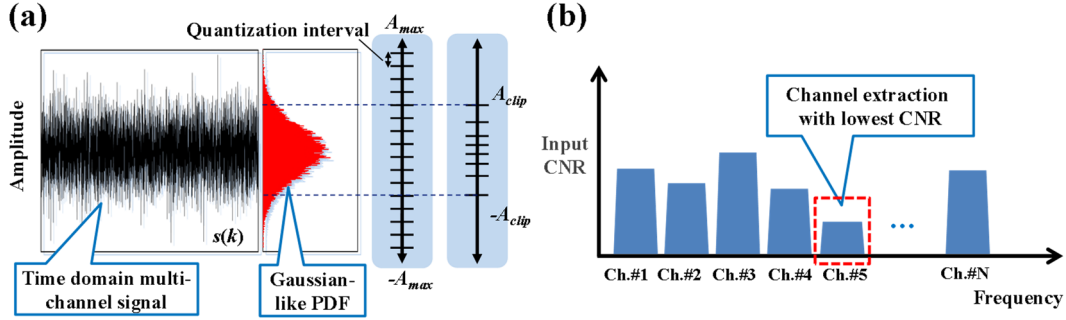
Fig. 3.4: Graphical understanding of signal processing in compression schemes. (a) is the graphical description of a schema that selects the channel with the lowest CNR from the input channels. (b) is the graphical description of compression process combining signal clipping and nonlinear transformation.

CNR of the quantized signal is monitored to detect the channel with the lowest CNR. The compression parameters are determined according to the channel with the lowest CNR. Signal compression is performed in the time domain based on the determined compression parameters. Details of compression scheme are described later. After the compressed signal is framed, it is transmitted through the optical network composed of core/metro network and access network. In the access network, the signal is transmitted through a PON consisting of an OLT and ONUs. At the receiver side, the electrical signal output from the ONU is input to the DRoF-Rx, where it is de-framed and de-compressed. The de-compressed signal is D/A converted by a high bit DAC. Since the bandwidth of the signal output from the DAC is IIF, it is collectively frequency converted from IIF to RF / IF. The frequency converted multi-channel RF / IF signals are output from the DRoF-Rx.

As described above, the existing communication networks are utilized, and the multi-channel broadcasting signals are optically re-transmitted.
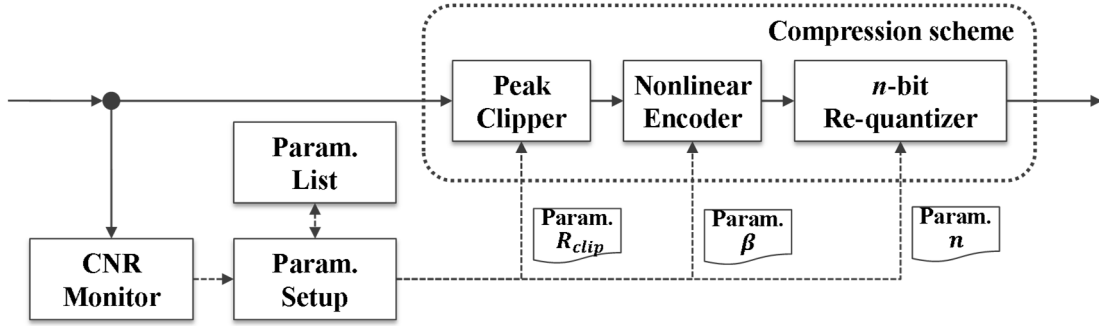
Fig. 3.5: Signal processing details of the compression scheme.

3.2.2 Adaptive Signal Compression Scheme

The DRoF-Rx in our system is deployed at the subscriber side. From the perspective of cost, the devices deployed must be implemented as simply as possible. In addition, in order to realize network sharing while assuring the transmission bandwidth of communication signals, a method that can achieve a high compression rate is required. Therefore, we utilize the simple and highly effective nonlinear compression scheme discussed in Chapter 2, which combines signal peak clipping and nonlinear transformation in the time domain.

Figure 3.4(a) visualizes the compression scheme. The time waveform of the multiplexed multi-channel RF / IF signal has a Gaussian-like probability distribution density. Therefore, our proposal first clips the less informative amplitude part away from the center. Next, we reduce the quantization error of the signal by nonlinear quantization according to the amplitude distribution of the clipped signal. The CNR margin obtained by reducing the quantization error is used to reduce the quantization number. The dotted line in Fig. 3.5 shows the signal processing flow of the compression scheme. It consists of Peak Clipper, Nonlinear Encoder, and n-bit Re-quantizer. First, the Peak Clipper clips the time domain signal at a certain clipping depth. The following equation shows input

signal s(k) clipped at the clipping amplitude of A_{clip}.

$$s_{clip}(k) = \begin{cases} s(k) & for \ |s(k)| < A_{clip} \\ A_{clip} & for \ |s(k)| \geq A_{clip} \end{cases} \tag{3.1}$$

where s_{clip} is the clipped signal and k is the k-th sample. Also, the clipping depth R_{clip} is defined as the backoff from the root mean square (RMS) value of the signal by the following equation.

$$R_{clip} = 20 \log_{10} \left(\frac{A_{clip}}{\sigma_{RMS}} \right) \tag{3.2}$$

Here, σ_{RMS} represents the RMS value of the signal. While clipping the signal reduces the quantization interval, clipping noise increases with clipping depth. As a result, the CNR of the signal is degraded. Therefore, peak clipping at the optimal clipping depth is required. In the Nonlinear Encoder, the clipped signal is nonlinearly transformed by the following equation.

$$u = A_{clip} sgn(s_{clip}) \frac{log(1 + \beta|s_{clip}|/A_{clip})}{log(1 + \beta)} \tag{3.3}$$

where u is the nonlinear transformed signal and β represents a nonlinear parameter. This nonlinear parameter adjusts the nonlinearity of the signal. The n-bit Re-quantizer re-quantizes the transformed signal by n-bit by subtracting the quantization bit number from 16-bits. This combination of signal clipping, nonlinear transformation, and re-quantization, offers effective and significant reductions in the transmission rate.

It is obvious that setting the optimal compression parameters is critical in achieving high compression ratios while suppressing signal CNR degradation. There is a trade-off between the compression ratio of the transmission rate and the degradation of the signal CNR. In other words, increasing the compression ratio degrades the signal CNR. In addition, the input CNR to DRoF-Tx varies depending on weather conditions. Therefore,

depending on the input CNR, it is necessary to determine the compression parameters that yield acceptable compression ratios. In our proposal, the compression parameters are dynamically assigned to the Peak Clipper, Nonlinear Encoder, and n-bit Re-quantizer of the compression scheme as shown in Fig. 3.5. As shown in Fig. 3.4(b), the input signal has different CNR for each channel. Therefore, the CNR of each channel is monitored. The channel with the lowest CNR is extracted by monitoring, and Param.Setup determines the compression parameters according to that channel. Here, the compression parameters are determined in advance and listed in Param.List; they are referenced regularly. Clipping depth R_{clip}, nonlinear parameter β, and re-quantization bit n are assigned to the Peak Clipper, Nonlinear Encoder, and n-bit Re-quantizer, respectively. Signal compression is performed using these parameters.

3.3 System Level Design Assuming Rainfall Attenuation

Channel state fluctuations in satellite broadcasting are a significant determiner of the CNR of the signal input to the DRoF-Tx. The main cause of the decrease in CNR is rainfall [71]. At frequencies above 10 GHz, rainfall attenuation often results in lower CNR. Therefore, we calculated the signal CNR received at the antenna site on the ground via the satellite channel and modeled the CNR of the DRoF-Tx input. First, to permit statistical analysis, the rainfall attenuation was calculated using the rainfall attenuation prediction model of ITU-R P. 618-13 [70], and used to calculate the DRoF-Tx input CNR. In calculating the rainfall attenuation, the prediction model shown in ITU-R P. 618-13 was used. With this model, the rainfall attenuation for some percentage of time p is calculated by inputting the point rainfall rate for the location for 0.01 % of an average

Table 3.1: Parameters used in rainfall attenuation analysis.

Parameters	Abbreviation	Set value
Point rainfall rate for the location for 0.01 % of an average year [mm/h]	$R_{0.01}$	69
Height above mean sea level of the earth station [km]	h_s	0.03
Elevation angle [degrees]	θ	46
Latitude of the earth station [degrees]	φ	35.64
The predicted attenuation exceeded for 0.01% of an average year	$A_{0.01}$	10.31
Frequency [GHz]	f	12.130

year. Rainfall attenuation A_p with percentage of time p is expressed by the following equation.

$$A_p = A_{0.01} \left(\frac{p}{0.01} \right)^{-\left(\frac{0.655 + 0.033 \ln(p)}{-0.045 \ln(A_{0.01}) - \beta(1-p)\sin\theta} \right)} \tag{3.4}$$

Here, β is expressed by the following equation.

$$\beta = -0.005(|\varphi| - 36) \tag{3.5}$$

The parameters used in the analysis are listed in Table 3.1. The parameters were set based on the values in reference [72].

On the other hand, the received CNR in satellite communication is determined by equation (3.6) using effective isotropic radiation power (*EIRP*) and parameter *G/T* [73]. Rainfall attenuation A_p included in the term of equation (3.6) is defined by equations (3.4) and (3.5) as a function of the percentage of time p. Therefore, the received CNR (i.e. input CNR to DRoF-Tx) is also expressed as a function of percentage of time p. Parameter *EIRP* represents the transmission power intensity in the antenna directivity direction.

Table 3.2: Signal parameters used in received CNR calculation.

Parameters	Abbreviation	Set value
Equivalent isotropic radiated power [dBW]	$EIRP$	60
Free space propagation loss [dB]	L_s	205.8
Boltzmann constant	k	1.38×10^{-23}
Bandwidth [MHz]	B	33.7561
Wavelength [m]	λ	0.024
Antenna diameter [m]	δ	1.2
Aperture efficiency	η	0.6
Feed line loss [dB]	L_f	0.5
Receiver noise figure [dB]	NF	0.8
Reference temperature [K]	T_0	290
Average propagation temperature [K]	T_m	273

Parameter G/T is generally called the *figure of merit* [74].

$$CNR = EIRP - L_s - A_p + G/T - 10 \log kB \qquad (3.6)$$

Here, L_s represents free space propagation loss, while k and B indicate Boltzmann's constant and signal bandwidth, respectively. Parameter G/T in equation (3.7) is given by the following equation.

$$G/T = G_r - 10 \log T_s \qquad (3.7)$$

Parameter G_r is antenna gain, and indicates the equivalent total noise temperature of the receiving system. Here, G_r is given by aperture efficiency η of a parabolic antenna, antenna diameter δ, and wavelength λ [75].

$$G_r = \eta \left(\frac{2\pi\delta}{\lambda}\right)^2 \tag{3.8}$$

Also, T_s of equation (3.7) is represented by antenna noise temperature T_a, reference temperature T_0, and receiver noise temperature T_r.

$$T_s = T_a + (L_F - 1)T_0 + L_F T_r \tag{3.9}$$

Here, L_F represents the feed line loss. The antenna noise temperature T_a of equation (3.9) is refined by the following equation.

$$T_a = T_m\left(1 - 10^{-(A/10)}\right) \tag{3.10}$$

Here, T_m represents the average propagation temperature. Further, T_r of equation (3.9) is expressed by the following equation using receiver noise figure NF.

$$T_r = (NF - 1)T_0 \tag{3.11}$$

The input CNR to DRoF-Tx is calculated using equations (3.4) to (3.11). Here, the parameters used in the CNR calculation are given in Table 3.2. The parameters were determined based on the typical receiving facilities at the head-end. Parameter A_p, the statistical rainfall attenuation value calculated from ITU-R P. 618-13, was used to calculate the input CNR to DRoF-Tx.

3.4   Evaluation

3.4.1 Experimental Setup

In order to investigate the dependency of the transmission rate on the fluctuating input CNR, we experimentally confirmed the required quantization bit number corresponding to the DRoF-Tx input CNR as determined in 3.2.3

Figure 3.6 shows the experimental setup for the transmission of UHD BS signals. The
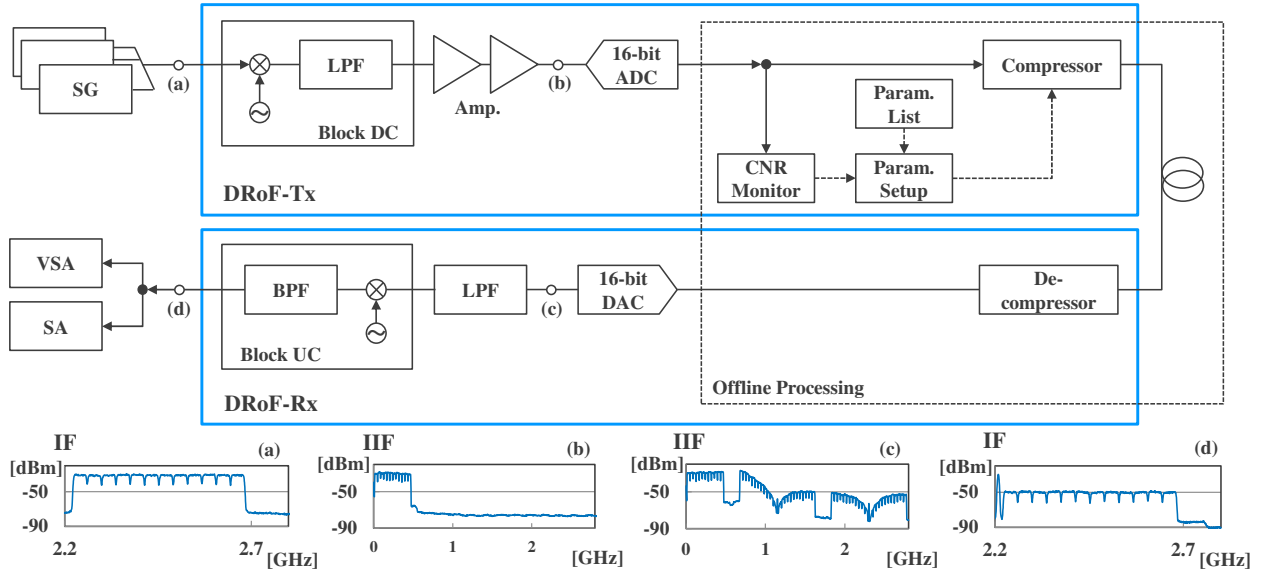
Fig. 3.6: Experimental setup for BS 4K UHD signals transmission using proposed system.

11ch frequency-multiplexed integrated services digital broadcast signals for satellite 3rd generation (ISDB-S3) were output from a signal generator (SG) [76]. The detailed parameters of the ISDB-S3 signals used in the experiment are shown in Table 3.3. They were generated by employing 16-amplitude and phase shift keying (APSK) [76]. The 11ch output signal was generated as an IF signal with frequencies from 2224.41 MHz to 2625.26 MHz. These IF signals simulate the signals after frequency conversion from the 12 GHz RF band used in the satellite communication channel. The FDM signal was block-down converted directly from IF to IIF using a 2209.41 MHz local oscillator. The high frequency band of the converted signal was cut by a LPF. The signal after passing through the LPF was amplified by the amplifier. The amplified signal was input to the 16-bit ADC and digitized. Part of the digitized signal was branched and the CNR of each channel was monitored by the CNR Monitor. Monitoring detected the channel with the lowest CNR, which was used in determining the compression parameters. The compression parameters were referenced from the pre-determined Param.List and applied by the Compressor to

46

Table 3.3: Signal parameters used in the experiment.

Parameters		Set value
Channel number		11
Occupied bandwidth [MHz]		34.5
Channel bandwidth [MHz]		38.36
Modulation scheme		16APSK
Forward error correction	Inner code	LDPC code (Code length: 44880)
	Coding rate	7/9
	Outer code	BCH (65535, 65343) Shortened code
Roll off factor		0.03
Symbol rate [Mbaud]		33.7561

compress the signal. The compressed signal was transmitted from the DRoF-transmitter to the DRoF-receiver. On the other hand, on the DRoF Receiver side, the transmitted signal was decompressed by the De-compressor and converted into an analog signal by 16-bit DAC. The DAC output was input to the LPF, and the harmonic components generated by the DAC were cut off. The signal output by the LPF was directly block-up converted by the 2209.41 MHz local oscillator. The out-of-band component was cut by the band pass filter (BPF) and output from the DRoF-receiver. The signal quality of the output signal was measured by using a vector signal analyzer (VSA) and signal analyzer (SA).

3.4.2 Required Quantization Bit against Percentage of Time

The transmission rate of the proposed system varies with the state of the satellite

47
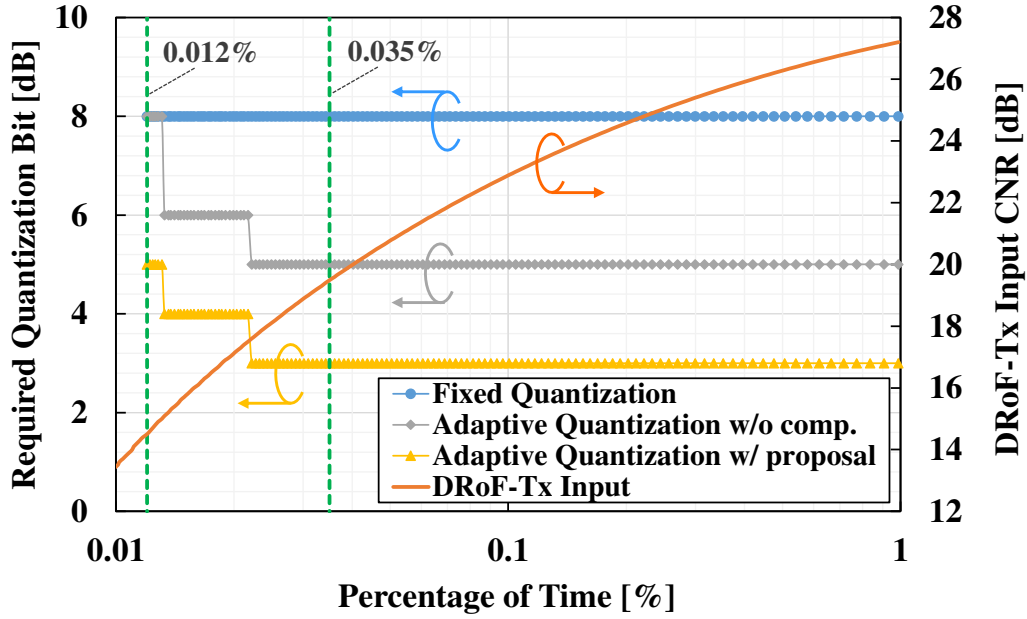
Fig. 3.7: Required quantization bit and input CNR for percentage of time.

communication. This is because the minimum quantization bit needed for DRoF-Tx may change depending on the input CNR. Therefore, the required quantization bit was experimentally evaluated in order to investigate the transmission rate according to the input CNR assuming it was varied due to rainfall attenuation. Here, the minimum quantization bit number that allowed the output signal CNR from DRoF-Rx to satisfy the required value (CNR≥14 dB) is defined as the required quantization bit number [77].

Figure 3.7 shows the required quantization bit number and the input CNR to DRoF-Tx for the percentage of time *p*. Three cases were compared; 1) Fixed quantization, 2) Adaptive quantization w/o compression, and 3) Adaptive quantization w/ proposal. 1) Fixed quantization; At the minimum allowable input CNR (i.e. 14.5 dB) without quantization bit reduction, the minimum quantization bit that satisfies the required CNR was set. 2) Adaptive quantization w/o compression; For each input CNR, the lowest quantization bit that satisfies the required CNR at the receiver side was assigned
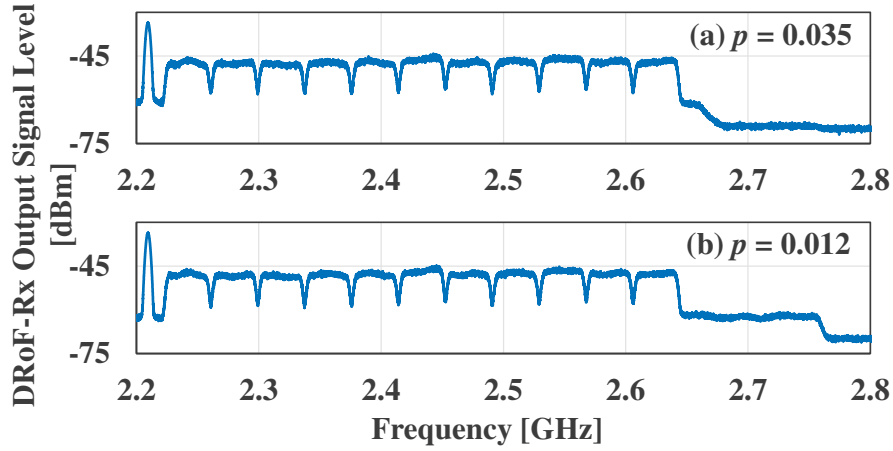
Fig. 3.8: Spectral result of output signal from DRoF-Rx. (a) shows the output signal from DRoF-Rx under the condition of p=0.035. (b) shows the output signal from DRoF-Rx under the condition of p=0.012.

dynamically. 3) Adaptive quantization w/ proposal; Our proposal was applied and the lowest quantization bit satisfying the required CNR at the receiver side was assigned dynamically. The vertical axis on the left plots the required quantization bit number, and the vertical axis on the right plots the DRoF-Tx input CNR. The horizontal axis plots the percentage of time p. From Fig. 3.7, it can be seen that 8-bits are required for the case of fixed quantization. On the other hand, in adaptive quantization w/o compression and adaptive quantization w/ proposal, the required quantization bit number increases as the percentage of time p decreases. This is because the input CNR decreases as the percentage of time p decreases, i.e. rainfall attenuation worsens. Focusing on the percentage of time 0.035 %, which indicates the service availability of existing satellite broadcast services, adaptive quantization w/o compression requires 5-bits. On the other hand, the proposed method can reduce the quantization bit number to 3-bits. It was experimentally confirmed in that the requirements for DRoF-Rx output were met even when the percentage of time p was 0.012 %. When the percentage of time p was 0.012 %, the quantization bit number
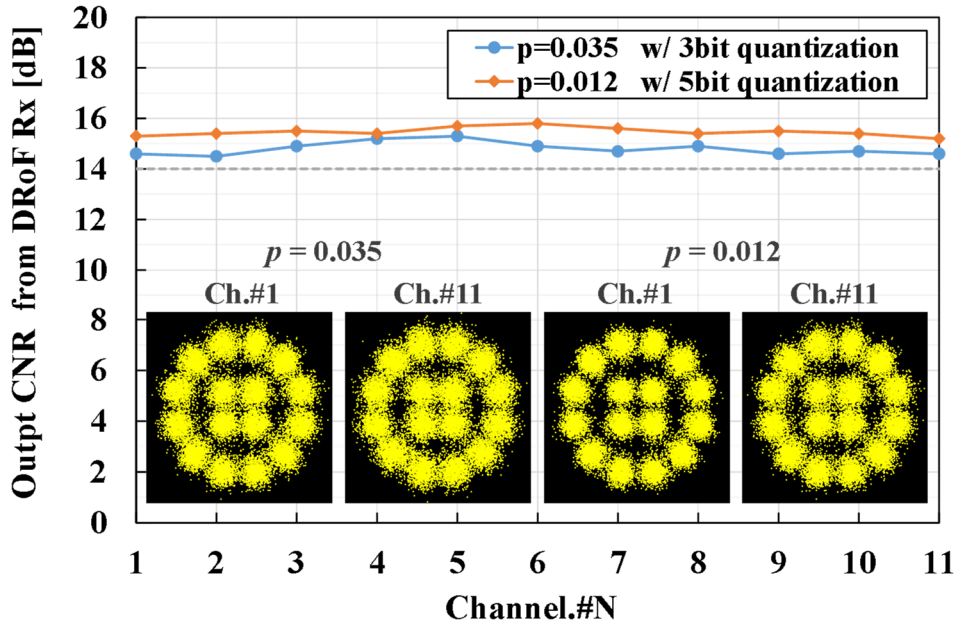
Fig. 3.9: All channel CNR measurement of output signals from DRoF-Rx. The inset shows a screenshot of the constellation diagram under the conditions p=0.035 and p=0.012.

required for adaptive quantization w/o compression was 8-bits. On the other hand, we confirmed that our proposal can satisfy the required CNR using only 5-bits. Furthermore, the average quantization bit number was investigated in the range of $p \geq 0.012$ % to statistically evaluate adaptive compression. The average quantization bit number for fixed quantization and adaptive quantization w/o compression were 8.000 and 5.000, respectively. With the proposal, on the other hand, the average quantization bit number for adaptive quantization was 3.000. This indicates that for most of the time, the adaptive compression scheme yields successful transmission with just 3-bits.

To indicate that all channels met the required quality against the percentage of time p, we scanned all the channels. Fig. 3.8 shows the captured signal spectrum. Snapshots for the case of p=0.035 % and p=0.012 % are shown. Fig. 3.9 shows the CNR measurement results of all transmitted channels. Adequate channel CNR was achieved under the
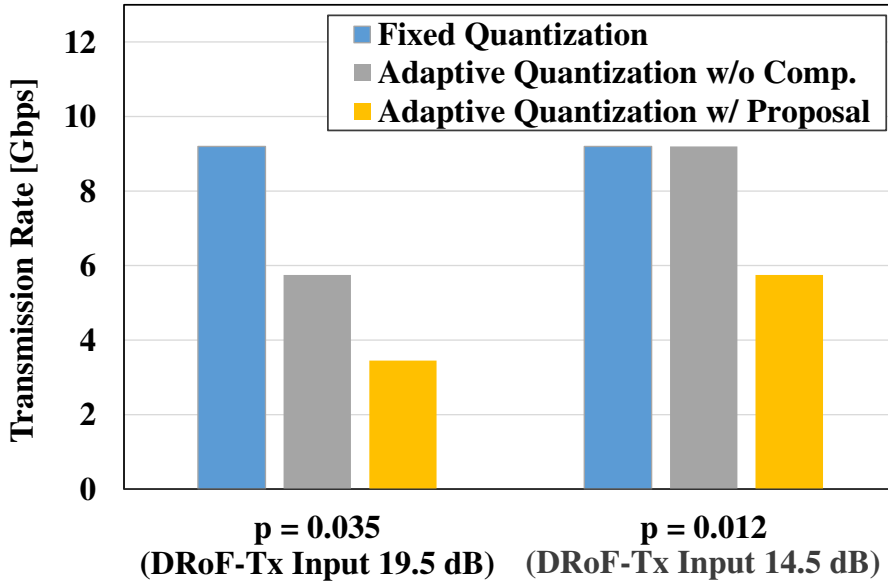
Fig. 3.10: Transmission rate results for percentage of time. The transmission rate results under the conditions of percentage of time 0.035 and 0.012 are shown. Three transmission methods are compared: 1) Fixed quantization, 2) Adaptive quantization w/o comp. and 3) Adaptive quantization w/ proposal.

conditions of p=0.035 % and p=0.012 %. From the output CNR results, it is clearly understood that the required CNR of all channels was satisfied for 0.035 % and 0.012 %. The inset in Fig. 3.9 shows Ch.#1 and Ch.#11 constellations for 0.035 % and 0.012 %. These constellation plots confirm that signal reception was realized while maintaining the signal quality even in Ch.#1 and Ch.#11, which are weak against the negative effects of frequency conversion and filtering.

All these results clearly show that our proposal achieved signal transmission and reception with fewer quantization bits at various input CNR values while satisfying the required CNRs in all channels.

3.4.3 Transmission Rate Reduction by Adaptive Quantization

Figure 3.10 shows the transmission rate results for the percentage of time p. Transmission

rates for the percentages of time p=0.035 and p=0.012 are shown. Three transmission methods were compared: 1) Fixed quantization, 2) Adaptive quantization w/o comp. and 3) Adaptive quantization w/ proposal. In fixed quantization, the quantization bit was fixed at 8-bits, so the transmission rate was also fixed regardless of the input CNR. On the other hand, in adaptive quantization, the minimum quantization bit was assigned according to the input CNR. Therefore, the transmission rate was reduced compared to fixed quantization. However, when the proposal is not applied, the effect of reducing the transmission rate is limited due to quality deterioration triggered by quantization error. On the other hand, it is understood that the transmission rate can be dramatically reduced by using the proposal. At p=0.035, a reduction of 62.5 % was achieved compared to Fixed quantization. In addition, 40 % reduction was obtained compared to Adaptive quantization w/o comp. At the transmission limit of p=0.012, no transmission rate reduction effect was obtained in the case of Adaptive quantization w/o comp. However, by using the proposal, a 25 % transmission rate reduction could be achieved.

From these results, our system can achieve a high transmission rate reduction of 62.5 % compared to Fixed quantization and 40 % reduction compared to Adaptive quantization w/o compression within 99.978 % service operation time (p≥0.022). This means that it covers most of the service operating time. More notably, our system was able to cover 99.988 % (p≥0.012) of the service operating time with the transmission rate reduction effect of 25 %.

3.5   Summary

In this chapter, we have proposed the adaptive optical re-transmission system; it applies combination compression with non-linear conversion and peak clipping to UHD BS/CS satellite broadcast signals whose input CNR to DRoF-Tx fluctuates significantly due to

rainfall attenuation. Our system dynamically assigns compression parameters according to the input CNR to the DRoF-Tx to achieve the highest possible compression ratio while satisfying the required quality on the receiver side. By reducing the transmission rate as much as possible according to the input to the DRoF-Tx, the transmission rate of the communication signal shared over PON can be maximized as much as possible. The applicable service operation range of our proposed system was experimentally investigated using the prediction model of ITU-R P.618-13. The proposed system achieved to cover 99.988 % of service operating time. Furthermore, we investigated the quantization bit number required for the input CNR values created by the rainfall attenuation range, and showed its impact on the transmission rate. Experiments showed that the service operation time of 99.978 % can be achieved with 3-bit quantization. This means our system can reduce the transmission rate by 62.5 % compared to conventional fixed quantization. In addition, the average quantization bit number for service operation times ($p \geq 0.012$) was investigated. The average quantization bit number in our system was 3.000. Most of the service operation times are covered by just 3-bit transmission; this is a significant transmission rate reduction effect compared to conventional approaches.

Chapter 4

Wireless LAN System Architecture Applying Optical Wireless to the Control Plane for Location-Aware Wireless Services

4.1 Introduction

Wireless LAN services are being provided as an added value for commercial services such as cafes and malls, and the quality of their communication services is becoming more demanding than ever before [34]. One of the factors for reducing communication quality is the movement of users within the wireless service area. In a distribution model in which there are many users and the distribution of users fluctuates with time, the deterioration of communication quality such as throughput becomes remarkable. This is one of the challenges of high-density wireless LAN systems.

To solve such problems, there are various connection methods for connection between UE and AP. They are classified as UE-driven and network-driven. The UE-driven type has the UE select and connect to an AP. In existing wireless LAN systems, the UE takes the initiative in connecting to the AP with the strongest RSSI among connectable APs

[40]. An alternative method uses the round trip time (RTT) between the UE and AP to trigger connection switching [41]. In these techniques, the individual initiative of the UE determines which APs should connect.

On the other hand, network-driven type methods assess the entire network and distribute UE connections from the viewpoint of network resources. The AP and controller basically perform centralized connection control based on the collected UE information. For example, one method changes the physical locations of the access points based on the information of UE location distribution. Dynamically changing AP placement is expected to improve the communication quality adaptively, even if the UE distribution fluctuates [78, 79]. However, the APs need to be equipped with a mobility mechanism. An alternative dynamically changes the transmission power according to UE location. These so-called cell-breathing methods control the transmission power of the AP, and a UE experiencing weak RSSI is forcibly reconnected to another AP [80, 81]. In the cell-breathing scheme, the control granularity of UEs to be load balanced is limited, and fine-grained connection control is difficult.

There are also several load balancing schemes for the AP side based on parameters that can be collected at each AP. The parameters collected by the AP vary, such as the number of active UEs, RSSI between UE and AP, and data rate [42,43,82]. However, in these RSSI-based schemes, the uncertainty in RSSI determination makes it difficult to select the correct UE for balancing in environments where the number of UEs is extremely high or they are unevenly distributed. Hence, throughput bias among UEs or APs will occur.

In addition to the relevant parameters mentioned above, a method has been proposed that uses the geographic location of the UE for connection selection. In [83], the location information of UEs is estimated from the RSSI of beacons and a distribution map is

created, which is then used to select the connection destination. This is based on the RSSI of the beacons. It is affected by uncertainty in environments where the distribution is skewed. [84] proposed a method that uses deep learning to estimate UE location from the radio signal (radio parameters other than RSSI) to achieve advanced location awareness and use location results for AP selection. However, achieving accurate location estimation incurs heavy computation costs. This problem worsens as UE number increase.

It is possible to apply a combination of such RSSI-based positioning methods and other positioning methods. The global positioning system (GPS) is well known as a source of location information [85]. Although GPS can determine location with high accuracy when used outdoors, it is well known that its accuracy is poor indoors. An indoor positioning technique that uses sound waves has been proposed [25, 86]. This can estimate the position in three dimensions. There is also a positioning technique that uses the channel characteristics of wireless signals [27, 87]. [27, 87] proposed a position estimation technique using channel state information (CSI). It has been reported that using CSI improves the accuracy of position estimation compared to using RSSI. Unfortunately, these proposals require the use of special devices dedicated as transmitters and receivers. To ensure convenience and practicality in implementing area-based connection restriction in hotspots, it is desirable to use an approach that does not use special devices and does not involve UE modification.

Therefore, in this chapter, in order to realize a location-aware wireless LAN system, we propose a wireless LAN system architecture that divides the wireless LAN service area into small cells by light source and controls the AP connection destination for each small cell. Specifically, optical wireless is applied to the control plane of the wireless LAN system, and the optical identifier (ID) corresponding to the wireless LAN control

information is transmitted to the UE under the small cell via the optical wireless. The UE that receives the optical ID is centrally guided to the optimum connection destination based on the wireless LAN control information. The proposed system controls the connection destination of the UE based on the positional relationship between the optical cell and the AP. This realizes location-aware wireless control without actively collecting location information from the UE. In addition, it is possible to flexibly construct a connection restricted area that has not been realized in the conventional wireless LAN service.

Section 4.2 describes the overall architecture of the proposed system. In addition, in order to realize the transmission and reception of optical IDs with a simple and low-cost device, we propose an optical ID transmission / reception method that utilizes IoT smart lighting and a smartphone illuminance sensor. Furthermore, in order to improve the communication quality of the system, we also propose an optical cell control algorithm for ensuring the communication quality of the UE against changes in the UE's location. Section 4.3 describes the results of an experimental evaluation of the implemented optical ID transmission / reception method. Section 4.4 describes the results of a simulation evaluation of the effect of load balancing based on the optical cell control algorithm. Finally, Section 4.5 summarizes the suggestions.

4.2 Application of Optical Wireless to Control Plane of Wireless LAN

4.2.1 Proposed Overall Architecture

Figure 4.1 shows the proposed system architecture. We assume a hotspot service with multiple APs that overlap each other. In addition, we also assume that there are multiple
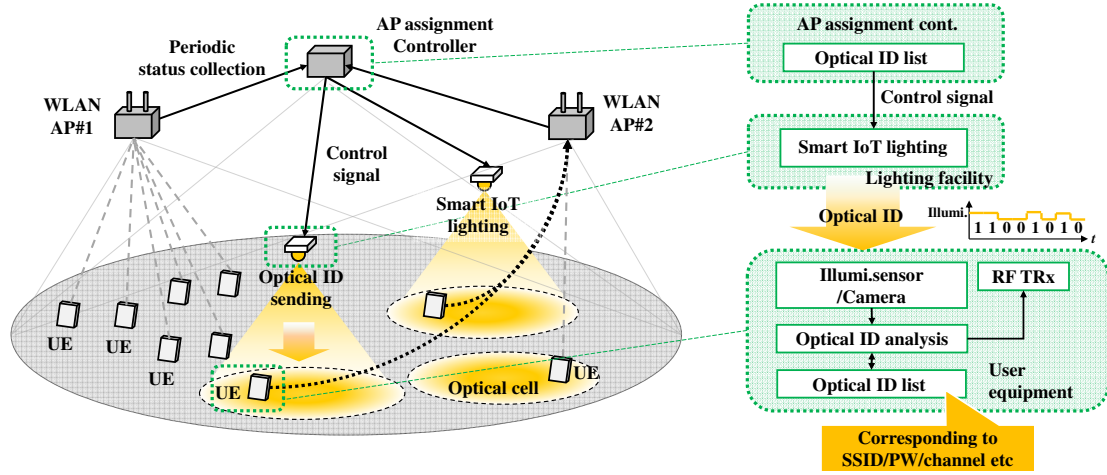
Fig. 4.1: Proposed system architecture that applies optical radio to the control plane of wireless LAN.

optical cells with smaller areas in the wireless LAN area. Specifically, the optical cells are created by smart Internet of Things (IoT) lighting using LEDs that can be dimmed by external control. The smart IoT lighting is used as an array of optical wireless transmitters; the modulation level is so low that it cannot be perceived by humans, and its lighting function is retained.

In our system architecture, AP selection is centrally controlled for each optical cell. The optical cells distribute the optical IDs, which are used for authentication and connection control. By knowing the installation location of the optical cell in advance, we can flexibly establish permitted and restricted areas. In addition, location-based connection control, which utilizes the installation location of optical cells, is expected to effectively realize load balancing, even when UEs move their locations or crowd together. The mechanism of connection control by optical cells and its flow are shown below.

In our system architecture, APs and smart IoT lighting are connected to a central AP assignment controller in a basic star network topology. The status of UEs under each AP

is managed, and the connection status is periodically collected from APs by the central AP assignment controller. Here, the status indicates information related to wireless LAN such as the number of UEs, channels, and frequencies of each AP. Based on this status, the optical ID is determined by the AP assignment controller for each optical cell. Here, the optical ID is an arbitrary orthogonal bit sequence. Individual bit sequences are associated with individual service set identifier (SSID) / password (PW). Optical IDs can be operated locally rather than globally to reduce the bit length. For example, in a small area such as the wireless service area of a commercial facility, about 8-bits is sufficient. A control signal for modulating the determined optical ID is sent from the AP assignment controller to the light source. The optical ID is broadcast to the UE in the optical cell. By transmitting the optical ID, the transmission rate required is reduced compared to sending the SSID/PW directly, making it possible to utilize IoT lighting with lower modulation facto and illuminance sensors with lower sampling rates as transmitters and receivers (TRx). The UE that receives an optical ID refers to an optical ID list loaded in advance and tries to connect to the specified AP. Here, the optical ID list associates the optical ID with connection information (i.e. SSID/PW etc.,). After receiving the optical ID, the UE makes the connection specified by the authentication process.

Instead of a dedicated optical wireless transceiver, we utilize general IoT lighting as the transmitter and a smartphone's illuminance sensor as the receiver. The advantage of the proposed system is that it is expected to become widespread given the rapid penetration of IoT. For example, the spread of IoT lighting systems is expected to increase more and more for the purpose of energy saving [88, 89, 90, 91]. However, there are trade-offs due to the use of general IoT equipment. One is that it is difficult to increase the transmission speed. Due to the limited speed of IoT lighting modulation and the

sampling frequency of most illumination sensors, the amount of information that can be transmitted is limited. This makes it difficult to insert the synchronous bits. As a result, it becomes difficult to achieve low error communication. In the next section, we detail our optical ID-based transmission/reception method that overcomes these problems. Another issue with our proposal is that the AP assignment controller and the UEs need to have a common optical ID list in advance. Our system enables UE control even at low speeds by maintaining an optical ID list that contains the optical IDs corresponding to the information to be transmitted. Considering these points, TRx must be economical and convenient in order to break down the hurdles of system diffusion and implementation, so it should be possible to use existing devices and smartphones without modification.

4.2.2 Optical ID Transmission and Reception Scheme Using Consumer Devices

In order to improve the economy and convenience of sending and receiving optical IDs, existing lighting and smartphones must be used instead of dedicated optical transmission/reception devices such as Li-Fi [92]. In addition, the optical ID receivers must be implemented as a simple smartphone application. Therefore, we propose an optical ID transmission and reception scheme to utilize IoT smart lighting as the transmitter, and the illuminance sensor of the smartphone as the receiver.

However, there are several technical issues. First, the transmission speed depends on the sampling frequency of the TRx, which is extremely low. Since it is difficult to use synchronous bits such as preambles, asynchronous communication must be used, resulting in high error rates. Also, due to the limited transmission speed, it takes time to receive and authenticate the optical ID.
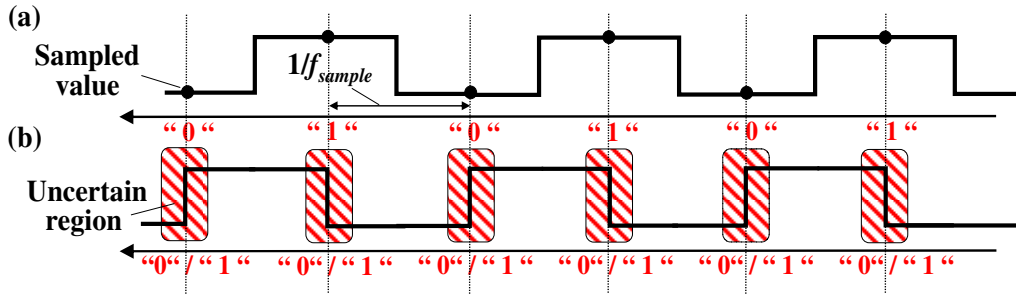
Fig. 4.2: Reception error in asynchronous correlation receiving scheme.
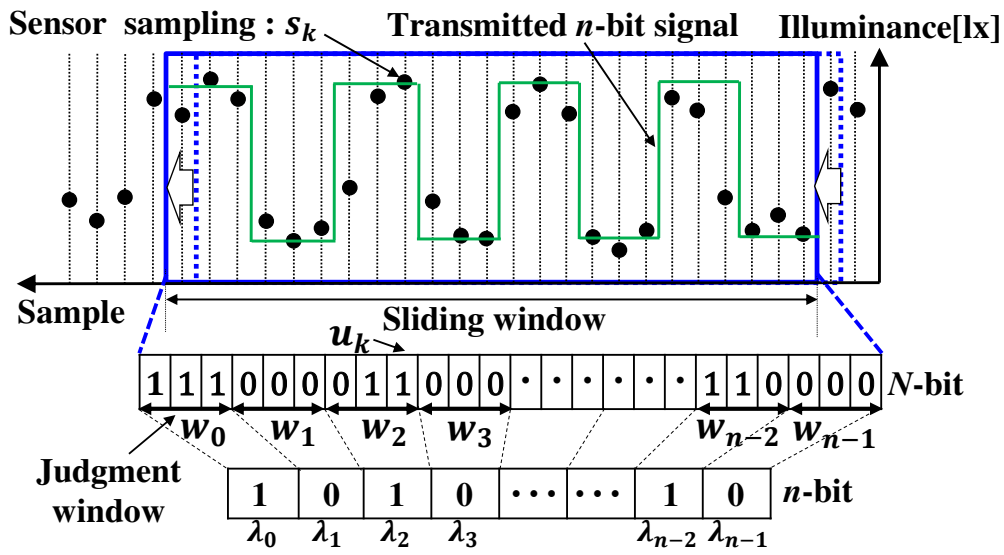
Fig. 4.3: Detailed understanding of the oversampled edge-excluded receiving scheme (OE).

One well known pattern matching method is that used in an intelligent lighting system [93]. This approach has the advantage of simplicity as optical correlation receiving is used. As shown in Fig. 4.2(a), there is no reception error when sampling is performed at the correct position for the received pulse. However, in the case of asynchronous communication, as shown in Fig. 4.2(b), errors are likely to occur when sampling is performed in an uncertain region, such as at the rising/falling edge of a pulse, where 1/0 judgment is uncertain. To address this issue, we propose an oversampled edge-excluded receiving scheme (OE). OE makes it possible to ignore uncertain regions (the edges) that

hinder ID determination. OE can estimate the optical ID by oversampling the transmitted n-bit signal and performing window-based decision for each defined window length. Fig. 4.3 details the proposed receiving process. The received illuminance is binarized using a threshold value calculated from the average illuminance value in the sliding window. OE uses this sliding window to extract oversampled N-bit arrays. Here, signal u_k after binarization is represented by the following equation.

$$u_k = \begin{cases} 1 & \text{if } s_k \geq \dfrac{\sum_{l=1}^{l=N} s_{k-N+l}}{N} \\ 0 & \text{if } s_k < \dfrac{\sum_{l=1}^{l=N} s_{k-N+l}}{N} \end{cases} \tag{4.1}$$

Here, s_k represents the sensor sampling instances in the sliding window; sliding window length for binarization is N. The binarized N-bit signal is converted into an n-bit optical ID by using a judgement window. λ_k, which constitutes the optical ID after window-based judgement, is given by the following equation.

$$\lambda_k = \begin{cases} 1 & \text{if } sum\{w_k\} > \dfrac{K}{2} \\ 0 & \text{if } sum\{w_k\} \leq \dfrac{K}{2} \end{cases} \tag{4.2}$$

Here, the window length for window-based is, for the k-th judgement window, set to K (=N/n). By performing these processes at the UE, uncertain regions (the edges) of the transmitted signal that hinder the determination of optical ID can be avoided, and the error rate can be reduced even with asynchronous signaling.

4.2.3 Fast Optical ID Authentication Method

In the OE proposal described in advance, oversampling is performed K times compared to the existing receiving method. This means that the matching cycle between the received optical ID and the reference ID is also K times longer. A matching cycle is represented by the following equation.
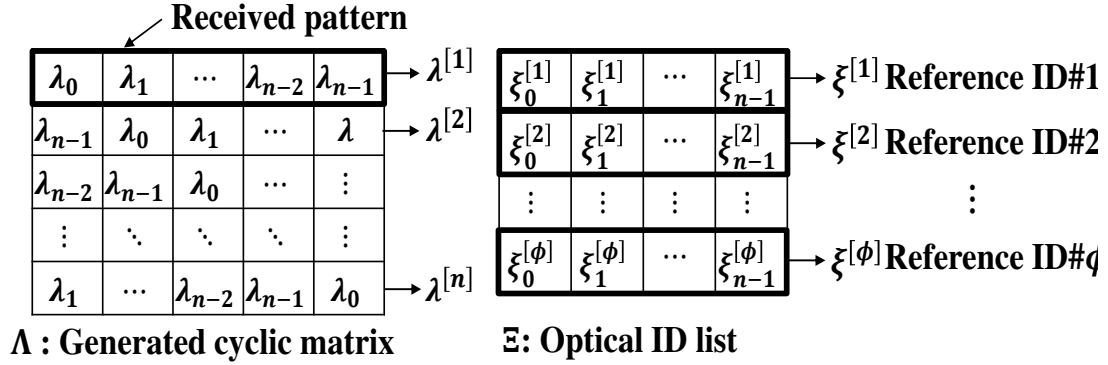
Fig. 4.4: Generated cyclic matrix and optical ID list.

$$T_{periodic} = K \cdot n \cdot 1 / f_{sample} \tag{4.3}$$

n is the number of bits of the optical ID, and f_{sample} indicates the sampling frequency of the illuminance sensor. $T_{periodic}$ increases in proportion to n and K. The $T_{periodic}$ indicates the shortest period during which optical ID can be pattern matched. Therefore, in order to ensure usability, it is necessary to reduce $T_{periodic}$ as much as possible. Therefore, we also propose a fast optical ID authentication scheme (FA) that reduces the authentication cycle. The proposed method compares not only the optical ID itself, but also n bit-shifted patterns of the optical ID and the reference ID on the optical ID list in each sampling cycle. The optical ID is given by

$$\Lambda_{received} = [\lambda_0 \quad \lambda_1 \quad \cdots \quad \lambda_{n-2} \quad \lambda_{n-1}]. \tag{4.4}$$

As shown in Fig. 4.4, cyclic matrix Λ is generated by bit-shifting the received optical ID. The optical ID list Ξ is prepared in advance. Here, ϕ indicates the number of reference IDs in optical ID list, and $\xi^{[\phi]}$ indicates the reference ID#ϕ. The k row of the cyclic matrix (i.e. $\lambda^{[k]}$) and the j row of the optical ID list (i.e. $\xi^{[j]}$) are extracted, and the correlation coefficient $\gamma_{\lambda^{[k]}\xi^{[j]}}$ is calculated by the following equation.

$$\gamma_{\lambda^{[k]}\xi^{[j]}} = \frac{\frac{1}{n}\sum_{i=0}^{n-1}\left(\lambda_i^{[k]} - \overline{\lambda^{[k]}}\right)\left(\xi_i^{[j]} - \overline{\xi^{[j]}}\right)}{\sqrt{\frac{1}{n}\sum_{i=0}^{n-1}\left(\lambda_i^{[k]} - \overline{\lambda^{[k]}}\right)^2} \cdot \sqrt{\frac{1}{n}\sum_{i=0}^{n-1}\left(\xi_i^{[j]} - \overline{\xi^{[j]}}\right)^2}} \tag{4.5}$$

The correlation coefficient between each row in the cyclic matrix and each row in the optical ID list (i.e. reference ID) is calculated by in round-robin manner. The reference ID#*j* with the highest correlation coefficient is determined by using following equation.

$$\xi^{[j]} = \arg\max_{\substack{k,j\in\mathbb{N} \\ 1\le k\le n \\ 1\le j\le\phi}}\left\{\gamma_{\lambda^{[k]}\xi^{[j]}}\right\} \tag{4.6}$$

Finally, the reference ID#*j* corresponding to the received optical ID is extracted from the optical ID list. The matching cycle when FA is applied to the OE is expressed by using sampling frequency of illuminance sensor f_{sample}.

$$T_{periodic\_FA} = K \cdot 1/f_{sample} \tag{4.7}$$

Matching cycle duration can be reduced by the factor of *n* compared to when only OE is used.

These processes can be implemented in software and run on the UE.

4.2.4 Optical Cell Operation Policy

The proposed architecture controls the optical ID distributed in each optical cell based on UE connection state. Our cell operating objective is to reduce the excessive network load on individual APs (i.e. bias of traffic among APs) and the unfairness among UEs under different APs, caused by UE mobility and local clusters. Therefore, optical cell control is based on the following policy.

- Reduce the difference in average capacity per UE among the APs.

- Reduce the network load bias of each AP

To satisfy the above policy, the optical ID sent to each optical cell is determined based on
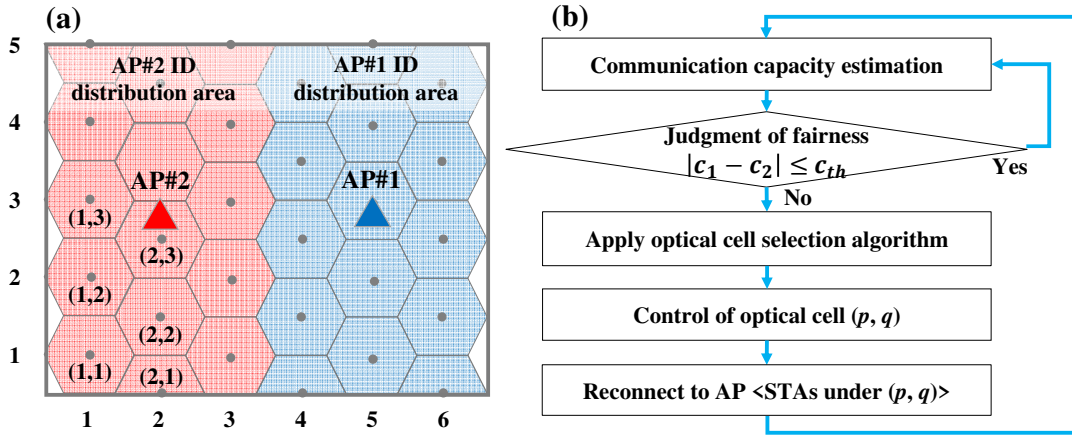
Fig. 4.5: Optical cell operation framework. (a) Arrangement and configuration of AP and optical cell. (b) Overall flow chart of optical cell operation.

the algorithm described below.

Figure 4.5 shows the framework for optical cell control. In the framework, a threshold based on fairness is first defined. Until the threshold is satisfied, the following operations are repeated: select an optical cell in the order given by the algorithm described below, changing the optical ID to be delivered, and switching the AP to which the UE is connected. As shown in Fig 4.5(a), we assume that two APs, AP#1 and AP#2, are deployed in a wireless service area hosting a large number of UEs. The placement coordinates (x, y) of the visible light source and the placement coordinates of AP#1 and AP#2 are known in advance. Fig 4.5(b) shows the flow of optical cell control. First, estimate the average capacity per UE for AP#1 and for AP#2 based on the traffic and number of UEs for each AP. If the following is satisfied, monitoring is continued.

4.2.5 Optical Cell Control Algorithm

Changing the optical cell selection order for determining which AP the optical cell belongs to, will significantly change the overall network capacity. This is because the

Table 4.1: Notation for Optical Cell Control.

Variable	Definition
c_1, c_2	Capacity per UE under AP#1 or AP#2
c_1', c_2'	Capacity per UE under AP#1 or AP#2 (value in previous loop)
c_{th}	Threshold of capacity difference per UE
(m, l)	Previously controlled optical cell coordinates
(p, q)	Optical cell coordinates to be controlled
M	Number of optical cells deployed in the horizontal direction
L	Number of optical cells deployed in the vertical direction
Ω	Total number of optical cells
ω	Total number of optical cells attributed to AP#1
δ	Identification number of the optical cell attributed to AP#1
τ	Identification number of the optical cell attributed to AP#2
d_δ^{12}	Distance between the optical cell belonging to AP#1 (identification number δ) and AP#2
d_τ^{21}	Distance between the optical cell belonging to AP#2 (identification number τ) and AP#1
$(a_\varepsilon, b_\varepsilon)$	Optical cell coordinates of identification number ε

capacity is affected by the modulation and coding scheme (MCS) chosen to suit the different RSSI values which depend on the distance between the optical cell and the AP [94]. Therefore, we introduce an optical cell selection algorithm that considers the physical distance between the optical cell and the AP. Two algorithms, ScanLine-based and MinDist-based, are presented; the notations for ScanLine-based and Min Dist-based are given in Table 4.1.

Figure 4.6 shows a graphical representation of ScanLine-based. In ScanLine-based, optical cells are selected in raster scan manner. As an example, we consider the case that the distribution of UEs fluctuates from the equilibrium state in Fig. 4.5(a) and the capacity

Fig. 4.6: Optical cell control using ScanLine-based algorithm.

(a) Optical cell operation in the situation of $c_1-c_2>0$. (b) Optical cell operation in the situation of $c_1-c_2<0$.
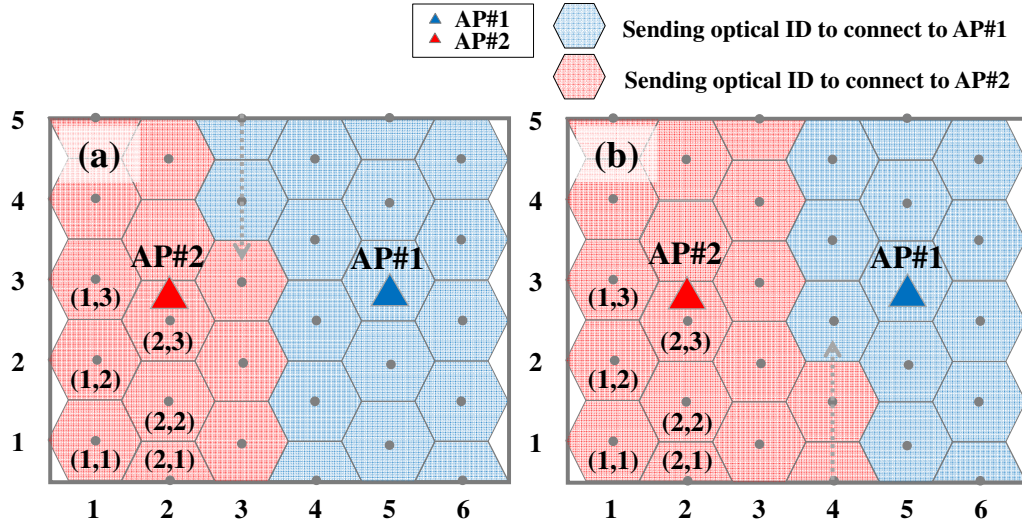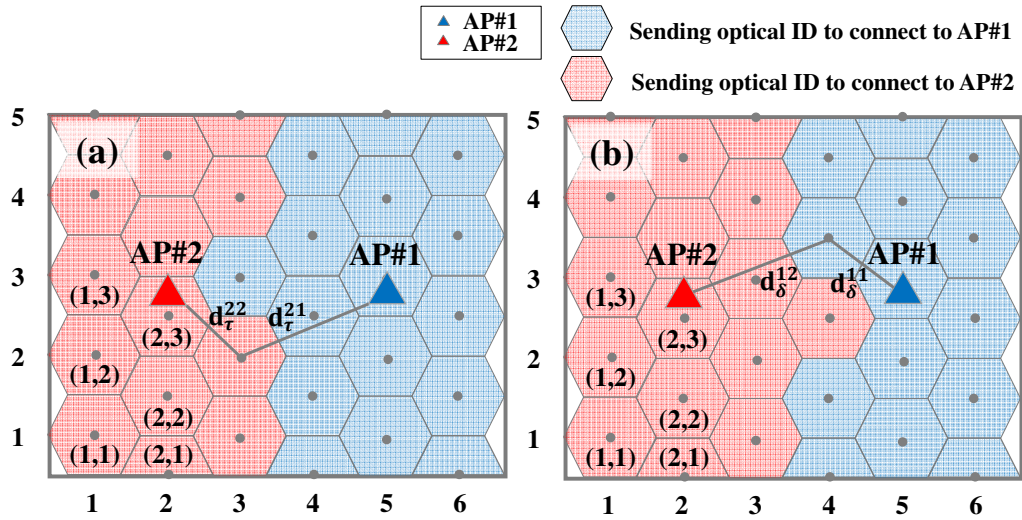

Fig. 4.7: Optical cell control using MinDist-based algorithm.

(a) Optical cell operation in the situation of $c_1-c_2>0$. (b) Optical cell operation in the situation of $c_1-c_2<0$.

of each UE changes. When the distribution of UEs changes, the AP allocation of optical

cells is changed from the initial cell allocation in the central equilibrium shown in Fig.

Algorithm 1: ScanLine-based

Require: (m, l), c_1', c_2', c_1, c_2

Ensure: (p, q)

1:    **if** $|c_1 - c_2| > c_{th}$
2:       **if** $c_1 - c_2 > 0$
3:          **if** $c_1' - c_2' < 0$
4:             stop cell operation
5:         **else**
6:            **if** $l = 1$ **then**
7:           **if** $m = 1$ **then**
8:                stop cell operation
9:              **else**
10:                 $p \Leftarrow m-1$, $q \Leftarrow L$
11:             **end if**
12:           **else**
13:             $p \Leftarrow m$, $q \Leftarrow l-1$
14:           **end if**
15:       **else**
16:          **if** $c_1' - c_2' > 0$ **then**
17:            stop cell operation
18:         **else**
19:            **if** $m = M$ **then**
20:             **if** $l = L$ **then**
21:                stop cell operation
22:             **else**
23:               $p \Leftarrow m+1$, $q \Leftarrow 1$
24:             **end if**
25:            **else**
26:             $p \Leftarrow m$, $q \Leftarrow l+1$
27:            **end if**
28:         **end if**
29:       **end if**
30:    **return** (p, q)

4.5(a) according to the cases $c_1 - c_2 > 0$ or $c_1 - c_2 < 0$, respectively. Here, the initial state varies depending on AP placement. In the initial state, each optical cell is assigned to the AP with the smallest distance.

In the situation where $c_1 - c_2 > 0$, as shown in Fig. 4.6(a), the optical cells belonging to AP#2 are reassigned to AP#1 in order from optical cell (3,5). On the other hand, in the situation where $c_1 - c_2 < 0$, as shown in Fig. 4.6(b), the optical cells belonging to AP#1 are reassigned to AP#2 in order from optical cell (4, 1). Optical cells are reassigned until

---

Algorithm 4.2: MinDist-based

Require: c_1', c_2' , c_1, c_2
Ensure: (p, q)
1:     **if** $|c_1 - c_2| > c_{th}$ **then**
2:         **if** $c_1 - c_2 > 0$ **then**
3:             **if** $c_1' - c_2' < 0$ **then**
4:                 stop cell operation
5:             **else**
6:                 $\varepsilon \Leftarrow \mathrm{argmin}(d_\tau^{21})$ for τ $\{\tau \in 1, 2, \cdots, (\Omega - \omega)\}$
7:                 $p \Leftarrow a_\varepsilon,\quad q \Leftarrow b_\varepsilon$
8:             **end if**
9:         **else**
10   **if** $c_1' - c_2' > 0$ **then**
11:             stop cell operation
12:         **else**
13:             $\varepsilon \Leftarrow \mathrm{argmin}(d_\delta^{12})$ for δ $\{\delta \in 1, 2, \cdots, \omega \}$
14:         $p \Leftarrow a_\varepsilon,\quad q \Leftarrow b_\varepsilon$
15:         **end if**
16:     **end if**
17:     **return (p, q)**

---

the condition of equation (4.6) is satisfied.

The other approach, Min Dist-based, is shown in Fig. 4.7. The optical cells to be changed are determined by considering the distance between optical cell centers and AP#1 or AP#2. When $c_1 - c_2 > 0$, as shown in Fig. 4.7(a), among the optical cells belonging to AP#2, the optical cells with the shortest distance between the optical cell center and AP#1 (i.e. d_τ^{21}) are reassigned to AP#1 in decreasing order of distance.

On the other hand, when $c_1 - c_2 < 0$, as shown in Fig. 4.7(b), among the optical cells belonging to AP#1, the optical cells with the shortest distance between the optical cell center and AP#2 (i.e. d_δ^{12}) are reassigned to AP#2 in decreasing order of distance. Optical cell reassignment is repeated until equation (4.6) is satisfied.

4.3 Evaluation of Optical ID Transmission and Reception Scheme

4.3.1 Experimental Setup

We implemented and evaluated the transmission and reception of optical IDs using commercial IoT lighting as the transmitter and an illuminance sensor as a receiver. Fig. 4.8 shows the processing blocks of each component. We utilized the commercial Philips Hue as smart IoT lighting hardware. Intel NUC (Linux PC) was used as the external IoT lighting controller. Moreover, an optical module (GY-30) equipped with illuminance sensor integrated circuit (IC) (BH1750FVI) was used on the receiver side. GY-30 was connected to Raspberry Pi 3B+ (representing the UE) by inter-integrated circuit (I2C) communication. The smart IoT lighting consisted of a lighting controller and light source. The lighting controller was externally driven, and optical ID was transmitted from the lighting controller to the light source. The light source emitted the n-bit ($n = 8$) optical ID as a modulation signal with the visually imperceptible optical modulation factor of 7 %
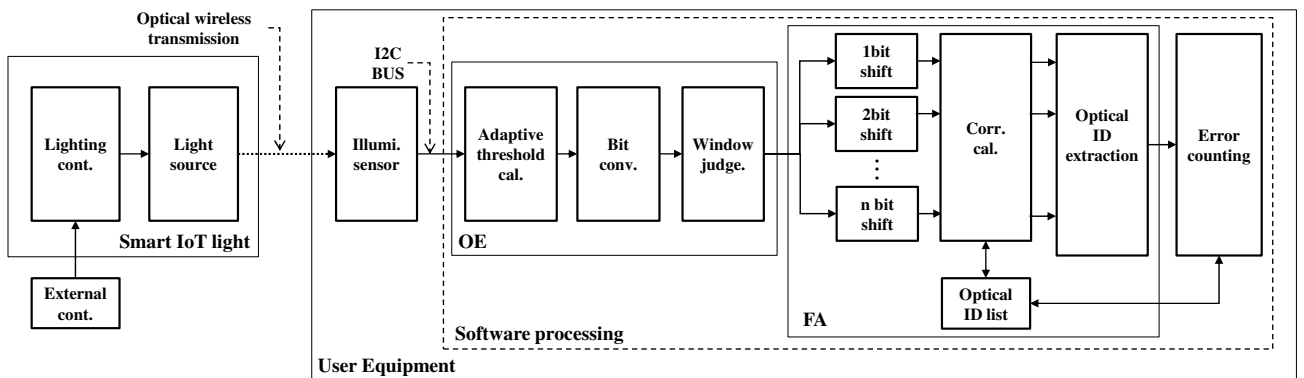

Fig. 4.8: Implementation of the optical ID transmission and reception scheme.
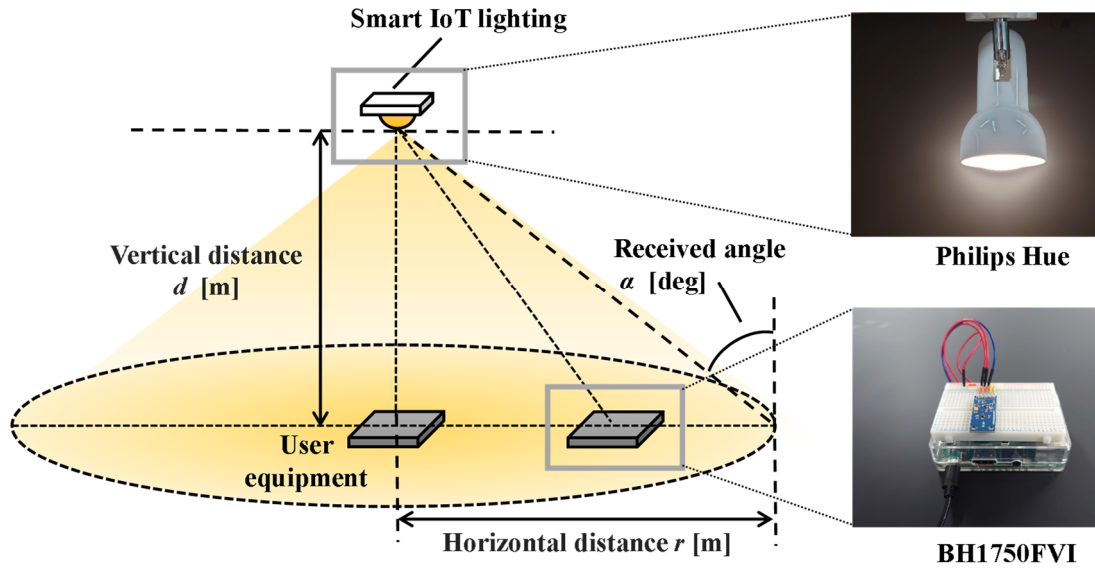
Fig. 4.9: Experimental layout of light source and UE equipment for evaluation.

[95]. The optical ID, "11000101", was repeatedly transmitted at the slow bitrate of 2.2 bps. Here, the optical ID took the form of an orthogonal bit sequence. The UE was placed 1.5 m below the light source. The illuminance sensor captured the optical wireless transmission. Here, the sampling cycle of the illuminance sensor was set to 150 ms. The signal is oversampled with $K = 3$. By using the received illuminance values, the average value was calculated for each N-bit ($N = 24$) sliding window, and 1/0 bit conversion was performed using the average value as a threshold. Window-based judgement was performed on the bit-converted signal, and an 8-bit optical ID was estimated. The optical ID was bit-shifted and a cyclic matrix was generated. Correlation was performed using the columns of the generated cyclic matrix and the columns of the optical ID list. Finally, the reference ID corresponding to the estimated optical ID was extracted.
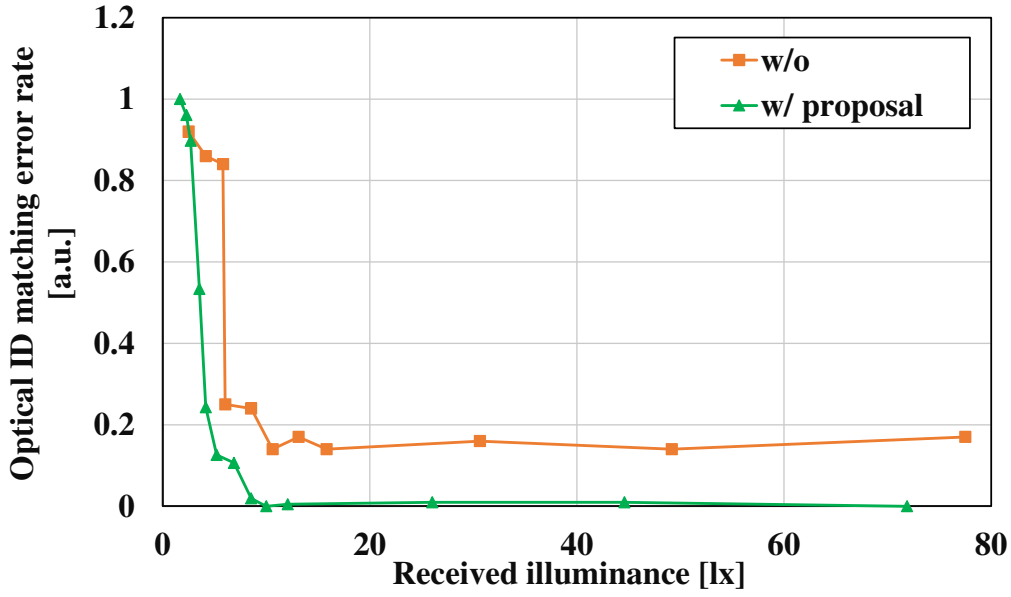
Fig. 4.10: Optical ID matching error rate using proposal.

4.3.2 Results of Optical ID Transmission and Reception Performance

Figure 4.9 shows the evaluation setup of the light source and UE. Smart IoT lighting height was set to $d = 1.5$ m. Fig. 4.10 shows the dependency of the optical ID reception error rate on the received illuminance level. This level is defined as the value obtained by subtracting the background illuminance from the measured illuminance sensor value. Here, the background illuminance is 226.67 lx. The existing method that uses optical correlation reception is shown as w/o. It permits reception error even if the received light illuminance is high. The error rate increased as the received illuminance fell under 16 lx. On the other hand, it is clear that our proposal, OE, reduced the error rate. OE error rate increased as the received illuminance level fell under 8.5 lx. It can be clearly understood that the proposed method can expand the acceptable range of received illuminance level

Fig. 4.11: Authentication cycle reduction by using fast authentication scheme.

Fig. 4.12: Relationship between optical cell radius and normalized illuminance of smart IoT lighting.

while reducing the error rate compared with the existing method.

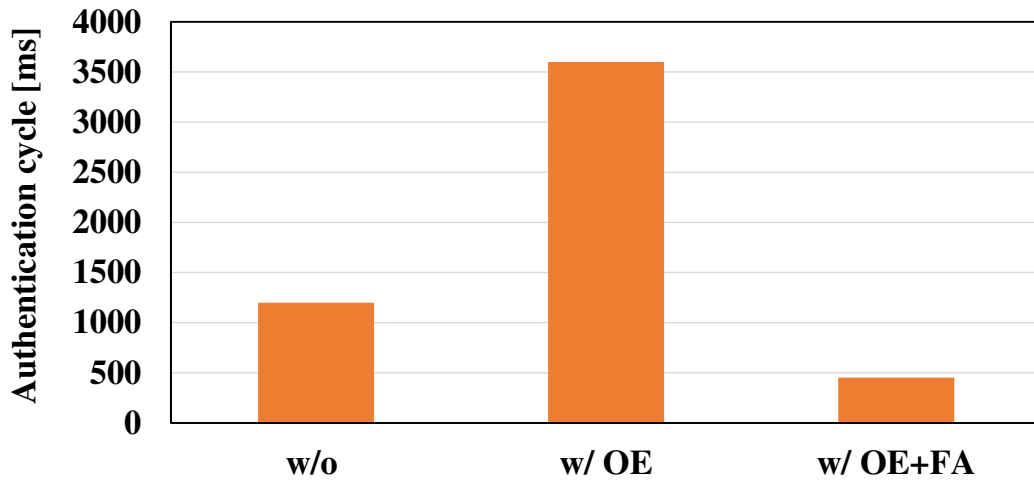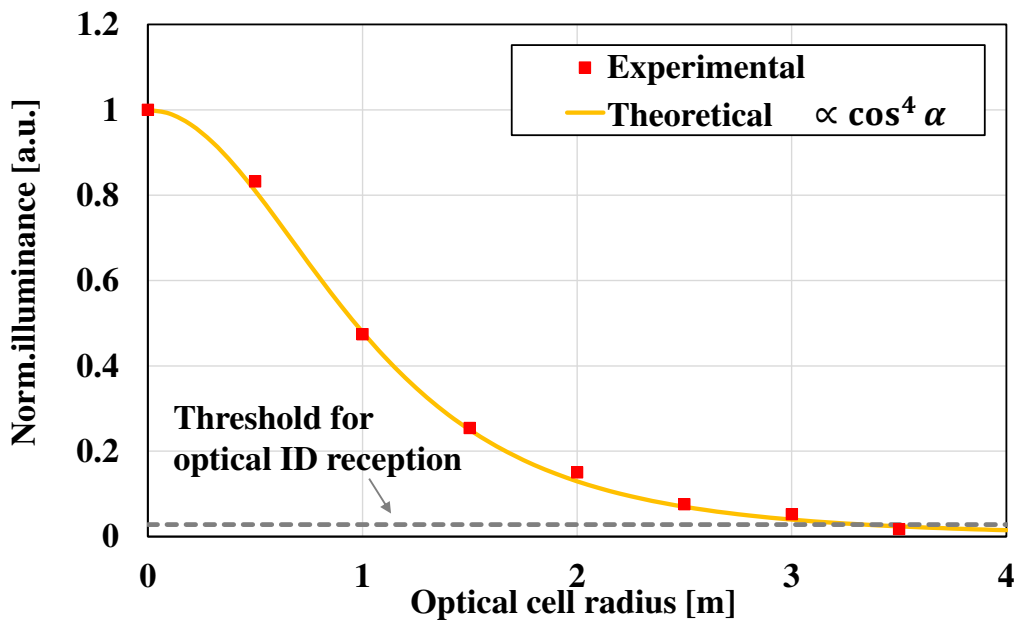Figure 4.11 quantifies the reduction in authentication cycle duration. For w/o, the duration is 1200 ms (8-bit × 150 ms). In the case of w/OE, the duration is 3600 ms (24-

bit × 150 ms) because of its 3 times upsampling. As shown in Fig.4.10, the error rate can be reduced, but the time required for pattern detection is extended. However, by introducing FA, authentication can be realized on a 3-sample cycle, so that the duration is just 450 ms (3-bit × 150 ms). Therefore, the authentication cycle can be reduced by 87.5 % compared to w/OE, and by 62.5 % compared to w/o. These results confirm that the combined use of the OE and FA proposals reduces the authentication cycle while maintaining low error rates.

Figure 4.12 plots the relationship between the optical cell radius (horizontal distance *r*) and the normalized irradiance of the smart IoT lighting. It can be seen that the illuminance characteristic of the IoT lighting used in this study is proportional to $\cos^4\alpha$ (where $\alpha = \tan^{-1}(d/r)$). Based on the fact that the recommended illuminance for a typical office is 300 lx or more, the threshold illuminance of 8.5 lx, where the error rate increases with the "w/proposal" shown in Fig. 4.10, is plotted as a dashed line. From this result, if a light source offering the illuminance of 300 lx at *d* = 1.5 m and *r* = 0 m is deployed, transmission and reception of optical ID can be realized with a modulation level of 7 % or less within an optical cell radius of *r* = 3.3 m, even if there are external disturbances such as natural light or other illumination sources.

4.4 Load Balancing Effect of Optical Cell Control Algorithm

4.4.1 Simulation

In order to evaluate the effectiveness of the proposed method in countering UE distribution fluctuations, we evaluated several scenarios. Table 4.2 shows the evaluation parameters. AP#1 and AP#2 were deployed in a space of 40 m × 40 m. 50 UEs were
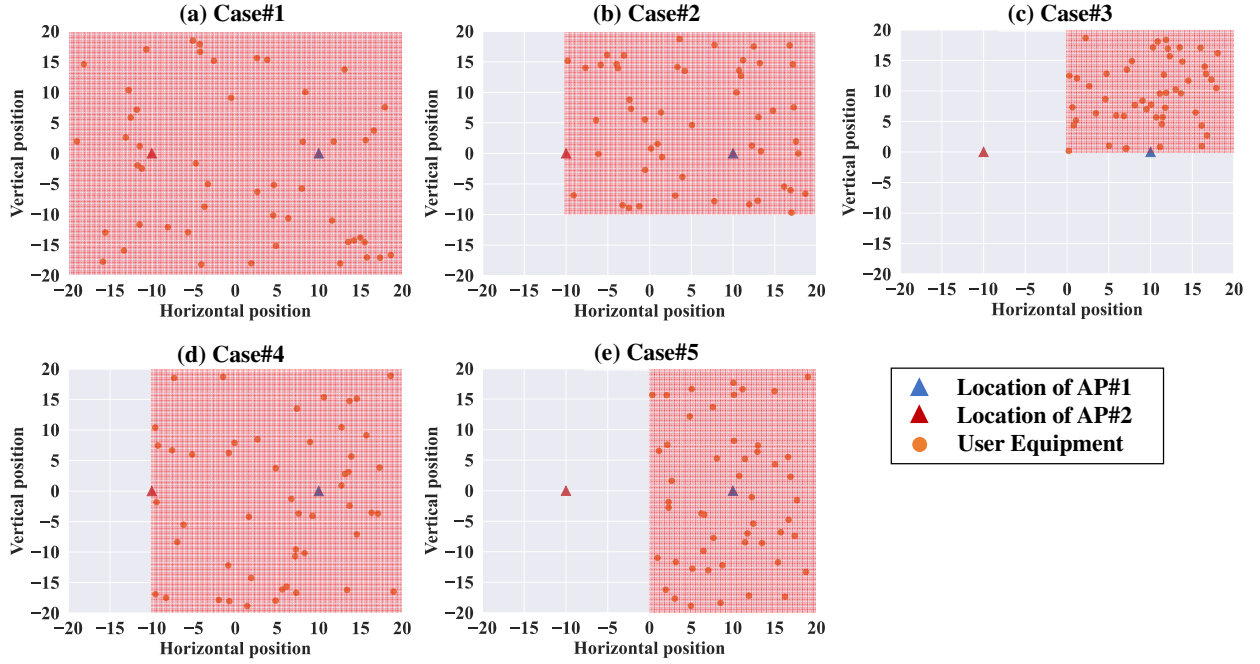
Fig. 4.13: Example of UE distribution for scenario-based evaluation.

arranged within the wireless service area. We used site-general models so propagation followed the ITU model [96]. UEs were assumed to be randomly distributed within a region. As an example, optical cell radius was set to 2 m. The capacity difference threshold, c_{th}, was set to 1 Mbps.

In evaluating the proposal, we considered five scenarios. Fig. 4.13 shows the UE distribution in five scenarios. Case#1: UEs were distributed throughout the wireless service area. That is, Case#1 represents uniform user distribution. Case#3 concentrates all users into the first quadrant. Case#2 represents an intermediate state between Case#1 and Case#3. On the other hand, Case#5 represents a case where all users are concentrated in first and fourth quadrant. Case#4 represents an intermediate state between Case#1 and Case#5. Cases#3 and Case5# are examples of the extreme distribution concentration in which all UEs concentrate on AP#1as controlled by RSSI. To benchmark the proposal,

Table 4.2: Parameters for Evaluation

Parameters	Set value
Wireless service area	40 m × 40 m
Number of UEs	50
UE distribution function	Random model
Coordinates of AP#1	(10, 0)
Coordinates of AP#2	(-10, 0)
Wireless system	802.11 n
Frequency	2.4 GHz
Bandwidth	40 MHz
Spatial Stream	3
Propagation model	Site-general models (ITU-R P.1238-7)
MCS	Active
Optical cell radius	From 1 m to 10 m
Capacity difference threshold value c_{th}	1 Mbps

we also evaluated a conventional RSSI-based scheme that determines the connection based on the strength of RSSI.

4.4.2 Results of Load Balancing Effects

Figure 4.14 shows the average capacity per UE for Case#1-5. Looking at RSSI-based, we can see a significant capacity decrease in Case#3 and Case#5. This is because the connections are concentrated on one AP due to the extreme bias in the distribution of UEs. On the other hand, ScanLine-based and MinDist-based maintained a capacity of at least 20 Mbps in all cases. In particular, stable capacity was obtained even in the situations of Case#3 and Case#5.

Figure 4.15 shows the difference in average capacity per UE between AP#1 and AP#2 for Case#1-5. RSSI-based yields extreme differences in Case#2-5. In particular, in Case#2
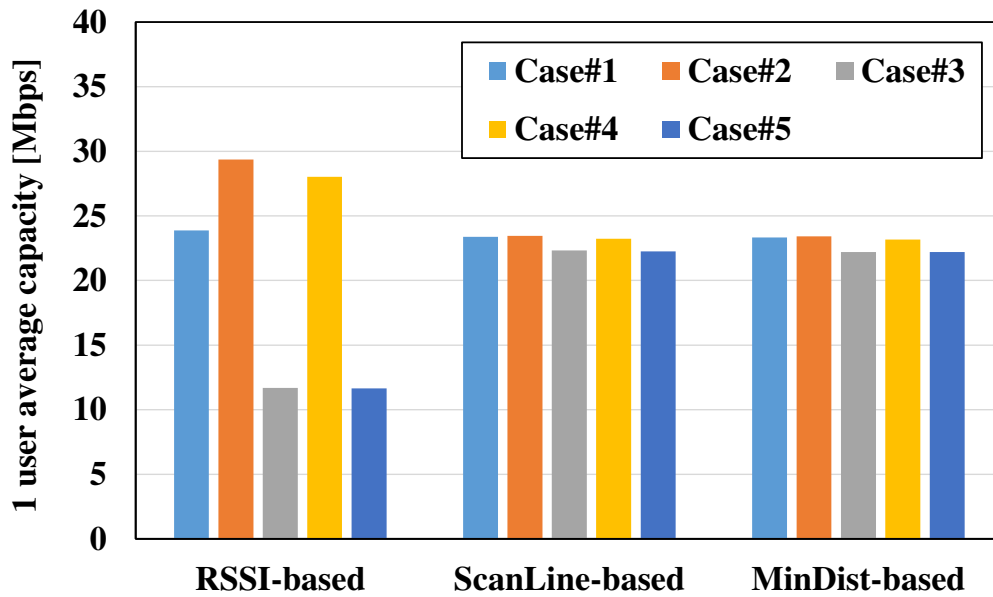
Fig. 4.14: Comparison of average capacity per UE in Case#1-5.
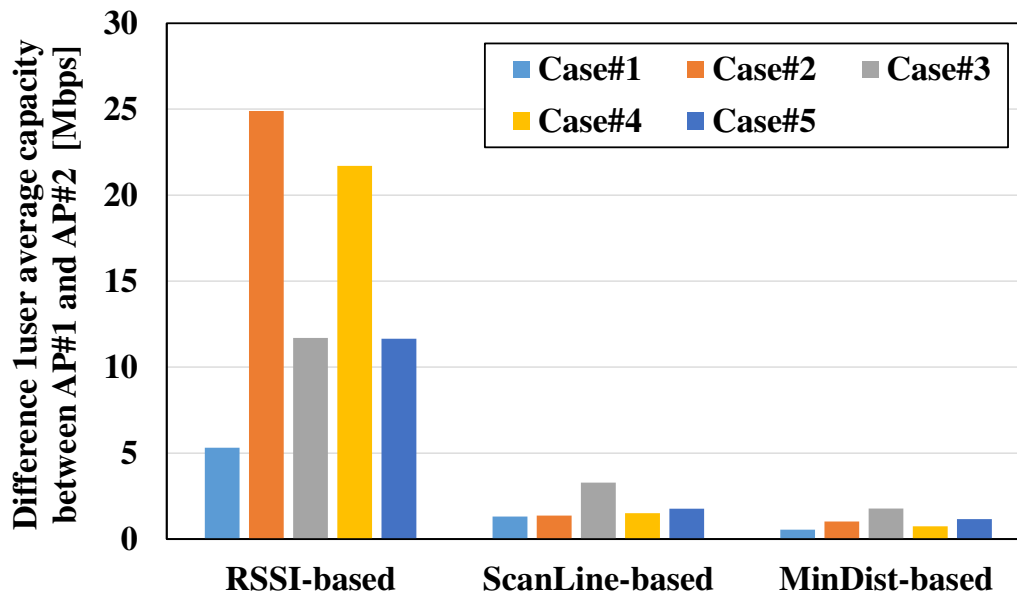
Fig. 4.15: Comparison of the difference in average capacity per UE between AP#1 and AP#2 in Case#1-5.

and Case#4, it can be seen from Fig. 4.15 that the difference in average capacity per UE exceeds 20 Mbps. In addition, there is a difference exceeding 10 Mbps in Case#3 and
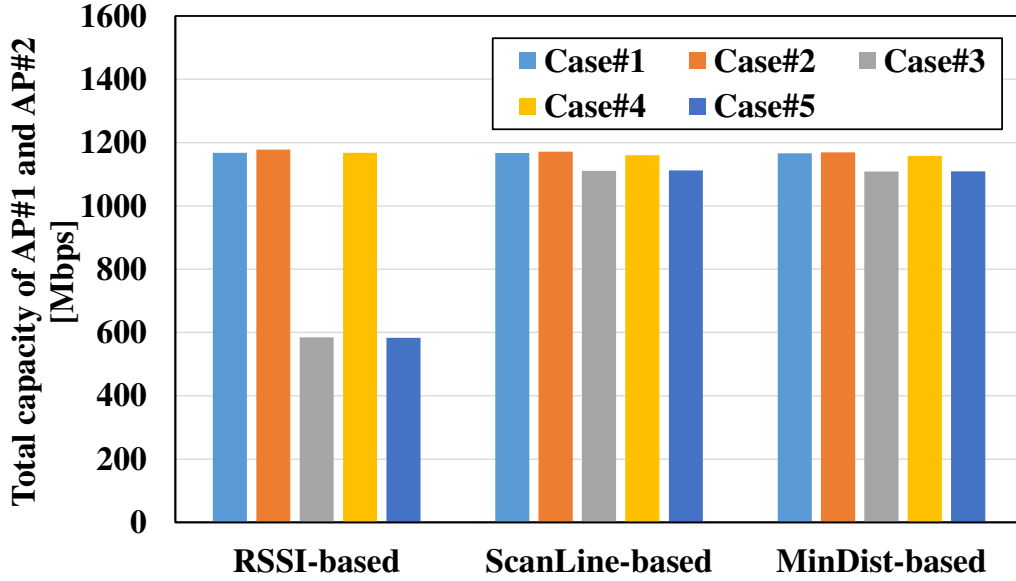
Fig. 4.16: Comparison of the total capacity of AP#1 and AP#2 in Case#1-5.

Case#5. On the other hand, ScanLine-based and MinDist-based reduced the difference to within 3 Mbps in all cases, with MinDist-based offering the smallest throughput difference. Here, the capacity difference increases according to the set value of c_{th} (i.e. capacity difference threshold). If c_{th} is set extremely small, the capacity difference may not converge within the set value stochastically. This depends on the number of UEs in the optical cell that should be controlled. Reducing the optical cell radius, stochastically reduces the number of UEs existing in the target optical cell. This makes it possible to reduce the average capacity difference.

Figure 4.16 shows the total capacity of AP#1 and AP#2. RSSI-based reduces the total capacity in Case#3 and Case#5. It can be said that the decrease in capacity is caused by the extreme bias in UE distribution. On the other hand, ScanLine-based and MinDist-based have slightly reduced total capacity in Case#3 and Case#5. However, they are superior to RSSI-based. This is because the UE is intentionally connected to an AP with
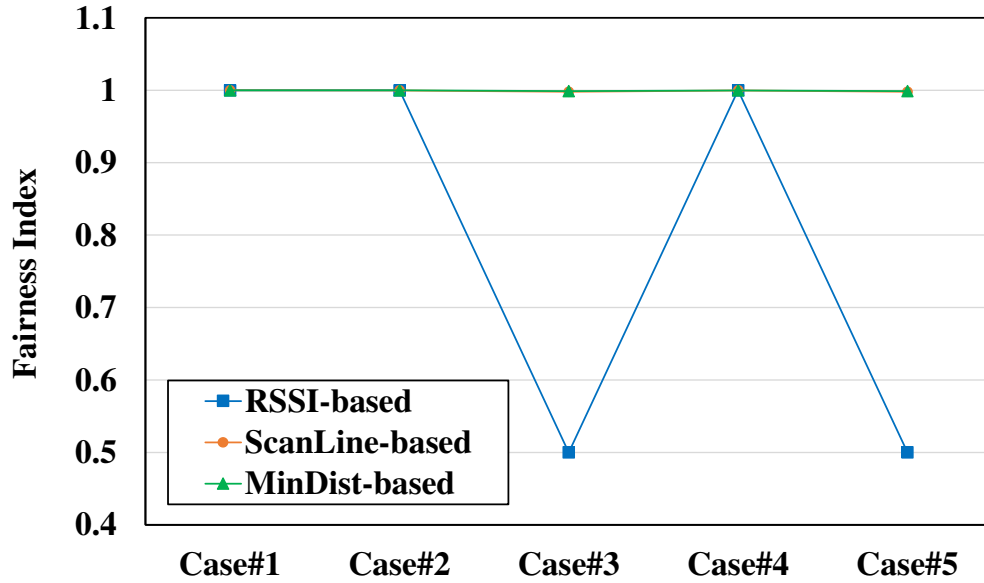
Fig. 4.17: Fairness Index between AP#1 and AP#2 in Case#1-5.

a small RSSI to avoid concentration on one AP. Here, the capacity of the UE depends on the RSSI. This is because the MCS changes the modulation scheme according to RSSI. In other words, UE capacity is reduced by intentionally connecting it to an AP with a small RSSI. However, in the proposal, the reduction in capacity is suppressed as much as possible by strategically selecting the optical cell to be offloaded in consideration of the positional relationship of the optical cell center and the AP.

Figure 4.17 shows the Fairness Index between AP#1 and AP #2. With reference to the results in Fig. 4.16, RSSI-based suffered a drop in Fairness Index in Case#3 and Case#5. However, ScanLine-based and MinDist-based offered improved fairness compared to RSSI-based. In particular, MinDist-based attained better Fairness Index values than ScanLine-based. Even if the wireless system frequency is changed to 5GHz, as long as each AP covers the wireless service area, the total capacity fluctuates slightly, but it does not significantly affect the results of the fairness index.
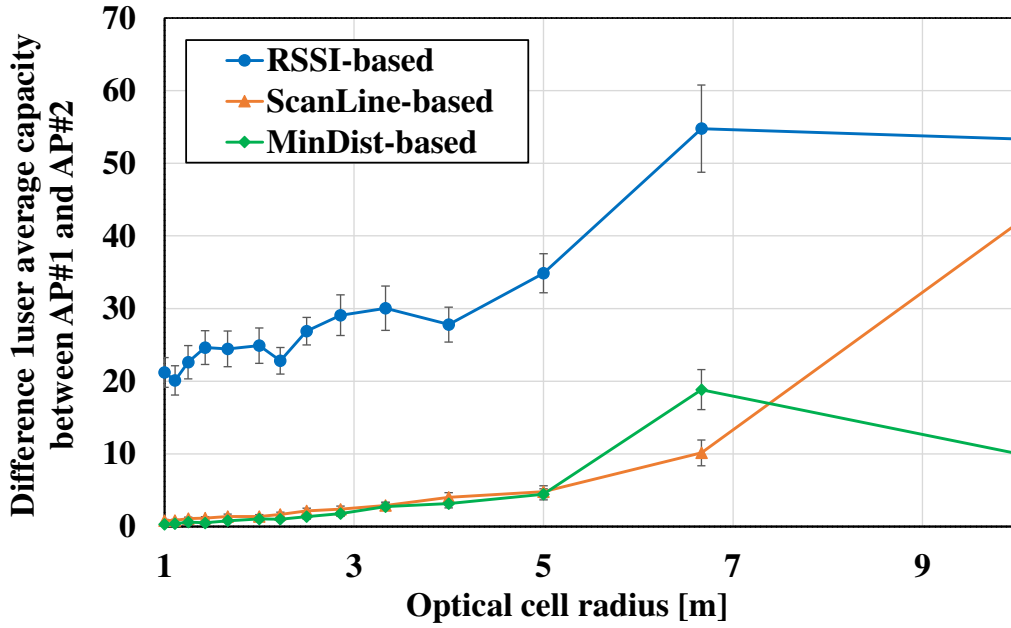
Fig. 4.18: Optical cell size dependence of the difference of UE capacity between AP#1 and AP#2 in Case#2.

4.4.3 Optical Cell Size Design

The design of the overlaid optical cell size is considered to be a parameter that affects the communication capacity and the difference among UEs. Therefore, we evaluated the difference in UE capacity and overall capacity as a function of optical cell size. Here, optical cell radius ranged from 1 m to 10 m. Among the five scenarios shown in Fig. 4.13, Case#2 and Case#3 with biased UE distribution were shown as examples. A random UE distribution was generated for the configurations of Case#2 and Case#3. The number of trials was set to 100, and the average value was calculated.

Figure 4.18 shows the optical cell size dependency of the average capacity difference per UE between AP#1 and AP#2 in Case#2. The legend shows the RSSI-based, ScanLine-based, and MinDist-based values. The 95 % confidence interval is also added. Under the condition of relatively large optical cell radius, all methods have a large average capacity
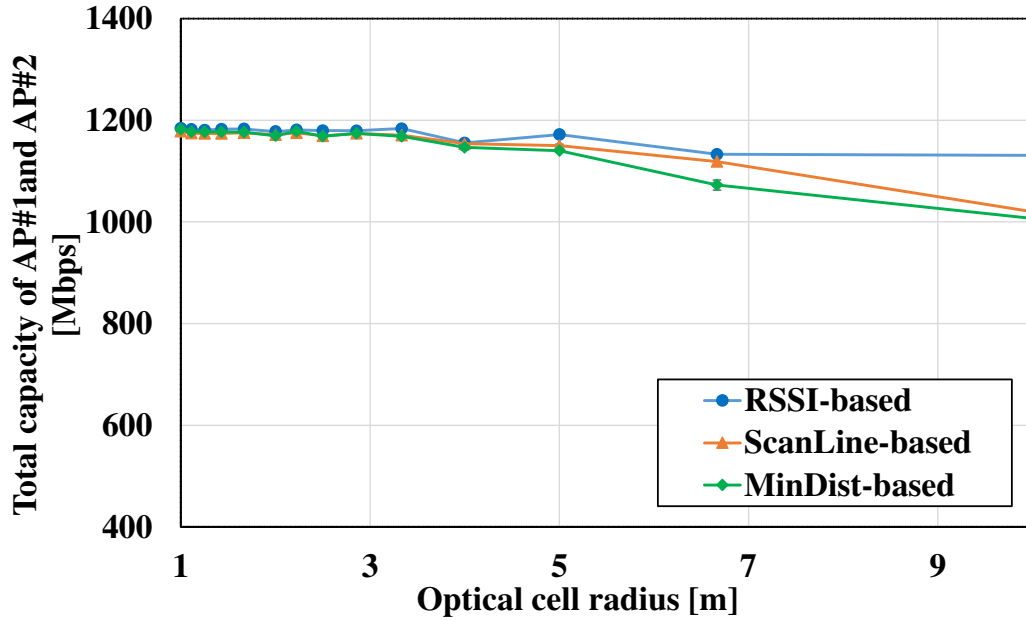
Fig. 4.19: The relationship between optical cell size and the total capacity of AP#1 and AP#2
in Case#2.

difference per UE between AP#1 and AP#2. This is because the number of UEs under one

optical cell is stochastically large, and the destination APs of many UEs are changed at

the same time. On the other hand, with relatively small optical cell radius, the number of

UEs under one optical cell is stochastically small, so the destination APs of only a small

number of UEs are changed at the same time. Therefore, by reducing the optical cell

radius, more fine-grained control can be achieved. Although RSSI-based shows a limited

improvement in the average capacity difference per UE, ScanLine-based and MinDist-

based offer a significant reduction in the average capacity difference per UE. Fig. 4.19

shows the relationship between optical cell size and the total capacity of AP#1 and AP#2

in Case#2. With relatively large optical cell radius, all methods suffer a drop in total

capacity. This can be attributed to the coarse granularity of the connection control. On the

other hand, it can be seen that the total capacity is improved by decreasing the optical cell
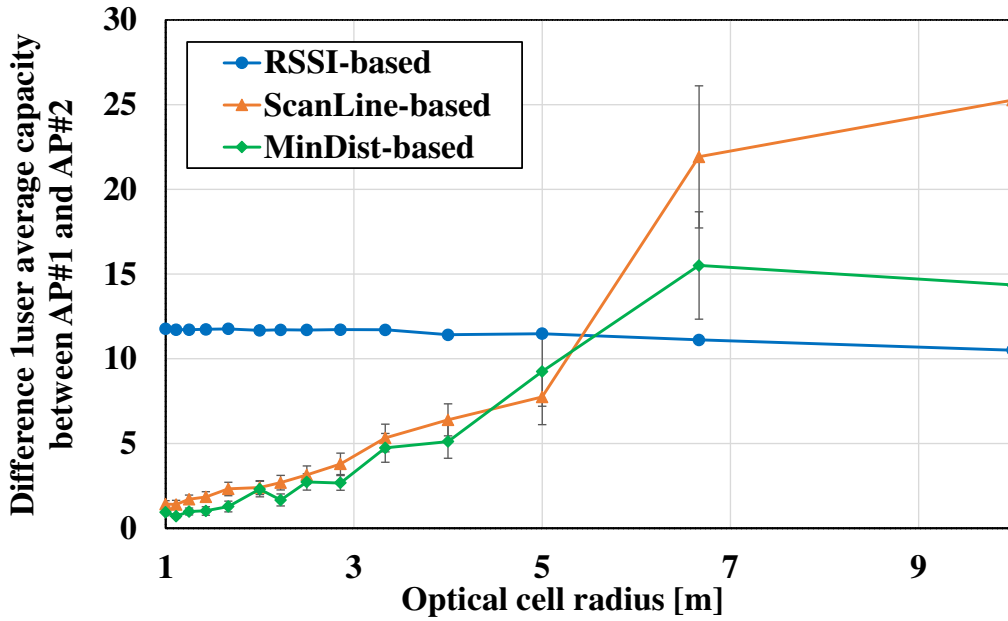
Fig. 4.20: Optical cell size dependence of the difference of UE capacity between AP#1 and AP#2 in Case#3.

radius.

Figures 4.20 and Fig. 4.21 show the average capacity difference per UE and the total capacity of AP#1 and AP#2 in the extreme UE distribution scenario of Case#3. In Case#3, UE distribution is more concentrated than in Case#2, and all UEs are assigned to AP#1 with RSSI-based. However, ScanLine- based and MinDist-based force the UEs in some optical cells to connect to AP#2, which has a lower RSSI, thereby preventing all UEs from connecting to AP#1. Fig. 4.20 shows that RSSI-based does not reduce the average capacity difference per UE, even if the optical cell radius is reduced. This is due to the fact that all UEs are attributed to AP#1. On the other hands, ScanLine-based and MinDist-based improve the average capacity difference compared to RSSI-based, with the demarcation point around 5 m. In addition, by further reducing the optical cell radius, the capacity difference is further improved with ScanLine-based and MinDist-based. These
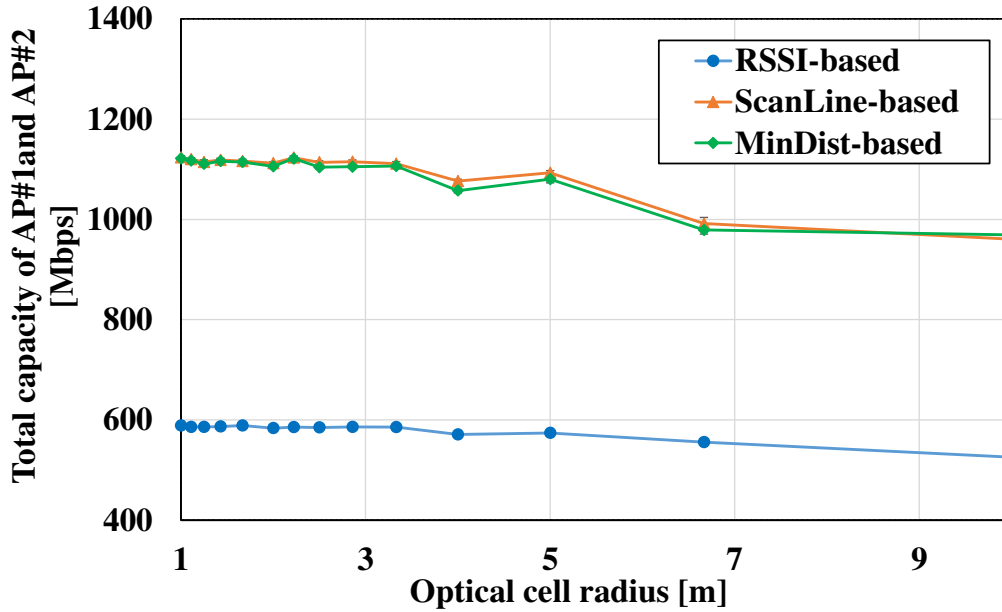
Fig. 4.21: The relationship between optical cell size and the total capacity of AP#1 and AP#2 in scenario Case#3.

results show that using more fine-grained optical cell control, using our ScanLine-based and MinDist-based methods, enables fair wireless connections between APs. As can be seen from Fig. 4.21, it is shown that the total capacity of RSSI-based is smaller than that of ScanLine-based and MinDist-based. This is also due to the fact that all UEs were biased towards AP#1, as described in Fig. 4.20. It can be clearly seen that the total capacity is improved by reducing the optical cell radius with ScanLine-based and MinDist-based.

Figures 4.22 and Fig. 4.23 summarize the comparison of RSSI-based and proposal in Case#1-5. Fig. 4.22 shows the results of the capacity difference per user between AP#1 and AP#2 in ScanLine-based and MinDist-based compared to RSSI-based. The vertical axis, Δdifference 1user capacity, represents the absolute difference between the RSSI-based 1user average capacity and the ScanLine-based/MinDist-based 1user average capacity. In other words, it means that the proposed method has superior performance in
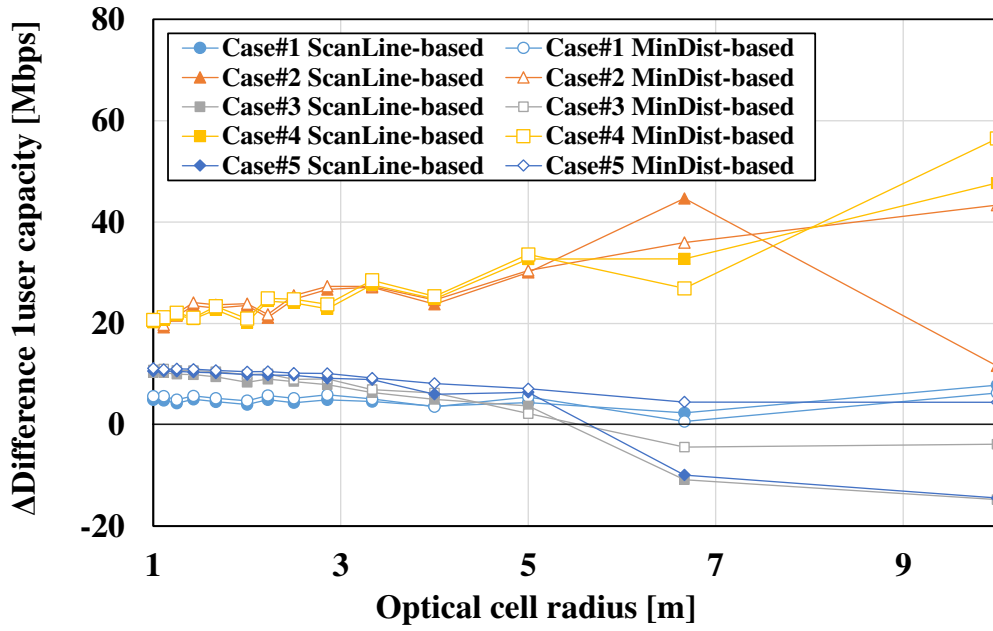
Fig. 4.22: The comparison result with RSSI-based in the difference of UE capacity between AP#1 and AP#2 for all scenario.

the region where Δdifference 1user capacity is a positive value (i.e. the capacity difference per user can be reduced compared to RSSI-based). From Fig. 4.22, with optical cell radius of 5 m or less, the proposal reduced the capacity difference per user compared to the RSSI-based in all scenarios.

Figure 4.23 shows the total capacity of ScanLine-based and MinDist-based compared to RSSI-based. The vertical axis Δtotal capacity represents the absolute difference between the average total capacity of RSSI-based minus the average total capacity of ScanLine-based/MinDist-based. In other words, in the region where Δtotal capacity is negative, the proposed method improves the total capacity compared with RSSI-based. From Fig. 4.23, it is understood that the improvement in total capacity by the proposed method is remarkable in Case#3 and Case#5 as compared with the other cases. In the other cases, RSSI-based has higher total capacity. However, by reducing the optical cell radius, the difference in total capacity between the RSSI-based and the proposal becomes
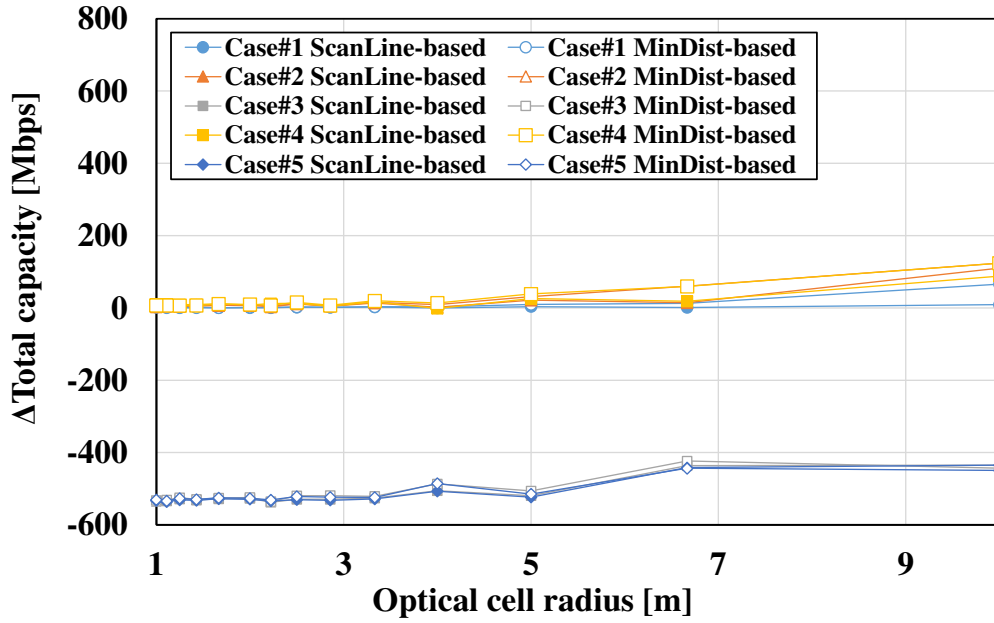
Fig. 4.23: The comparison result with RSSI-based in the total capacity between AP#1 and AP#2 for all scenario.

smaller. At 5 m or less, use of the proposed method suppresses the deterioration to just a few several percent of the expected maximum total capacity.

These results indicate that by making the optical cell smaller, the average capacity difference per user can be reduced and total capacity can be improved. A reduction in optical cell size means a stochastic decrease in the number of UEs existing in the optical cell. Therefore, by making the optical cell smaller, we approach personal connection control for each UE. Depending on cell size, the proposed method is closer to the case of trying to acquire the individual position of the user as in related research. As already mentioned, many methods for grasping UE position have been studied and are advancing day by day. However, for highly accurate position estimation, it is necessary to attach a new device to the UE or modify the UE [44, 86, 45, 87]. In contrast, our proposal does not specifically need to collect the location of the UE itself. It also allows location-based

control without changing UE/AP or adding devices on the wireless system side. Since RSSI-based location awareness is utilized in [83], the RSSI map is formed in the AP based on the RSSI of the signal received from the UE. The relative position of the UE determines the connection to the AP. However, since [83] collects only the position relative to the AP, it offers inadequate connection control according to the area, which is one of the goals of our system. (i.e., flexibly constructing a wireless connection restriction area or connectable area within the wireless service area) Furthermore, another originality of our proposal is the optical cell control algorithm. In our algorithm, the optical cell that offers less capacity reduction is selected from among many optical cells in consideration of the positional relationship between the optical cell center and the APs. Strategic optical cell control that also takes into account the optical cell radius reduces the average capacity difference per user while reducing the capacity deterioration in extremely biased user distribution scenarios.

It is also important to note that there is a trade-off between the granularity of equipment placement and performance improvement. It is necessary to design optical cell radius that take into account the cost of equipment and the performance improvement from each perspective.

4.5   Summary

In this chapter, we have proposed a novel wireless control architecture that applies optical wireless to the control plane of wireless LAN systems. To reduce the deployment barrier, we proposed a software-based optical ID transmission and reception scheme using consumer-based smart IoT lighting and the illumination sensors widely implemented in smartphones. Experiments confirmed that the proposed OE algorithm reduces the error rate compared to the existing optical correlation-based receiving scheme, while the FA

algorithm can shorten the authentication cycle, which is a challenge when using OE. The results of the experiments showed that the combined use of OE and FA can reduce the authentication cycle by 62.5 % (1200 ms to 450 ms) and reduce the error rate compared to existing methods.

Furthermore, we also proposed two optical cell control algorithms (i.e. ScanLine-based and MinDist-based) to guarantee high network quality against temporal variations in UE location density. Compared to the existing RSSI-based scheme, our proposals showed improvements in terms of average per-user capacity difference and fairness among APs, while maintaining the total capacity in several highly-skewed UE distribution scenarios. In addition, for optical cell design, an evaluation against optical cell radius was performed. It was shown that the average per-user capacity difference between APs and the overall capacity are improved as the optical cell radius is reduced. In particular, the optical cell radius of 5 m was found to be the threshold for improving the average capacity difference per user. Since there is a trade-off between installation granularity and the resulting performance improvement, it is necessary to deploy optical cells considering each aspect.

Chapter 5

Conclusion

This paper proposes a technology to solve the problems in two aspects for the future optical access network. The first is an optical network accommodating technology for optical re-transmission service of broadcast signals, which aims to integrate various services into an optical access network efficiently and economically from the operator's point of view. The second technology is a wireless local area network (LAN) system technology that aims to realize high-quality services even in a high-density environment by utilizing optical resources for wireless LAN services, which is one of the promising services accommodated in optical access networks. The following is a summary of the results obtained in Chapter 2 to 4, and concludes.

In Chapter 2, we have proposed an optical re-transmission system that applies digitized radio-over-fiber (DRoF) technology in order to realize optical re-transmission of broadcast signals via a shared optical network for communication. By applying DRoF technology, the following advantages can be obtained by providing the same coaxial interfaces as before at both ends of the optical network.

- Reduce capital expenditure / operating expenditure (CAPEX / OPEX) by utilization of sharing the optical network.

- Achieves a significant reduction in the number of re-transmission facility due to a significant increase in transmission distance.

- By utilizing the coaxial interface, community antenna television (CATV) operators can reduce the barriers to implementation and use the subscribers' television (TV) viewing environment as it is.

In DRoF-based systems, since the radio frequency (RF) signal is directly digitized, the increase in transmission rate becomes a serious technical problem. To address this issue, we investigated an approach to realize quantization bit reduction to reduce the transmission rate. Through the signal-to-noise ratio (SNR) analysis of the system, it is shown that the number of quantization bits in the analog-to-digital converter (ADC) of DRoF-transmitter (Tx) has a significant impact on the received carrer-to-noise ratio (CNR). 7-bit quantization is the minimum number of quantization bits to satisfy the requirements of DRoF-receiver (Rx) output. To further reduce the number of quantization, we have proposed improved nonlinear quantization (INL), which combines signal clipping and nonlinear quantization to quantize the signal according to the probability distribution characteristics of the target signal. The proposal is a low-cost and simple way to realize receivers in subscriber's side. In order to show the effect of the proposal, an optical re-transmission experiment using a commercial 9ch multiplexed digital terrestrial broadcasting (DTT) signal was carried out. In the experiment, it was confirmed that 7-bit transmission is possible when the method of reducing the number of quantization bit is not applied. This was the same as the theoretically derived result. On the other hand, INL has shown that 5-bit transmission is possible. This means that it can be further reduced compared to the 6-bit result of the existing Mu-law. In terms of transmission rate reduction, INL achieved a 28.6% reduction. Therefore, it was confirmed that it is possible to transmit at 0.625 Gbps when collectively transmitting 9 ch of DTT signal. These results indicate that the proposed DRoF-based optical re-transmission system can accommodate

digital terrestrial broadcasting service even in the current 10G-class or 1G-class communication passive optical network (PON) systems.

Chapter 3 described an approach for achieving adaptive transmission rate reduction, focusing on satellite broadcasting signals such as broadcasting satellite (BS) / communications satellite (CS). BS / CS, which is propagated using a super-high frequency (SHF) band of 11GHz to 12GHz, is affected by rainfall attenuation during radio propagation compared to DTT of ultra-high frequency (UHF) band. Therefore, the input signal CNR at the head-end of the optical re-transmission facility fluctuates, and as a result, the input CNR to the DRoF-Tx also fluctuates. When the CNR of received signal changes, the acceptable CNR margin in the network section also changes. Since there is a trade-off between the signal compression ratio and the signal quality at the network, it is necessary to relax the compression ratio by assuming the worst case of the received signal at the head-end in order to satisfy the required CNR at the receiver. Therefore, in order to reduce the transmission rate as much as possible against the fluctuation of CNR due to rainfall attenuation, we have proposed a DRoF-based adaptive optical re-transmission system based on combination compression. The proposed system achieves the highest possible compression ratio while satisfying the required CNR of DRoF-Rx by dynamically assigning compression parameters according to the input CNR. In the proposal, based on the INL shown in chapter 2, three parameters (i.e. signal quantization number, clipping depth, and nonlinear constant) are dynamically assigned. In our approach, first, we modeled the received CNR at the head-end using the prediction model of ITU-R P.618-13 in order to utilize the statistical index of rainfall attenuation. Furthermore, in order to show the effect of adaptive compression, an optical re-transmission experiment of ultra-high definition (UHD) -BS signal 11ch was performed.

The required quantization bit was experimentally confirmed for the modeled received CNR at head-end. Throughout the experiment, the average quantization bit number for the service operation time was 8.000-bit for the conventional fixed quantization, while it was 3.000-bit for the proposal. It was shown that 99.978% of service time can be covered by 3-bit quantization. In terms of transmission rate, an average reduction of 62.5% was achieved compared to fixed quantization. By applying our proposal, it was clarified that the transmission rate when multiplexing 11ch UHD-BS signals is 5.75 Gbps at the peak and 3.45 Gbps at the minimum. From the viewpoint of transmission rate, it was difficult to accommodate satellite broadcasting signals in a 1G class PON system. However, it has been revealed that the current 10G class PON system is sufficient to support these signals. By applying the proposal, the transmission rate when multiplexing 11ch UHD-BS signals is 5.75Gbps at the peak and 3.45Gbps at the minimum. From the standpoint of transmission rates, it is difficult to accommodate satellite broadcast signals on a 1G-class PON system even if the proposed compression technology is applied. However, it has been shown that the current 10G-class PON system is sufficient to accommodate these signals.

On the other hand, the service perspective of the proposed system will be discussed below. The media is diversifying, especially among young people, and the proportion required to watch TV is declining. However, looking at all ages of the population, it is thought that TV viewing still accounts for a large proportion of the time spent in various media [2]. In addition, in the video content market in Japan, the market size of RF content such as terrestrial broadcasting, satellite and CATV broadcasting shows a high proportion [2]. It can be inferred that these market structures will be maintained in the short to medium term. On the other hand, the market structure may change in the long run. In

response to future changes in the market structure, it will be possible to extend some of the proposed technologies to future applications.

The feature of the proposed system is that the RF signal waveform is directly digitized and transmitted, so the signal is transmitted while maintaining the radio wave information. This makes it possible to transmit information without depending on the wireless system, and is expected to be applied to various applications. For example, it is possible to consider the application of the proposed system as a means to realize centralization of base station functions of multiple wireless systems and simplification of deployed antennas. In addition, the proposed system can be expected to be applied to use cases where wireless areas are expanded via a network and direct communication is performed among terminals.

Chapter 4 focused on wireless LAN services among the services accommodated in optical access network, and showed the wireless LAN system architecture for the realization of high-quality wireless service. We have shown a solution that utilizes optical resources to solve the problem that it is difficult to provide location-aware services with conventional wireless LAN system. Specifically, we have proposed a wireless LAN system architecture that divides the wireless LAN service area into small cells using a light source and controls the access point (AP) connection destination for each small cell. This system realizes location-based user equipment (UE) connection control using the positional relationship between the optical cell and the AP. The following advantages can be obtained by our system.

- Location-aware wireless control can be realized without actively acquiring location information from the UE.

- Enables the construction of flexible accessible/inaccessible areas for wireless LAN

services.

In the proposed system, the optical identifier (ID) corresponding to the AP connection information is transmitted to the UE under the optical cell. In order to realize low cost transmission and reception of optical ID without using a dedicated transmitter / receiver, we proposed an optical ID transmission / reception method that utilizes (Internet of Things) IoT smart lighting and a smartphone illuminance sensor. The first is the oversampled edge-excluded receiving scheme (OE). In order to reduce the reception error rate of optical ID, OE oversamples and carryout a majority decision by window processing. The second is the fast authentication scheme (FA), which aims to suppress the increase in the matching cycle of optical ID caused by the application of OE. FA is a correlation-based reception method that uses a bit-circulated optical ID array. An experimental evaluation of the reception error rate and matching cycle was performed using a UE with OE and FA. It was confirmed that the application of OE can significantly reduce reception errors compared to the conventional. It was also shown that the application of FA can reduce the matching cycle by 62.5% while applying OE compared to the conventional.

Furthermore, in order to realize location-aware wireless control, which is one of the features of the proposed system, we proposed two optical cell control algorithms for the deterioration of communication quality caused by temporal fluctuations in user distribution. One is ScanLine-based, which changes the optical cell in a scanning line according to the average capacity of the UE. The other is MinDist-based, which changes the optical cell according to the average capacity of the UE, considering the positional relationship between the AP and the optical cell. These two algorithms were evaluated by five scenario-based simulations that simulated the distribution bias of the UE. As a result

93

of the evaluation, it was confirmed that the improvement of 1 user capacity difference among APs and fairness among APs were confirmed while maintaining the total capacity in APs for various distribution scenarios of UEs. It was also found that the optical cell radius that can confirm the effectiveness of the proposal is 5 m or less. The control particle size becomes smaller by increasing the number of installed light sources and making the optical cell radius smaller. This is expected to improve performance. However, the introduction of light sources incurs costs and increases with the number. Therefore, since there is a trade-off in terms of performance improvement and cost, it is necessary to consider both perspectives. Through these results, we can conclude that the application of optical wireless to the control plane of wireless LAN enables location aware service provision and the effectiveness of its communication quality improvement effect has been realized.

As for the outlook for the service deployment of the proposed system, for example, in commercial facilities, the separation of wireless service areas and the improvement of wireless service quality can be considered. One of the features of the proposal system is that it is possible to perform authentication and connection control according to the position without collecting the user's position, so it is possible to perform authentication according to the area. This makes it possible to separate the wireless service area from the rest of the area. In addition, connection control according to the position is realized for user terminals in the separated service provision area. However, there are future works for service provision. It will be necessary to make detailed settings for the light source assuming the actual service environment. Specifically, in the actual service environment, there are various restrictions such as the placement position and height of the lighting, so it is necessary to adjust the light source illuminance and automate the optical cell design

in consideration of these restrictions.

Finally, in future access networks, we hope that DRoF-based system technology will become one of the basic technologies to realize efficient and economical accommodation of optical re-transmission service. We also hope that a wireless LAN system that utilizes optical wireless will be one solution for further improvement of communication services.

Reference

[1]   Hiromichi Shinohara, "FTTH experiences in Japan," *Journal of Optical Networking*, vol. 6, no. 6, pp. 616-623, May 2007.

[2]   "Information and communication in Japan, Chapter4: Basic Data on the ICT Field," Ministry of Internal Affairs and Communications, Japan, White Paper 2020, Dec. 2020. (in Japanese)

[3]   J. Prat, "Next-Generation FTTH Passive Optical Networks: Research Towards Unlimited Bandwidth Access," Springer, New York, USA, 2008

[4]   E. Harstead, "25G Based PON Technology," *Proc. 2018 Optical Fiber Communications Conference and Exposition* (*OFC*), pp. 1-3, Mar. 2018.

[5]   V. Houtsma and D. van Veen, "Optical Strategies for Economical Next Generation 50 and 100G PON," *Proc. 2019 Optical Fiber Communication Conference* (*OFC*), pp. 1-3, Mar. 2019.

[6]   S. Nishihara, M. Hajduczenia, H. Mukai, H. Elbakoury, R. Hirth, M. Kimura, and M. Kato, "Power-saving methods with guaranteed service interoperability in Ethernet passive optical networks," *IEEE Commun. Mag.*, vol. 50, no. 9, pp. 110-117, Sept. 2012.

[7]   R. Kubo, J. Kani, Y. Fujimoto, N. Yoshimoto and K. Kumozaki, "Sleep and Adaptive Link Rate Control for Power Saving in 10G-EPON Systems," *Proc. 2019 IEEE Global Telecommunications Conference* (*GLOBECOM*), pp. 1-6, Dec. 2009.

[8]   R. Kubo, J. Kani, Y. Fujimoto, N. Yoshimoto, and K. Kumozaki, "Adaptive power saving mechanism for 10 Gigabit class PON systems," *IEICE Trans. Commun.*, vol. E93-B, no. 2, pp. 280-288, Feb. 2010.

[9] A. M. Mikaeil, W. Hu, T. Ye and S. B. Hussain, "Performance evaluation of XG-PON based mobile front-haul transport in cloud-RAN architecture," *Journal of Optical Communications and Networking*, vol. 9, no. 11, pp. 984-994, Nov. 2017.

[10] T. Kobayashi, H. Ou, D. Hisano, T. Shimada, J. Terada and A. Otaka, "Bandwidth allocation scheme based on simple statistical traffic analysis for TDM-PON based mobile fronthaul," *Proc. 2016 Optical Fiber Communication Conference* (*OFC*), pp. 1-3, Mar. 2016.

[11] S. Zhou, X. Liu, F. Effenberger and J. Chao, "Mobile-PON: A high-efficiency low-latency mobile fronthaul based on functional split and TDM-PON with a unified scheduler," *Proc. 2017 Optical Fiber Communication Conference* (*OFC*), pp. 1-3, Mar. 2017.

[12] Hiroyuki Uzawa, Kazuaki Honda, Hirotaka Nakamura, Yukio Hirano, Ken-ichi Nakura, Seiji Kozaki, and Jun Terada, "Dynamic bandwidth allocation scheme for network-slicing-based TDM-PON toward the beyond-5G era," *Journal of Optical Communications and Networking*, vol. 12, no. 2, pp. A135-A143, Feb. 2020.

[13] T. Yokotani, "Application and technical issues on Internet of Things," *Proc. the 10th International Conference on Optical Internet* (*COIN*), pp. 67-68, May 2012.

[14] M. M. Alenazi, B. A. Yosuf, T. El-Gorashi and J. M. H. Elmirghani, "Energy Efficient Neural Network Embedding in IoT over Passive Optical Networks," *Proc. 22nd International Conference on Transparent Optical Networks* (*ICTON*), pp. 1-6, July 2020.

[15] H. Q. Al-Shammari, A. Lawey, T. El-Gorashi and J. M. H. Elmirghani, "Energy Efficient Service Embedding In IoT over PON," *Proc. 21st International Conference on Transparent Optical Networks* (*ICTON*), pp. 1-5, 2019.

[16] Jun-ichi Kani, Manabu Yoshino, Kota Asaka, Hirotaka Ujikawa, Takashi Yamada, Keita Nishimoto, Ken-Ichi Suzuki, and Akihiro Otaka, "Flexible Access System Architecture (FASA) to Support Diverse Requirements and Agile Service Creation," *Journal of Lightwave Technology*, vol. 36, no. 8, pp. 1510-1515, April 2018.

[17] F. Slyne, A. Elrasad, C. Bluemm and M. Ruffini, "Demonstration of Real Time VNF Implementation of OLT with Virtual DBA for Sliceable Multi-Tenant PONs," *Proc. 2018 Optical Fiber Communications Conference and Exposition* (*OFC*), pp. 1-3, Mar. 2018.

[18] M. Tadokoro, K. Nishimoto, T. Mochida, T. Tanaka, T. Yamada, A. Takeda, and T. Inoue, "Design of softwarized EPON OLT and its transmission jitter suppression techniques over MPCP," *Proc. 2017 Optical Fiber Communications Conference and Exposition* (*OFC*), pp. 1-3, Mar. 2017.

[19] N.Egi, D.Ikegami, J.Okamoto, T.Shobudan, "A Study on QoE geographic visualizing model for mobile network services," *IEICE Technical Report*, vol. 118, no. 192, pp. 95-99, Aug. 2018.

[20] A. Valenti, A. Rufini, S. Pompei, F. Matera, S. Di Bartolo, C. Da Ponte, D. Del Buono, G. Tosi Beleffi, "QoE and QoS comparison in an anycast digital television platform operating on passive optical network," *Proc. 2012 15th International Telecommunications Network Strategy and Planning Symposium* (*NETWORKS*), pp. 1-6, Oct. 2012.

[21] F. Aurzada, M. Lévesque, M. Maier and M. Reisslein, "FiWi Access Networks Based on Next-Generation PON and Gigabit-Class WLAN Technologies: A Capacity and Delay Analysis," *IEEE/ACM Transactions on Networking*, vol. 22, no.

4, pp. 1176-1189, Aug. 2014.

[22] Satou, Hiroaki. "State and Issues of Video Delivery on IP Networks," *IEICE Technical Report*, vol. 110, no. 119, pp. 39-44, 2010.

[23] T. Shitaba, T. Taniguchi, H. Shimizu, T. Fujiwara, H. Yoshinaga and T. Sugawa, "Feasibility Study on In-Band Unidirectional ONU Control of the 10G-class WDM Overlaid Digital Baseband UHD Video Distribution System," *Proc. 42nd European Conference on Optical Communication* (*ECOC*), pp. 1-3. Sept. 2016.

[24] R. Gaudino, V. Curri and S. Capriata, "Propagation impairments due to Raman effect on the coexistence of GPON, XG-PON, RF-video and TWDM-PON," *Proc. 39th European Conference and Exhibition on Optical Communication* (*ECOC*), pp. 1-3. Sept. 2013.

[25] Toshiaki Shibata, Tomoaki Yoshida, Jun Terada, "Optical Video Transmission Technique using FM conversion," *IEICE Technical Report*, vol. 2019-AVM-107, no. 18, pp. 1-5, Nov. 2019.

[26] "Transmission equipment for multi-channel television signals over optical access networks by sub-carrier multiplexing (SCM)," *Rec. ITU-T J.186*, June 2008.

[27] M. Khanal, C. J. Chae and R. S. Tucker, "Selective broadcasting of digital video signals over a WDM passive optical network", *IEEE Photon. Technol. Lett.*, vol. 17, no. 9, pp. 1992-1994, Aug. 2005.

[28] "Transmission equipment for transferring multi-channel television signals over optical access networks by frequency modulation conversion," *Rec. ITU-T J.185*, June 2012.

[29] A. Nirmalathas, P. A. Gamage, C. Lim, D. Novak and R. Waterhouse, "Digitized Radio-Over-Fiber Technologies for Converged Optical Wireless Access Network,"

Journal of Lightwave Technology, vol. 28, no. 16, pp. 2366-2375, Aug. 2010.

[30] A. Nirmalathas, P. A. Gamage, C. Lim, D. Novak, R. Waterhouse and Y. Yang, "Digitized RF transmission over fiber," *IEEE Microwave Magazine*, vol. 10, no. 4, pp. 75-81, June 2009.

[31] D. Novak et al., "Radio-Over-Fiber Technologies for Emerging Wireless Systems," *IEEE Journal of Quantum Electronics*, vol. 52, no. 1, pp. 1-11, Jan. 2016.

[32] P. Roshan and J. Leary, "802.11 Wireless LAN Fundamentals," Cisco, San Jose, CA, USA, 2005.

[33] Hongqiang Zhai, Xiang Chen and Yuguang Fang, "How well can the IEEE 802.11 wireless LAN support quality of service?," *IEEE Transactions on Wireless Communications*, vol. 4, no. 6, pp. 3084-3094, Nov. 2005.

[34] Reyes-Menendez, A., Palos-Sanchez, P.R., Saura, J.R., Martin-Velicia, F., "Understanding the influence of wireless communications and Wi-Fi access on customer loyalty: A behavioral model system," *Wireless Communications and Mobile Computing*, vol. 2018, pp. 1–16, Dec. 2018.

[35] Won Seok Lee, Joonho Moon and Myungkeun Song, "Attributes of the coffee shop business related to customer satisfaction," *Journal of Foodservice Business Research*, vol. 21, no. 6, pp. 628–641, Oct. 2018.

[36] Noorhaiza Masri, Faiz Izwan Anuar and Astri Yulia, "Influence of Wi-Fi service quality towards tourists' satisfaction and dissemination of tourism experience," *Journal of Tourism, Hospitality and Culinary Arts*, vol. 9, no. 2, pp. 383–397, Oct. 2017.

[37] Jiyeon Jeon, Myongjee Yoo, Natasa Christodoulidou, " The impact of Wi-Fi service on millennial diners," *Journal of Hospitality and Tourism Technology*, vol. 10, no.

3, pp. 383-400, June 2019.

[38] Weiping Sun, Okhwan Lee, Yeonchul Shin, Seongwon Kim, Changmok Yang, Hyoil Kim and Sunghyun Choi, "Wi-Fi Could Be Much More," *IEEE Commun. Mag.*, vol. 52, no. 11, pp. 22-29, 2014.

[39] Hui Luo, "A secure server-paid hot spot Wi-Fi Internet service method," in Proc. IEEE 6th Circuits and Systems Symposium on Emerging Technologies: Frontiers of Mobile and Wireless Communication, Shanghai, China, pp. 1-12, June 2004.

[40] Mishra Arunesh, Minho Shin, and William Arbaugh, "An Empirical Analysis of the IEEE 802.11 MAC layer Handoff Process," *ACM Computer Communications Review*, vol. 33, no. 2, pp. 93-102, 2003.

[41] H.Kobayashi, E.Kameda, Y.Terashima and N.Shinomiya," Towards sustainable heterogeneous wireless networks: A decision strategy for AP selection with dynamic graphs," *Computer Networks*, vol. 136, pp. 99-107, Feb. 2018.

[42] H. Velayos, V. Aleo and G. Karlsson, "Load balancing in overlapping wireless LAN cells," *Proc. 2004 IEEE International Conference on Communications* (*ICC*), pp. 3833-3836, June 2004.

[43] U. Shafi, M. Zeeshan, N. Iqbal, N. Kalsoom and R. Mumtaz, "An Optimal Distributed Algorithm for Best AP Selection and Load Balancing in WiFi," *Proc. 15th International Conference on Smart Cities: Improving Quality of Life Using ICT & IoT* (*HONET-ICT*), pp. 65-69, Oct. 2018.

[44] Lok Wai Jacky Tsay, Tomoo Shiigi, Zichen Huang, Xunyue Zhao, Tetsuhito Suzuki, Yuichi Ogawa and Naoshi Kondo, "Temperature-Compensated Spread Spectrum Sound-Based Local Positioning System for Greenhouse Operations, " IoT, vol. 1, no. 2, pp. 147-160, July 2020.

[45] A. Sobehy, E. Renault and P. Muhlethaler, "NDR: Noise and Dimensionality Reduction of CSI for Indoor Positioning Using Deep Learning," *Proc. 2019 IEEE Global Communications Conference (GLOBECOM)*, pp.1-6, Dec. 2019.

[46] M. Uysal and H. Nouri, "Optical wireless communications - An emerging technology," *Proc. 16th International Conference on Transparent Optical Networks (ICTON)*, pp. 1-7, July 2014.

[47] X. Bao, G. Yu, J. Dai, and X. Zhu, "Li-Fi: Light fidelity-a survey," *Wireless Netw.*, vol. 21, no. 6, pp. 1879-1889, Jan. 2015.

[48] F. Coppinger and D. Piehler, "RF video overlay in an Ethernet passive optical network," *Proc. 2006 Optical Fiber Communication Conference (OFC)*, pp. 1-3, Mar. 2006.

[49] M. Cantono, V. Curri and R. Gaudino, "Raman Crosstalk Suppression in NG-PON2 Using Optimized Spectral Shaping," *Journal of Lightwave Technology*, vol. 33, no. 24, pp. 5284-5292, Dec. 2015.

[50] J. Bae, J. Song, S. Ra, D. Choi and N. Hur, "A study on common phase rotation compensation for coaxial transmission systems in the HFC network," *Proc. 2015 International Conference on Information and Communication Technology Convergence (ICTC)*, pp. 159-163, Oct. 2015.

[51] D. Umeda, T. Ikagawa, K. Yamazaki, N. Hirakata and K. Yamagishi, "Bidirectional 3R Repeater for GE-PON Systems," *Proc. 2006 European Conference on Optical Communications (ECOC)*, pp. 1-2, Sept. 2006

[52] Noise Figure Measurement Methods [Online]. Available: https://dl.cdn-anritsu.com/en-en/test-measurement/files/Application-Notes/Application-Note/ms269xa-2830a-017-ef1300.pdf, 2016.

[53] A. Hajimiri and T. H. Lee, "A general theory of phase noise in electrical oscillators," *IEEE Journal of Solid-State Circuits*, vol. 33, no. 2, pp. 179-194, Feb. 1998.

[54] William H. Tranter, "Principles of communication systems simulation with wireless applications," Prentice Hall, pp-68, Jan. 2004.

[55] R. G. Lyons, "Reducing ADC quantization noise," *Microwaves and RF Magazine*, pp. 10–21, June 2005.

[56] B. Brannon, "Sampled systems and the effects of clock phase noise and jitter," Analog Devices App. Note, vol. AN-756, pp. 1-11, 2004.

[57] A. Viterbi, "Lower Bounds on Maximum Signal-to-Noise Ratios for Digital Communication Over the Gaussian Channel," *IEEE Transactions on Communications Systems*, vol. 12, no. 1, pp. 10-17, March 1964.

[58] IEEE Standard 802.3ab, Type 1000-BASE-T, June 1999.

[59] "The Broadcast Act (In Japanese), Chapter 2, Section 3, Article 15," Ministry of Internal Affairs and Communications, https://elaws.e-gov.go.jp/document?lawid=423M60000008095, May 2019.

[60] European Telecommunications Standard Institute ETSI, "Digital Video Broadcasting (DVB); Frame structure, channel coding and modulation for a Second Generation Digital Terrestrial Television Broadcasting System (DVB-T2)," EN 302 755 V.1.4.1, July 2015.

[61] ATSC: ATSC 3.0 Physical Layer Protocol Standard, document A/322, Adv. Television Syst. Committee, Washington, DC, USA, Dec. 2018.

[62] ATSC: ATSC 2.0 standard, document A/107, Adv. Television Syst. Committee, Washington, DC, USA, Dec. 2018.

[63] A. E. Kamal and B. F. Blietz, "A priority mechanism for the IEEE 802.3ah EPON,"

Proc. 2005 IEEE International Conference on Communications (*ICC*), vol. 3, pp. 1879-1883, May 2005.

[64] M. Xu, F. Lu, J. Wang, L. Cheng, D. Guidotti and G. Chang, "Key Technologies for Next-Generation Digital RoF Mobile Fronthaul With Statistical Data Compression and Multiband Modulation," *Journal of Lightwave Technology*, vol. 35, no. 17, pp. 3671-3679, Sept. 2017.

[65] M. Takada and M. Saito, "Transmission System for ISDB-T," *Proceedings of the IEEE*, vol. 94, no. 1, pp. 251-256, Jan. 2006.

[66] Hisashi Sujikai and Atsuro Ichigaya, "Source Coding and Transmission Technology of 4K/8K UHDTV Satellite Broadcasting." *IEICE Communications Society GLOBAL NEWSLETTER* vol. 45, no.1, Mar. 2021.

[67] A. Iwasaki, M. Nagasaka, Y. Koizumi, M. Kojima, S. Nakazawa, S. Tanaka, K. Ueda, "Hardware performance of optical distribution equipment for 12-GHz band satellite broadcasting using dual-polarization", *Transactions of the Japan Society for Aeronautical and Space Sciences, Aerospace Technology Japan*, vol. 16, no. 2, pp. 131-136, Mar. 2019.

[68] Yoichi Suzuki, Hisashi Sujikai, "Transmission System of 4K/8K UHDTV Satellite Broadcasting", *IEICE Transactions on Communications*, vol. E103.B, no. 10, pp. 1050-1058, Oct. 2020.

[69] J. D. Laster, W. L. Stutzman, "Frequency scaling of rain attenuation for satellite communication links", *IEEE Trans. Antennas Propagat.*, vol. 43, no. 11, pp. 1207–1216, Nov. 1995.

[70] "Propagation data and prediction methods required for the design of Earth-space telecommunication systems", Rec. ITU-R P.618-13, vol. 13, Dec. 2017.

[71] M. A. Samad, F. D. Diba, and D.-Y. Choi, "A survey of rain attenuation prediction models for terrestrial links—Current research challenges and state-of-the-art, " *Sensors*, vol. 21, no. 4, pp. 1207, Feb. 2021.

[72] M. Kamei, S. Nakazawa, S. Tanaka and K. Shogen, "A Study of Rain Attenuation with Measured Data in Japan for 21GHz-band Satellite Broadcasting," *Proc. 2011 International Symposium on Antennas and Propagation (ISAP)*, pp. 1-4, Oct. 2011.

[73] G. W. Beakley, "Television to Small Earth Stations," *IEEE Transactions on Broadcasting*, vol. BC-22, no. 3, pp. 96-100, Sept. 1976.

[74] J. J. Lee, "G/T and noise figure of active array antenna," IEEE Trans. Antennas Propag., vol. 41, pp. 241–244, Feb. 1993

[75] Ang Yu, Fan Yang, Atef Z. Elsherbeni, John Huang, Yahya Rahmat-Samii, "Aperture efficiency analysis of reflectarray antennas," *Microwave and Optical Technology Letters*, vol. 52, no. 2, pp. 364-372, Dec. 2009.

[76] ARIB STD-B44, "Transmission System for Advanced Wide Band Digital Satellite Broadcasting," ARIB, Mar. 2016.

[77] "The Broadcast Act (In Japanese), Chapter 2, Section 4, Article 19, "Ministry of Internal Affairs and Communications, https://elaws.e-gov.go.jp/document?lawid=423M60000008095, May 2019.

[78] Z. Zhi, J. Wu, X. Meng, M. Yao, Q. Hu and Z. Tang, "AP Deployment Optimization in Non-Uniform Service Areas: A Genetic Algorithm Approach," *Proc. IEEE 90th Vehicular Technology Conference (VTC)*, pp. 1-5, Sept. 2019.

[79] Y. Jian, Y. Liu, S. K. Venkateswaran, D. M. Blough and R. Sivakumar, "A Quantitative Exploration of Access Point Mobility for mmWave WiFi Networks," *Proc. 2020 IEEE International Conference on Communications (ICC)*, pp. 1-7,

June 2020.

[80] Y. Bejerano a nd S. Han, "Cell Breathing Techniques for Load Balancing in Wireless LANs," *IEEE Transactions on Mobile Computing*, vol. 8, no. 6, pp. 735-749, June 2009.

[81] S. Suherman, S. Andoni and A. H. Rambe, "Clustered beacon signal cell breathing for load balancing in mobile and wireless networks," *Proc. 3rd International Conference on Electrical, Telecommunication and Computer Engineering (ELTICOM)*, pp. 13-16, Sept. 2019.

[82] D. G. Narayan, R. Nivedita, S. Kiran and M. Uma, "Congestion adaptive multipath routing protocol for multi-radio Wireless Mesh Networks," *Proc. 2012 International Conference on Radar, Communication and Computing (ICRCC)*, pp. 72-76, Dec. 2012.

[83] H. C. Yu, K. Alhazmi and R. R. Rao, "Wi-Fi Roaming as a Location-based Service," *Proc. 2020 IEEE International Conference on Communications (ICC)*, pp. 1-7, June 2020.

[84] Z. Han, T. Lei, Z. Lu, X. Wen, W. Zheng and L. Guo, "Artificial Intelligence-Based Handoff Management for Dense WLANs: A Deep Reinforcement Learning Approach," *IEEE Access*, vol. 7, pp. 31688-31701, Feb. 2019.

[85] Y. Zheng, Y. Chen, X. Xie and W. Ma, "GeoLife2.0: A Location-Based Social Networking Service," *Proc. 2009 Tenth International Conference on Mobile Data Management: Systems, Services and Middleware*, pp. 357-358, May 2009.

[86] J. Qi and G.-P. Liu, "A robust high-accuracy ultrasound indoor positioning system based on a wireless sensor network," *Sensors*, vol. 17, no. 11, Nov. 2017.

[87] X. Wang, L. Gao, S. Mao and S. Pandey, "DeepFi: Deep learning for indoor

fingerprinting using channel state information," *Proc. 2015 IEEE Wireless Communications and Networking Conference* (*WCNC*), pp. 1666-1671, Mar. 2015.

[88] M. Castro, A. J. Jara and A. F. G. Skarmeta, "Smart Lighting Solutions for Smart Cities," *Proc. 27th International Conference on Advanced Information Networking and Applications Workshops*, pp. 1374-1379, Mar. 2013.

[89] P. Smallwood, "Lighting, LEDs and smart lighting market overview," presented at the U.S. Dept. Energy SSL Workshop, Raleigh, NC, USA, 2016.

[90] I. Chew, D. Karunatilaka, C. P. Tan, and V. Kalavally, "Smart lighting: The way forward? Reviewing the past to shape the future," *Energy Buildings*, vol. 149, pp. 180-191, Aug. 2017.

[91] A. M. Al-Ghaili, H. Kasim, N. M. Al-Hada, M. Othman and M. A. Saleh, "A Review: Buildings Energy Savings - Lighting Systems Performance," *IEEE Access*, vol. 8, pp. 76108-76119, April 2020.

[92] L. I. Albraheem, L. H. Alhudaithy, A. A. Aljaser, M. R. Aldhafian, and G. M. Bahliwah, "Toward designing a Li-Fi-based hierarchical IoT architecture," IEEE Access, vol. 6, pp. 40811–40825, 2018.

[93] M. Miki, K. Yoshida, and M. Yoshimi, "Faster Illuminance Convergence for the Intelligent Lighting System Using Visible Light Communication," *Proc. 2012 IEEE International Conference on Systems, Man, and Cybernetics* (*SMC*), pp. 3179–3184, Oct. 2012.

[94] V. Jones and H. Sampath, "Emerging technologies for WLAN," *IEEE Communications Magazine*, vol. 53, no. 3, pp. 141-149, March 2015.

[95] J. J. Koenderink, A. J. van Doorn, "Visibility of unpredictably flickering lights," *J. Opt. Soc. Amer.*, vol. 64, no. 11, pp. 1517-1522, Nov. 1974.

[96] P. Series, "Propagation data and prediction methods for the planning of indoor radio communication systems and radio local area networks in the frequency range 300 MHz to 100 GHz," Recommendation ITU-R P.1238-8, 2015.

[97] E. Wong, "Next-Generation Broadband Access Networks and Technologies," *Journal of Lightwave Technology*, vol. 30, no. 4, pp. 597-608, Feb. 2012.

[98] K. Grobe and J. Elbers, "PON in adolescence: from TDMA to WDM-PON," *IEEE Communications Magazine*, vol. 46, no. 1, pp. 26-34, Jan. 2008.

[99] Jun Shan Wey, "The Outlook for PON Standardization: A Tutorial," *Journal of Lightwave Technology*, vol. 38, no. 1, pp. 31-42, Jan. 2020.

[100] D. Nesset, "NG-PON2 Technology and Standards," *Journal of Lightwave Technology*, vol. 33, no. 5, pp. 1136-1143, Mar. 2015.

[101] C. Knittle, "IEEE 50Gb/s EPON (50G-EPON)," *Proc. 2020 Optical Fiber Communications Conference and Exhibition* (*OFC*), pp. 1-3, Mar. 2020.

[102] N. Tanaka, D. Umeda, Y. Sugimoto, T. Funada, K. Tanaka, S. Ogita, "25.78-Gbit/s Burst-mode Receiver for 50G-EPON OLT," *Proc. 2020 Optical Fiber Communications Conference and Exhibition* (*OFC*), pp. 1-3. Mar. 2020.